# Technobius

*A peer-reviewed open-access journal*

# Technobius

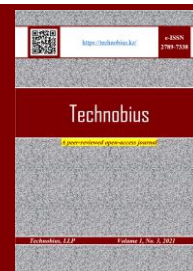## *Volume 5, No. 1, 2025*

# CONTENTS

*Review*

# Comprehensive overview of the macroscopic thermo-hydro-mechanical behavior of saturated cohesive soils

Victor N. Kaliakin[1,*], Meysam Mashayekhi[2]

[1]Department of Civil, Construction, and Environmental Engineering, University of Delaware, Newark, DE, USA
[2]Department of Civil Engineering, University of Isfahan, Isfahan, 81744-73441, Iran
*Correspondence: kaliakin@udel.edu

**Abstract.** Understanding the effects of temperature on the hydro-mechanical behavior of geomaterials (i.e., soil and rock) has gained significance over the past three decades. This is due to new applications in which these materials are subjected to non-isothermal conditions. Examples of such applications include geothermal systems, nuclear waste disposal, and energy geo-structures. The analysis and design of such applications requires a thorough understanding of the macroscopic thermo-hydro-mechanical (THM) behavior of the geomaterials. Although various aspects of this behavior have been documented in the literature, a comprehensive overview of such behavior is lacking. This article presents such an overview of the macroscopically observed THM behavior of saturated cohesive soils.
**Keywords:** saturated cohesive soils, temperature, thermo-hydro-mechanical, energy geo-structures.

## 1. Introduction

The effects of temperature changes on the hydro-mechanical behavior of geomaterials (i.e., soil and rock) assumes importance in many applications. During the 1930's, perhaps the largest concern related to temperature effects on soils was the disturbance, in terms of variations of strength, and compressibility during the sampling, handling, or laboratory testing of specimens.

The subsequent incentive for improved understanding the thermal response of geomaterials was the necessity to solve a rather diverse set of problems such as 1) the improved stability of soil masses realized through their heating, 2) the interaction between soils and buried pipes transporting fluids or high-voltage cables at elevated temperatures, 3) the integrity of pavements and subgrades that are subjected to daily temperature variations, 4) the behavior of foundations (e.g., for furnaces) that are subjected to cyclic variations in temperature, 5) the drilling of deep wells, both offshore and on land, for hydrocarbon extraction, and 6) the effect of temperature variations on the behavior of clay liners, possibly in conjunction with geosynthetics, used in landfills.

In the 20th century, the major challenge that motivated an improved understanding of the thermo-hydro-mechanical (THM) behavior of soils was the disposal of radioactive waste in deep underground or offshore repositories, primarily consisting of low-permeability clay soils.

In the 21st century, an understanding of the aforementioned behavior was required in addressing two significant international socio-economic issues, namely the production and use of energy. During the last few decades, concerns over energy equity and security, excessive energy consumption rates, and issues related to climate change have intensified a worldwide effort to address such issues [1]. Increases in the price of fossil fuels have also accelerated the investigation of alternate energy sources. One such alternative, which is a renewable and possibly "clean" source of energy, is geothermal energy [2].

The basic premise underlying geothermal energy is to make use of thermal energy that is generated by the decay of radioactive elements within the ground or, more likely, by the storage of solar radiation. Several mechanical systems have been developed to facilitate the use of geothermal energy. These are commonly divided into two main categories based on their temperature range, namely 1) low thermal gradient zones known as Ground Source Heat Pumps [3], and 2) high thermal gradient zones known as Enhanced Geothermal Systems [4].

One of the newer advances in geothermal systems are the so-called energy geostructures. In such systems, structural elements, often associated with buildings, are used for heat transfer. Perhaps the most significant challenge associated with energy geostructures is the proper account for the effect of temperature on the response of the structure. Temperature changes typically induce variations in the settlement of the soil and structure, as well as in the forces acting within the structure. Consequently, supplementary considerations are required in the design of energy geostructures. The difference in response of the structure (typically thermo-elastic) and the soil (typically inelastic) also increases the complexity of the response. It follows that design of energy geostructures should be executed with consideration of the inelastic thermo-mechanical response of soils (e.g., the effect of temperature changes on consolidation and subsequent time dependent deformation of the soil), of the mobilization of side friction between structural elements and the soil that they are in contact with, and the additional loads due to degree of fixity at the bottom and top portions of the structure [5].

Since geothermal applications involve geomaterials (i.e., a soil or rock), understanding the behavior of such materials related to thermal loading is vital. Soils are heterogeneous particulate materials consisting of solid, liquid and gaseous phases. Consequently, they possess rather complex heat dissipation mechanisms such as conduction, convection, radiation, ion exchange, as well as vaporization and condensation. In unfrozen soils, heat transfer occurs by conduction and, to a lesser degree, by convection [5]. Thus, thermal properties of the soils related to phenomena such as heat capacity, thermal diffusivity and thermal conductivity are essential.

To further complicate the problem, other phenomena that can also influence the heat transfer. These include 1) the temperature dependence of the thermal parameters characterizing the geomaterial, 2) the effect of physical changes on the values of these parameters during mechanical and thermal loading, and 3) the different rates of heat transfer between the solid and liquid phases in a geomaterial [5].

The behavior of geomaterials is influenced by variables associated with the solid phase (e.g., mineralogy, size, shape, surface charge, composition, etc.), by the value of bulk (index) variables (e.g., void ratio, moisture content, relative density, etc.), and by the characteristics of the pore fluid. The relative importance of both micro- and macro-level variables is, however, dependent on the particular soil under consideration.

In saturated cohesive soils, the solid phase consists primarily of fine-grained constituents such as clays and silty clays. Clay particles are crystalline, plate-like, and have high specific surface (i.e., the surface area per unit mass) [6]. They have negative net surface charges and, due to breaks in their crystalline structure, a net positive charge at the plate edges [7]. Such edges may attract negative ions, dipole molecules, or may themselves be attracted to the negatively charged surface of another particle [6].

The properties of any cohesive soil are known to significantly be influenced by the presence of water [6], [8]. In a general cohesive soil, water is present in three forms, namely as 1) Ordinary ("free" or "bulk") liquid water, 2) Adsorbed water, and, particularly in low-porosity clays 3) An "organized" fluid. Macroscopically, the charged nature of clay particles thus influences such macroscopic measures of response as plasticity, shrinkage and swelling potential, permeability, compressibility, and strength parameters (e.g., the cohesion and friction angle) [6].

It light of the above discussion, it is evident that the macroscopic thermo-hydro-mechanical (THM) behavior of saturated cohesive soils should be interpreted in terms of the microscopic and physicochemical aspects associated with such geomaterials. This behavior is complicated by the discontinuous and heterogeneous nature of the microstructure (i.e., the geometric arrangement of pore spaces, particles, and particle groups, along with the interparticle forces present in the geomaterial),

as well as by sundry physicochemical aspects. A rudimentary discussion of such aspects, as they apply to the THM behavior of saturated cohesive soils, was presented by Kaliakin et al. [9]; this was superseded by the updated and more in-depth treatment presented by Mashayekhi [10]. More thorough treatments of the microscopic and physicochemical aspects are given in books by Scott [11], Mitchell [6] and Mitchell and Soga [12].

When mathematically modeling the THM behavior of saturated cohesive soils, it is not yet possible to account for microscopic and physicochemical aspects in a manner that is both practical and robust, especially when simulating actual boundary value problems. Instead, in such models these aspects must be accounted for indirectly. This approach is largely based on the macroscopic THM behavior of saturated cohesive soils that is observed in laboratory tests. This article presents a comprehensive overview of such behavior. This overview updates and expands the earlier work of Kaliakin et al. [9] and Mashayekhi [10].

## 2. Methods

The subject matter related to the THM behavior of saturated cohesive soils has been available in the literature since the 1960's. As such, some of the older references were available only in hardcopy form. More current references were accessed from electronic databases such as Web of Science.

In searching through the available literature, only subject matter pertaining to saturated cohesive soils was considered. Herein, "cohesive soil" is restricted to clays and silty clays. Other fine-grained soils such as silts and clayey silts were not included in the literature reviewed for this article. This was done for reasons of brevity and because relatively little information is available regarding the THM behavior of such materials.

The search of pertinent subject matter included master theses and doctoral dissertations. Unfortunately, not all academic institutions provide easy access to such documents. Consequently, the theses and dissertations cited in this article do not constitute a complete collection such references.

A topic associated with the THM behavior of saturated cohesive soils is the variation, with temperature and possibly pressure, of the parameters used to characterize the thermal properties geomaterials. Such parameters include the density of the pore fluid and solid phase, the isotropic or anisotropic coefficients of thermal expansion for these two phases, the viscosity of the pore fluid, the hydraulic and thermal conductivities, and the heat capacity and specific heat of the solid and pore fluid phases. For brevity, the discussion of the aforementioned topic has been omitted from the present review article. A rather thorough overview of this topic has, however, been given by Mashayekhi in Chapter 4 of his dissertation [10].

## 3. Effect of Temperature on General Material Characteristics

Historically, the effect of temperature changes on the macroscopic behavior of cohesive soils was evaluated using standard soil mechanics laboratory experiments. To begin the present overview of the THM behavior of saturated cohesive soils, consider the effect of temperature on general material characteristics.

*3.1 Atterberg Limits*
The plasticity of cohesive soils is largely characterized by the values of the liquid limit ($w_L$) and plastic limit ($w_P$). As noted by by Mashayekhi [10], "the effect of temperature on the Atterberg limits has not been extensively investigated. This may, in part, be due to questions that have been raised regarding the reliability of the Atterberg limit tests". Consider the determination of $w_P$. In this test, an exchange of heat typically takes place between the soil and the hand of the individual performing the test [13], [14]. In addition, it is a well-known fact that the determination of $w_P$ is more subjective and more prone to error than the determination of $w_L$ [15], [16]. It is timely to note that

measurements of $w_L$ using the standard Casagrande device are more subjective and tend to be less repeatable than those obtained when using a cone penetrometer [17], [18].

The first experimental investigation of the effect that changes in temperature have on the Atterberg limits was that performed by Youssef et al. [19], who conclude that temperature increases lead to a reduction in the values of $w_L$ and $w_P$. These findings were explained by the observation that, since temperature increases reduce the moisture content ($w$) of a soil, index properties dependent on $w$ will likewise decrease under such conditions.

Similar reductions in $w_L$ at elevated temperatures were reported for the three major clay mineral types (kaolinite, illite, and monmorillonite) by Laguros [13]. In this study, the results obtained for $w_P$ were, however, rather inconsistent. Reductions in $w_L$ and $w_P$ with increases in temperature were also observed by Ctori [14] and by Wohlbier and Henning [20].

After reviewing the aforementioned results of Youssef et al. [19] and Laguros [13], Mitchell [21] concluded that the reductions in $w_L$ with increases in temperature to be consistent with the reductions in strength observed at elevated temperatures (to be discussed in sub-section 3.3), especially since $w_L$ is considered to be an indirect measure of shear strength of cohesive soils.

The results of more recent investigations seem to indicate that the *mineralogy* of the cohesive soil plays a significant role in determining the effect of temperature changes on the Atterberg limits. This observation stems from the rather contradictory results [22], [23], [24], [25] which indicated that such limits for kaolinite were essentially unaffected by changes in temperature. However, for kaolinite-bentonite mixtures, Reifer [23] found that $w_L$ increased with increases in temperature. Such increases intensified as the percentage of bentonite was increased. The value of $w_P$ was, however, essentially unaffected by these increases in temperature.

A somewhat more systematic study of the effects of mineralogy on the temperature dependence of $w_L$ was carried out by Jefferson and Rogers [26]. In this study, it was determined that although $w_L$ decreased with temperature for kaolinite, it increased for specimens that contained percentages of bentonite. Jefferson and Rogers [26] attributed these variations in $w_L$ to the specific surface of the particular clay mineral. Thus, for clays with relatively high specific surface (e.g., bentonite), $w_L$ will increase with increased temperature; in clays with low specific surface (e.g., kaolinite), it will slightly decrease for these same temperature increases.

*3.2 Elastic Response*

Although it is widely accepted that soils exhibit elastic response only at very low strains [27], [28] their elastic response has been rather extensively studied in the past. Of particular interest to the present development is elastic response under non-isothermal conditions.

The first experimental study of the effect of temperature changes on the response of clays, consisting of drained stress relaxation tests performed on saturated, undisturbed specimens, was performed by Murayama and Shibata [29]. Based on the results of this study, an analytical formulation in which the solid phase of the soil was idealized as being *viscoelastic* was proposed. Subsequent work by Murayama [30] extended this formulation by basing it on statistical mechanics (i.e., the rate process theory).

As summarized by Mashayekhi [10], Murayama and Shibata [29] conjectured that "the elastic resistance of clay particles is due, in part, to an imbalance of attractive and repulsive physicochemical forces, as well as to the viscous resistance due to adsorbed water between particles. Thus, although the elasticity of the skeleton is likely due to bending of the thin plate particles, it is also attributed to physicochemical interparticle forces. According to the Gouy-Chapman theory, temperature increases reduce the thickness of the diffuse double layer, thus also reducing the electric repulsion between clay particles" [31]. As a result, it follows that the elastic response of the clay tested will be a function of temperature changes.

Another important observation attributed to Murayama and Shibata [29] is the apparent existence of a "threshold" axial strain value (on the order of 1.0%), below which the elastic moduli will be unaffected by changes in temperature. Once this value is exceeded, temperature increases will cause the elastic moduli to *decrease* in magnitude. Murayama and Shibata [29] attributed this

behavior to "fracture" of the solid phase once the aforementioned "threshold" axial strain value was exceeded.

With an eye towards using the mathematical theory of elastoplasticity to simulate the behavior of cohesive soils, investigations have been made into the effect of temperature changes on the size of the elastic domain in such simulations [32], [33], [34]. Based on these investigations, there appears to be general consensus that the size of this domain *decreases* with increases in temperature.

### 3.3 Shear Strength

One of the most fundamental material characteristics associated with geomaterials is their shear strength. The variation of shear strength of saturated cohesive soils, as a function of temperature, has been the subject of a number of studies [31], [35], [36], [37], [38], [39], [40], [41], [42], [43], [44], [45]. However, as noted by Mashayekhi [10], a general consensus regarding the effect of temperature variations on the shear strength of saturated cohesive soils has not been reached.

In their study of compacted cohesive soils, Hogentogler and Willis [35] found that increases in temperature *decreased* the strength of such materials. Lambe [31], on the other hand, postulated that an increase in temperature should result in an *increase* in shear strength. Citing the earlier findings of other investigators [35], [36], [37], Leonards [38] postulated that increases in temperature should cause a *reduction* in the shear strength of clays, thus contradicting Lambe's [31] hypothesis. From undrained axisymmetric triaxial tests performed on specimens of San Francisco Bay Mud, Mitchell [40] found that higher temperatures produced *lower* shear strength and higher excess pore pressure generation. Duncan and Campanella [42] acquired experimental data for soils first consolidated and then sheared under undrained axisymmetric triaxial conditions. Their findings also indicated that an increase in temperature causes a *reduction* in strength. Sherif and Burrous [44] investigated the undrained strength of kaolin subjected to undrained thermal loading and also found substantial *reductions* in strength. Figure 1 summarizes some of their findings.

Noble and Demirel [43] sheared specimens of a highly plastic alluvial clay at temperatures that were lower than the temperature at which they were consolidated. It was observed that the higher the consolidation temperature, the greater the shear strength at any given temperature. This observation, which agrees with the results of Laguros [13], is attributed to the greater decrease in volume (and thus void ratio) at higher consolidation temperatures. However, for a given consolidation temperature, the strength decreases in a regular manner with increasing test temperature. Leroueil and Marques [46] concluded that the undrained shear strength of saturated cohesive soils decreases by approximately 10% per $12^{\circ}$C change in temperature.

In the case of undrained shearing that follows heating under *drained* conditions, the shear strength of soil tends to *increase*. This is explained by the fact that thermal compression of the soil during drained heating reduces the soil's void ratio and thus increases its shear strength.

By contrast, following undrained heating, the undrained shear strength tends to decrease. Hueckel and Baldi [34] attribute this phenomenon to the decrease in effective stress due to the increase in the generation of excess pore pressure during the process of undrained heating.

### 3.4 Anisotropy

The results of many experiments indicate that the mechanical properties of many natural and remolded soils are associated with certain preferred directions in space [47], [48]. Mathematically, such soils are thus classified as being *anisotropic* [49].

The anisotropy of cohesive soils is commonly attributed to preferred orientations of particles or clusters of particles, and possibly to the development of residual microstructural stresses [49]. Such preferred orientations result in both elastic and inelastic anisotropy. According to Dafalias [50], the consideration of elastic anisotropy is important for small strain levels. For larger strains, however, inelasticity is predominant, and elastic anisotropy can thus be neglected.
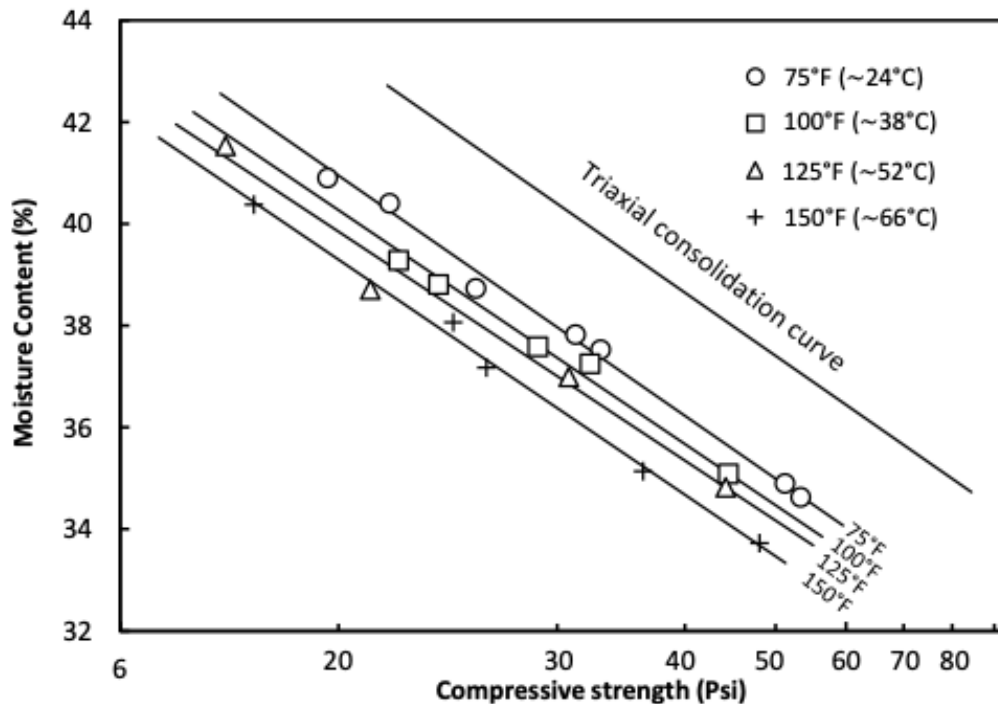
Figure 1 – Effect of temperature on the undrained shear strength of kaolinite in unconfined compression (after Sherif and Burrous [44])

Very few experimental studies have been performed to investigate the effect that changes in temperature have on the behavior of anisotropically consolidated cohesive soils. In such studies, the specimens are assumed to be transversely isotropic [49].

One important contribution in this area is the critical review by Hueckel and Pellegrini [51] of experimental data for two deep ocean clays [52], [53] that exhibited pronounced anisotropy. Hueckel and Pellegrini [51] noted that when these clays are isotropically compressed under isothermal conditions, they exhibit greater compression in the "vertical" direction (i.e., the direction perpendicular to the plane of isotropy) than in the "horizontal" direction (i.e., the direction parallel to the plane of isotropy). They attributed such behavior to the past loading history for these clays, which consisted largely of one-dimensional straining in the "vertical" direction, followed by unloading. Due to such a loading history, the clay particles and particle clusters tend to align themselves at right angles to the "vertical" direction, thus giving rise to a primarily horizontal orientation [54]. Upon subsequent laboratory re-loading, these clays tend to deform more easily in the "vertical" direction. When both of these clays were subjected to isotropic heating, the irreversible strain in the "horizontal" direction was larger than in the "vertical" direction. Although Hueckel and Pellegrini [51] could not definitively explain such results, their conjecture was that under isotropic conditions, lateral strains tend to be larger than for anisotropic ($K_0$) conditions.

Somewhat limited experimental evidence seems to indicate that the largest degree of anisotropy in cohesive soils is present during elastic deformation [55]. Then, under isotropic inelastic re-loading, it essentially disappears. Such behavior is consistent with the aforementioned hypothesis of Dafalias [50].

The effect of temperature changes on the behavior of overconsolidated anisotropic cohesive soils has received precious little attention in past studies. The only work in this area appears to be that reported by Virdi and Keedwell [56]. In this study, overconsolidated kaolin specimens were subjected to transient temperature distributions. The higher deviatoric stresses that resulted were attributed by Virdi and Keedwell [56] to stress-induced anisotropy, which tended to make the specimens stiffer in the axial ("vertical") direction.

In a more recent study, Russell Coccia and McCartney [57] employed a true triaxial apparatus to study the effect of anisotropy on thermally induced volume changes of a saturated silt tested under drained conditions. They concluded that such volume changes are not significantly influenced by stress-induced anisotropy.

## 4. Effect of Temperature on Behavior Under Drained Conditions

In drained tests, the drainage valves in the test apparatus remain open. The stresses are applied very slowly so that essentially no excess pore pressure is developed in the specimen.

The earliest investigation of the effect of temperature on the drained response of saturated cohesive soils appears to be that of Gray [58]. Based on the results of this, as well as subsequent investigations, there is general consensus that at constant levels of stress under drained conditions, normally consolidated (NC) and lightly overconsolidated (OC) cohesive soil specimens compress when heated. Temperature decreases typically cause such specimens to swell; pore fluid is adsorbed by such specimens [42], [59]. The aforementioned compression in heated NC specimens appears to be independent of the material state but to be dependent on the mineralogy and porosity of the specimen [52].

The behavior of saturated NC specimens subjected to cycles of heating and cooling under drained conditions at constant stress states has also been investigated. During such thermal cycling, the behavior appears to be inelastic; that is, some part of the axial strain is irreversible [42], [60], [61]. The associated permanent decrease in void ration during such thermal cycling appears to be independent of the effective confining stress [25], [43], [60], [62], [63], [64], [65]. Specimens subjected to such temperature cycles behave as if they were overconsolidated [25], [33], [34], [42], [63], [66].

The magnitude of the volume change under drained conditions has been reported to reduce with increases in the overconsolidation ratio (OCR) [34], [53], [59], [60], [61], [63], [67]. The rate of this reduction seems to be a function of the stress level (typically represented in terms of the OCR [60]). In the case of cohesive soils of low plasticity, such reductions tend to be rather pronounced. For cohesive soils with high plasticity, the rate of such reduction appears to be less significant. For low porosity clays, volume contraction becomes dilative for high OCRs [25], [61].

When NC and OC cohesive soil specimens are cooled under drained conditions, the associated volumetric strains are generally independent of the stress state, thus implying elastic response. The volumetric strains generated during such cooling do not necessarily have the same sense. For example, in the case of illitic clays [21], [62], [63], and for Pontida silty clay [61], the volumetric strains are rather pronounced and dilative (and thus negative). In the case of soft Bangkok clay [65] and Boom clay [61], the volumetric strains generated during cooling are quite small as compared to the strains produced during heating. By contrast, when Spanish clay [53] is cooled, the volumetric strain generated tends to be compressive (and thus positive). As noted by Mashayekhi [10], "the aforementioned variations in the sign of the recoverable volumetric strain have, in some cases, necessitated the use of rather elaborate functional forms for the coefficients of thermal expansion for cohesive soils".

### 4.1 Compressibility Characteristics

The compressibility of soils is typically studied using oedometer and axisymmetric triaxial devices under drained conditions. Several experimental investigations have examined the effect that temperature cycling has on volume change characteristics in such tests that are carried out constant levels of confining stress. These investigations used a standard laboratory oedometer [25], [33], [63], [66], [68], [69], [70], a standard triaxial cell with isotropic confining pressure [42], [53], [67], and a special triaxial test cell [59], [60]. The tests performed using such devices tests were carried out at varying (constant) stress levels and temperatures.

The results of such tests indicate that, when subjected to temperature increases, NC and lightly OC specimens consolidate; temperature decreases lead to the swelling of such specimens. As a result,

the soil behaves as if it were overconsolidated [34], [42], [63], [66]. Consequently, the heating of such specimens at constant mean normal effective stress produces a quasi-preconsolidation behavior similar to that associated with long term consolidation [25], [33], [42], [63].

For NC specimens, the magnitude of irreversible volume change generated by heating, while material specific, was shown to be essentially *independent* of stress level. In particular, when subjected to temperature increases, illitic clays [62], [63] and smectites [43] exhibited a clear reduction of void ratio. For clays possessing high volume fractions of silt this was not, however, the case, as such soils did not undergo appreciable void ratio reductions when heated [63].

By contrast, in OC cohesive soils the thermally induced volume changes are typically independent of stress level. They are, however, a function of the stress history, which is typically quantified by the OCR.

The effect of temperature cycling on the volume changes in OC cohesive soils has also been investigated [34], [53], [60], [61], [63], [67]. As summarized by Mashayekhi [10], "the consensus appears to be that compared to normally consolidated specimens, thermally induced volumetric strains are relatively small, depend on the OCR [34], [63], [71], and are largely reversible". In support of this summary is the observation that the amount of compression exhibited under drained conditions appears to decrease with increasing OCR. In the case of clays with low porosity, the behavior of OC specimens was actually found to be *thermoelastic* [34], [53], [61]. Furthermore, when heated, highly OC specimens of such clays dilated. This is partly explained by the fact that when such clays are heated, the pore fluid expands to a greater degree as compared to the solid phase. Since the permeability of clays is relatively low, this fluid cannot quickly drain from the pores, resulting in dilative behavior.

## 4.2 Compression and Swell/Recompression Indices

The compressibility of soils is typically characterized by the values of compression index $C_c$ and the swell/recompression index $C_r$. Based on the available experimental findings, there does not appear to be consensus regarding the effect of temperature increases on the values of $C_c$ and $C_r$ (or on their critical state counterparts $\lambda$ and $\kappa$, respectively). The following findings are presented in support of this conclusion.

### 4.2.1 The Compression Index

Initially, most of the experimental studies were performed at relatively low stress levels [13], [63], [66], [69], [72]. The results of these studies indicated that the value of $C_c$ changed with temperature. Such changes were dependent on the stress level [72], the soil type, and on temperature [63], [66], and pressure [63].

At higher confining pressures, the value of $C_c$ was found to be practically temperature independent [32], [42], [60], [62], [67], [68], [73], [74], [75]. Increases in temperature tended to displace the virgin compression line in void ratio versus logarithmic of stress space to lower void ratios; the slope of the line, which is equal to $C_c$, remained essentially the same. These findings were supported by the results of a subsequent analytical study that was based on the Gouy-Chapman theory [76].

The effect of stress history on the thermally induced variation in $C_c$ was also studied by Habibaghi [69]. Based on the result of this experimental program, it was concluded that for NC clays at stresses greater than 300 kPa, the $C_c$ values were temperature independent. However, for OC specimens, such values were dependent on the temperature. Habibaghi [69] noted, however, that this dependency seemed to diminish with reductions in the OCR. Consequently, the effect of temperature on the value of $C_c$ appears to be a function of the stress history.

### 4.2.2 The Swell/Recompression Index

A few researchers [13], [34], [42] have reported that the value of $C_r$ was essentially temperature independent. Other findings [32], [73], [77], however, showed that $C_r$ was an increasing function of temperature.

This assessment of the temperature dependence of $C_r$ appears to depend on whether the *swell* or the *recompression* portion of the response was considered in a given experimental study. This conjecture is largely due to the findings of Campanella [62], who attributed the observed variation in $C_r$ to hysteresis effects (which is related to changes in a soil's compressibility), and to differences in unloading-reloading response. In support of this conclusion, is the fact that the tests of Eriksson [32] were performed on the recompression portion of the void ratio versus logarithm of stress curve. By contrast, the test results of Laguros [13] were, however, obtained from the swell portion.

The apparent discrepancies associated with the dependence of $C_r$ on temperature were investigated by Abuel-Naga et al. [67], who performed tests involving both the swell and recompression phases of the response. In tests that made use of the recompression line, $C_r$ was found to be temperature dependent, while in those involving the swelling line, $C_r$ was found to be temperature independent. These results led Abuel-Naga et al. [67] to conclude that, since the recompression portion of the response involves irreversible deformations, the proper assessment of the temperature dependence of $C_r$ must make use of the swell portion.

In an attempt to explain the elastic response associated with the swell portion, Mashayekhi [10] notes that "from a micromechanical viewpoint, temperature increases will tend to reduce interparticle bond strength and thus increase the elastic deformations. However, under drained conditions, the same temperature increase will cause a reduction in void ratio, thus compensating for the reduction in bond strength. The overall response may thus be largely temperature independent".

*4.3 Preconsolidation Stress*

The effective preconsolidation stress ($\sigma'_p$) is thought to be a "yield limit", that under both isotropic and anisotropic stress states, separates elastic response from inelastic response [46]. Based on the results of oedometer and constant rate of strain axisymmetric triaxial tests, it has been ascertained that, at a given value of void ratio, increases in temperature cause $\sigma'_p$ to decrease [32], [33], [34], [65], [74], [77], [78], [79], [80]. The change in $\sigma'_p$ appears to be greater for cohesive soils with increased clay content, as well as for those characterized by larger values of $w_L$ [33]. Figure 2 summarizes some experimental results related to the effect of temperature on $\sigma'_p$.

The reduction in $\sigma'_p$ appears to depend on the stress ratio, $\eta = q/p'$, where $q$ is the deviator stress and $p'$ is the mean normal effective stress. The higher the stress ratio, the smaller the reduction of $\sigma'_p$ [67].

## 5. Effect of Temperature on Behavior Under Undrained Conditions

In undrained tests, the drainage valves in the test apparatus are closed following consolidation. The stresses subsequently applied to a specimen generate excess pore pressures, which are recorded.

For NC and lightly OC saturated cohesive soils tested under undrained conditions at a constant level of total stress, temperature increases, even minor ones, lead to the development of excess pore pressure and thus to a decrease in effective stress [30], [45], [56], [81], [82]. Decreases in temperature cause the excess pore pressure to decrease.

The aforementioned changes in excess pore pressure are typically attributed to sundry physicochemical effects, and to the difference in thermal expansion characteristics associated with the pore fluid and solid phases. The *magnitude* of excess pore pressure change is thought to be a function of the 1) path followed in thermal loading, 2) temperature increments used in a given test, 3) compressibility of the soil being tested and, 4) thermal expansion properties of the pore fluid and solid phase [45].

Investigations of thermal cycling indicate that the resulting pore pressure changes are irreversible [81], [83], [84], [85]; the pore pressure response is characterized by hysteresis loops that may [81] or may not [63], [83], [84], [85], [86] be closed.

Campanella and Mitchell [42] hypothesized that continued temperature cycling and the dissipation of "secondary compression tendencies at high temperatures" would result in excess pore

pressure-axial strain hysteresis loops that were *closed*. In support of this conjecture was the lack of residual excess pore pressure for specimens of illite tested by Campanella and Mitchell [42]. Before being subjected to undrained conditions, these specimens were subjected to temperature changes under drained conditions.
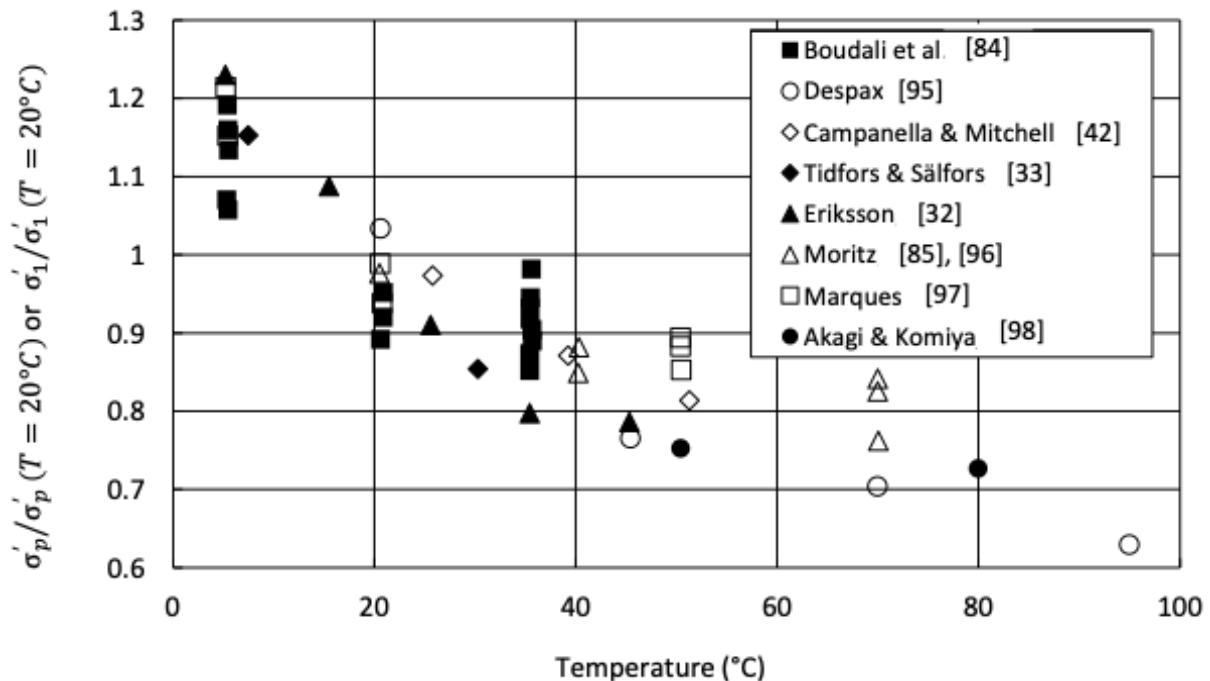


Figure 2. Effect of temperature on the normalized preconsolidation stress (after [46]).

Two important observations related to temperature dependent response of saturated cohesive soils under undrained conditions were made by Plum and Esrig [63]. First, they noted that hysteresis loops would only be expected to occur following several thermal loading-unloading cycles or after variations in temperature. Secondly, they noted that a closed hysteresis loop would be developed only when the soil is somewhat OC. This second observation leads credence to earlier results presented by Mitchell and Campanella [81] that produced closed hysteresis loops, for this study involved two OC cohesive soils.

## 6. Time Dependent Behavior

The effect of temperature changes on the time dependent behavior of saturated cohesive soils is somewhat complicated by the fact that it is rather difficult to isolate temperature effects from time effects [10]. When discussing the macroscopically observed time-related behavior of saturated cohesive soils, this subject is commonly divided into the following categories: a) constant stress creep, b) constant strain relaxation, and c) strain-rate effects. Such a division is admittedly somewhat artificial. Indeed, it is the feeling of many researchers that the same micromechanical mechanisms may be responsible for all three of these phenomena [9], [87]. Nevertheless, it successfully separates the different types of time dependent behavior for specific loading conditions, and it aligns with the manner in which this subject has been presented in past literature. Consequently, it facilitates the presentation of subject matter in this section.

*6.1 Constant Stress Creep*
Of the aforementioned categories related to time dependent behavior, the creep of saturated cohesive soils has been studied more comprehensively than relaxation or strain-rate effects. Constant stress creep is defined as the time dependent development of shear- and/or volumetric deformations

under a constant state of total stress. Creep occurs under both drained (constant effective stress), as well as undrained (constant volume) conditions. It is used to depict a number of field applications in which a constant load is applied to a soil deposit (e.g., from an embankment built on the ground surface), and causes either undrained or drained creep in the supporting soil.

In what appears to be one of the earliest systematic investigations of the effect of temperature on the time dependent behavior of cohesive soils, Murayama [30] performed creep tests, under drained conditions, on NC specimens of an alluvial marine clay. Based on the results of these tests, at a given temperature, the creep strain rate was determined to be linear with the logarithm of time. Although increases in temperature caused the strain rate to increase, it remained approximately linear with the logarithm of time.

A similar series of drained creep tests was performed by Campanella [62], albeit on specimens of illite. For a given (constant) level of total stress, and under isothermal conditions, only relatively small volume changes were measured during creep. If, however, a specimen's temperature was increased after consolidation, the volume changes measured during creep increased rather appreciably. Campanella [62] also found that, at a given time during creep, specimens consolidated at higher temperatures exhibited higher strain rates. Unlike the findings of Murayama [30], Campanella [62] noted that his experimental results were best represented by a linear relationship between the logarithm of strain rate versus the logarithm of time.

The subsequent drained creep tests performed by Virdi and Keedwell [56] were noteworthy because they not only maintained a constant temperature during the tests but also imposed a transient temperature state consisting of two full cycles. Based on the results of these tests, Virdi and Keedwell [56] noted that temperature increases reduced the volume of their specimens. Temperature decreases had the reverse effect. In all of the drained creep tests performed, the effect of temperature changes on the volumetric and axial strain rates was more pronounced at higher deviator stress levels. Virdi and Keedwell [56] also noted that, in response to temperature variations, the volume of pore fluid expelled from, or absorbed into a specimen appeared to be proportional to the moisture content.

The topic of secondary compression (drained volumetric creep [87]) is very often included in a discussion of consolidation. The effect of temperature increases on secondary compression has thus been the focus in several investigations [25], [42], [63], [88], [89]. The results of these investigations have not, however, been in general agreement. For example, the conclusion reached by Plum and Esrig [63] was that if sufficient time is allowed for thermally induced volume changes to occur, the rate of secondary compression will only slightly be affected by temperature increases. This conclusion, however, contradicted the findings of other investigators [25], [42], [88], [89]. As noted by Mashayekhi [10], "it is possible, however, that in the latter investigations insufficient time was allowed for thermally induced volume changes to fully manifest themselves".

In their study of thermal effects on secondary compression, Towhata et al. [25] increased the temperature at different times during the secondary phase of consolidation. The found that such actions accelerated the amount of volume change generated during this phase.

Burghignoli et al. [75] also performed thermal consolidation tests on NC specimens. They found that in heated specimens the variation in void ratio during secondary compression was relatively large. Burghignoli et al. [75] concluded that during the secondary phase of consolidation of NC clays, creep deformations were dominant. When such specimens were cooled, they did not exhibit any appreciable secondary compression. In their tests on OC specimens, Burghignoli et al. [75] reported essentially *identical* behavior during both heating and cooling phases. Such results underscore the importance of stress history when studying temperature and time dependent processes.

It is timely to note that in discussing the somewhat controversial subject temperature effect on secondary compression, there appears to be consensus that the overconsolidation of cohesive soils due to cooling reduces the rate of secondary compression [42], [63], [75].

Relatively few experimental studies have investigated the effect of temperature on creep of cohesive soils under undrained conditions. Before subjecting them to undrained creep, Houston et al. [45] consolidated specimens at constant temperatures under drained conditions. They found that, with increasing consolidation temperatures, undrained creep strain rates decreased. Houston et al. [45]

attributed such behavior to the greater degree of densification and higher stiffness that is obtained during consolidation at elevated temperatures. During undrained creep, specimens tested at higher temperatures were more likely to fail under undrained conditions.

Similar to the aforementioned drained creep tests, Virdi and Keedwell [56] also performed undrained creep tests in which a constant temperature was maintained and during which a transient temperature state consisting of two full cycles was imposed. In these tests, four different (constant) values of deviator stress (30, 50, 70, and 90% of the failure stress under isothermal conditions) were maintained. Virdi and Keedwell [56] found that the magnitude of excess pore pressures generated in a specimen increased with temperature; when cooled, such pore pressures decreased. During temperature increases, the axial strain in the specimens increased. For specimens subjected to thermal cycling, such increases decreased with each cycle. When the temperature of a specimen was decreased, the axial strain did not decrease appreciably; this was particularly true at the higher deviator stress levels.

*6.2 Constant Strain Relaxation*

Constant strain relaxation tests attempt to duplicate the behavior of loaded soil masses whose dimensions in-situ remain essentially unchanged. Prime examples of such scenarios are problems involving soil-structure interaction in which the presence of the structure prevents excessive deformation of the soil mass, or in the case of objects penetrating into soil that are held stationary for some period of time (e.g., a cone penetration test held stationary while load and pore pressure changes are measured). In such problems, the reduction (relaxation) of stresses in the soil mass is of primary interest.

As noted by Mashayekhi [10], "data concerning the effect of temperature on constant strain stress relaxation is quite scarce". Indeed, the only extensive experimental study of this subject was that performed by and Murayama and Shibata [29]. In this study, stress relaxation tests were performed in axisymmetric triaxial compression under undrained conditions. Based on the results of such tests, Murayama and Shibata [29] found that, during relaxation, the deviator stress decreased linearly with the logarithm of time and approached a non-zero limiting value. The results of these tests also showed that three initials as well as the fully relaxed levels of deviator stress decrease with increases in temperature.

*6.3 Strain-Rate Effects*

As in the case of constant stress creep, there have been two primary bodies of work performed for this subject. First are *undrained* shear tests using axisymmetric triaxial, direct simple shear, or other devices in which a shear stress can be applied to a specimen. Secondly are *drained* one-dimensional consolidation tests using either calculated strain rates in conventional, incrementally loaded consolidation tests or in the constant rate of strain consolidation test. Unfortunately, to date no systematic studies of the effect that temperature changes have on the behavior of saturated cohesive soils subjected to different rates of loading have been performed. In such studies, the THM behavior of saturated cohesive soils is a function of not only stress, strain, and temperature, but also of the strain-rate.

## 7. Discussion

This article presented a comprehensive overview of the macroscopically observed thermo-hydro-mechanical behavior of saturated cohesive soils. Several findings related this behavior are noteworthy. These are summarized below.

Based on the results of several experimental studies, it appears that clay *minerology* assumes importance in determining the temperature dependence of the liquid limit ($w_L$). Due to the subjective nature of the plastic limit test, no definitive conclusions have been reached regarding its temperature dependence.

The effect of temperature on $w_L$ is explained by the fact that mineralogy is intimately related to the specific surface associated with a particular clay mineral [6], [7]. In kaolinites, which have the lowest specific surface among clay minerals, the adsorbed water layer is relatively thin and the interparticle bonding would thus be realized mostly through solid bonds. When heated, kaolinite particles lose some of the adsorbed water and the interparticle forces are influenced by sundry physicochemical effects that cause some of the bonds to break. This results in, at most, a slight reduction in $w_L$. In smectites, which possess the largest specific surface among clay minerals, the adsorbed water layers are relatively thick. Since experimental results indicate that the heating of smectite-rich soils causes $w_L$ to increase, this implies that heating has caused an increase in the thickness of the adsorbed water layer. This, however, contradicts the observation [6] that changes in temperature have only a negligible on the thickness of the diffuse double layer. Clearly, additional research regarding the temperature dependence of $w_L$ is warranted.

The thermal response of saturated cohesive soils is affected by the soil type and, in the case of clays, by the minerology of the soil. Consequently, for heating under drained conditions, higher volume change will be observed for soils with higher plasticity indices. For heating under undrained conditions, higher excess pore pressures will be observed in such soils.

Based on the results of a somewhat limited number of experimental studies, temperature increases reduce the magnitude of elastic moduli. There is also general consensus that the extent of the elastic domain for a saturated cohesive soil decreases with increases in temperature.

A general consensus has not been reached regarding the effect of temperature on the shear strength of saturated cohesive soils. The strength of such soils can increase or decrease with changes in temperature. In certain cases, however, the shear strength appears to be unaffected by temperature changes. It is the feeling of some researchers [90] that this apparent confusion is attributed to the lack of consideration of the thermal and mechanical history of the soil prior to failure. This notwithstanding, clearly, this subject requires additional experimental investigation.

The effect that temperature increases have on the internal friction angle is rather inconclusive. For NC clays, temperature changes have little effect on the effective friction angle, at least for values lower than about 50ºC [46]. Depending on the specific conditions maintained during a test, increases in temperature can cause the magnitude of the friction angle at critical state either to slightly increase or to decrease.

Anisotropy does not appear to be induced in saturated cohesive soils by temperature increases, though pertinent experimental results are relatively scarce. Increases in temperature can reduce the degree of anisotropy in such soils.

In normally consolidated saturated cohesive soils subjected to temperature increases under drained conditions, the resulting reduction in void ratio appears to be independent of the stress state. The magnitude of this reduction depends on the predominant clay mineral present in the soil, as well as its moisture content.

Based on the available experimental results, there does not appear to be consensus regarding the effect of temperature increases on the values of the compression index $C_c$ and on the swell/re-compression index $C_r$. Except for very low confining stresses, the value of $C_c$ appears to be temperature independent. If it is measured from the re-compression portion of the void ratio versus logarithm of stress plot, the value of $C_r$ will likewise be essentially independent of temperature.

The effective preconsolidation stress ($\sigma'_p$) is affected by changes in temperature. Increases in temperature cause to $\sigma'_p$ to decrease. The rate of this decrease appears to a function of the material characteristics of the saturated cohesive soil.

Based on the results of several experimental studies, the excess pore pressures generated under undrained conditions by temperature increases depend on the magnitude of the applied temperature increment, on the stress state in the soil, and on the magnitudes of the thermal expansion coefficients for the fluid and solid phases.

During undrained heating, positive excess pore pressures are generated in normally consolidated specimens. The magnitude of such pore pressures decreases with increasing degree of overconsolidation.

When specimens are cooled under undrained conditions, the excess pore pressures decrease. In normally consolidated specimens, temperature cycles produce irreversible changes in excess pore pressure. In overconsolidated specimens, such pore pressures appear to be reversible.

Experimental investigations of temperature cycling under undrained conditions seem to indicate that the resulting changes in excess pore pressure are irreversible, thus implying that effective stresses will likewise be affected. During such thermal cycling, hysteresis loops shall be formed, though necessarily during the first cycle. In addition, the amount of residual excess pore pressure that is generated seems to decrease with the number of cycles, for the soil is becoming increasingly overconsolidated.

In constant stress creep tests performed on normally consolidated and on lightly overconsolidated cohesive soils, increases in temperature result in increased axial strain rates and increased excess pore pressures.

## Acknowledgments

## References

[1]  S. Sorrell, "Reducing energy demand: A review of issues, challenges and approaches," *Renewable and Sustainable Energy Reviews*, vol. 47, pp. 74–82, 2015, doi: 10.1016/j.rser.2015.03.002.

[2]  I. B. Fridleifsson, "Geothermal energy for the benefit of the people," *Renewable and Sustainable Energy Reviews*, vol. 5, no. 3, pp. 299–312, Sep. 2001, doi: 10.1016/S1364-0321(01)00002-8.

[3]  S. Kavanaugh and K. Rafferty, *Geothermal heating and cooling: design of ground-source heat pump systems*, vol. 1. Peachtree Corners, Georgia: ASHRAE, 2015.

[4]  J. W. Tester *et al.*, *The Future of Geothermal Energy - Impact of Enhanced Geothermal Systems (EGS) on the United States in the 21st Century*. Cambridge: Massachusetts Institute of Technology, 2006.

[5]  H. Brandl, "Energy foundations and other thermo-active ground structures," *Géotechnique*, vol. 56, no. 2, pp. 81–122, Mar. 2006, doi: 10.1680/geot.2006.56.2.81.

[6]  J. K. Mitchell, *Fundamentals of Soil Behavior*. New York: J. Wiley & Sons, 1976.

[7]  R. V. Whitman and T. W. Lambe, *Soil Mechanics, SI Version*. New York: J. Wiley & Sons, 1979.

[8]  I. Th. Rosenqvist, "Physico-Chemical Properties of Soils: Soil-Water Systems," *Journal of the Soil Mechanics and Foundations Division*, vol. 85, no. 2, pp. 31–53, Feb. 1959, doi: 10.1061/JSFEAQ.0000189.

[9]  V. N. Kaliakin, M. Mashayekhi, and A. Nieto-Leal, "The time- and temperature-related behavior of clays: Microscopic considerations and macroscopic modeling," in *Clays and Clay Minerals: Geological Origin, Mechanical Properties and Industrial Applications*, L. R. Wesley, Ed., New York: Nova Publishers, 2014, pp. 1–44.

[10]  M. Mashayekhi, "Modeling the Temperature-Dependent Response of Saturated Cohesive Soils in a Generalized Bounding Surface Framework," PhD dissertation, University of Delaware, Delaware, 2018.

[11]  R. F. Scott, *Principles of Soil Mechanics*. Reading, MA: Addison-Wesley Publishing Co., 1963.

[12]  J. K. Mitchell and K. Soga, *Fundamentals of Soil Behavior*, 3rd ed. New York: J. Wiley & Sons, 2005.

[13]  J. G. Laguros, "Effect of Temperature on Some Engineering Properties of Clay Soils," in *Proceedings of International Conference on the Effects of Temperature and Heat on Engineering Behaviour of Soils: Highway Research Board, National Research Council, Special Report 103*, J. K. Mitchell, Ed., Washington, D.C., 1969, pp. 186–193.

[14]  P. Ctori, "The effects of temperature on the physical properties of cohesive soil," *Ground engineering*, vol. 22, no. 5, pp. 26–27, 1989.

[15]  G. E. H. Ballard and W. G. Weeks, "The human factor in determining the plastic limit of cohesive soils," *Materials Research and Standards*, vol. 3, no. 9, pp. 726–729, 1963.

[16]  T. K. Liu and T. M. Thornburn, "Study of the reproducibility of Atterberg Limits," *Highway Research Record*, vol. 63, pp. 22–30, 1964.

[17]  C. P. Wroth and D. M. Wood, "The correlation of index properties with some basic engineering properties of soils," *Canadian Geotechnical Journal*, vol. 15, no. 2, pp. 137–145, May 1978, doi: 10.1139/t78-014.

[18] G. T. Houlsby, "Theoretical analysis of the fall cone test," *Géotechnique*, vol. 32, no. 2, pp. 111–118, Jun. 1982, doi: 10.1680/geot.1982.32.2.111.

[19] M. S. Youssef, A. Sabry, and A. H. El Ramli, "Temperature Changes and their Effects on Some Physical Properties of Soils," in *Proceedings of the 5th ICSMFE*, Paris, France, 1961, pp. 419–421.

[20] H. Wohlbier and D. Henning, "Effect of preliminary heat treatment on the shear strength of kaolinite clay," in *Proceedings of International Conference on the Effects of Temperature and Heat on Engineering Behaviour of Soils: Highway Research Board, National Research Council, Special Report 103*, J. K. Mitchell, Ed., Washington, D.C., 1969, pp. 287–300.

[21] J. K. Mitchell, "Temperature Effects on the Engineering Properties and Behavior of Soils," in *Proceedings of International Conference on the Effects of Temperature and Heat on Engineering Behaviour of Soils: Highway Research Board, National Research Council, Special Report 103*, J. K. Mitchell, Ed., Washington, D.C., 1969, pp. 9–28.

[22] T. Tippet, "An investigation into the effect of temperature upon the Atterberg Limits and mechanical properties of cohesive soils," Undergraduate Project Report, Lanchester Polytechnic, Coventry, U.K., 1976.

[23] J. H. Reifer, "The effect of temperature and mineralogy upon the Atterberg Limits and mechanical properties of cohesive soils," Undergraduate Project Report, Lanchester Polytechnic, Coventry, U.K., 1977.

[24] M. Wang, J. Benway, and A. Arayssi, "The Effect of Heating on Engineering Properties of Clays," in *Physico-Chemical Aspects of Soil and Related Materials*, ASTM International100 Barr Harbor Drive, PO Box C700, West Conshohocken, PA 19428-2959, 1990, pp. 139–158. doi: 10.1520/STP23553S.

[25] I. Towhata, P. Kuntiwattanakul, and H. Kobayashi, "A Preliminary Study on Heating of Clays to Examine Possible Effects of Temperature on Soil-Mechanical Properties," *Soils and Foundations*, vol. 33, no. 4, pp. 184–190, Dec. 1993, doi: 10.3208/sandf1972.33.4_184.

[26] I. Jefferson and C. D. Foss Rogers, "Liquid limit and the temperature sensitivity of clays," *Eng Geol*, vol. 49, no. 2, pp. 95–109, Mar. 1998, doi: 10.1016/S0013-7952(97)00077-X.

[27] B. O. Hardin and W. L. Black, "Closure to 'Vibration Modulus of Normally Consolidated Clay,'" *Journal of the Soil Mechanics and Foundations Division*, vol. 95, no. 6, pp. 1531–1537, Nov. 1969, doi: 10.1061/JSFEAQ.0001364.

[28] F. Tatsuoka, T. Uchimura, K. Hayano, J. Koseki, H. Di Benedetto, and M. S. A. Siddiquee, "Time-dependent deformation characteristics of stiff geomaterials in engineering practice," in *Proceedings of the Second International Symposium on Pre-Failure Deformation Characteristics of Geomaterials*, Amsterdam: Balkema, 1999, pp. 1161–1262.

[29] S. Murayama and T. Shibata, "Rheological Properties of Clays," in *Proceedings of the 5th International Conference on Soil Mechanics and Foundation Engineering*, Paris, France, 1961, pp. 269–273.

[30] S. Murayama, "Effect of Temperature on Elasticity of Clays," in *Proceedings of International Conference on the Effects of Temperature and Heat on Engineering Behaviour of Soils: Highway Research Board, National Research Council, Special Report 103*, J. K. Mitchell, Ed., Washington, D.C., 1969, pp. 194–203.

[31] T. W. Lambe, "The Structure of Compacted Clays," *Journal of the Soil Mechanics and Foundations Division*, vol. 84, no. 2, pp. 1–34, May 1958, doi: 10.1061/JSFEAQ.0000114.

[32] L. G. Eriksson, "Temperature effects on consolidation properties of sulphide clays," in *Proceedings of the International Conference on Soil Mechanics and Foundation Engineering*, Rio De Janeiro: Taylor & Francis, 1989, pp. 2087–2090.

[33] M. Tidfors and G. Sällfors, "Temperature Effect on Preconsolidation Pressure," *Geotechnical Testing Journal*, vol. 12, no. 1, pp. 93–97, Mar. 1989, doi: 10.1520/GTJ10679J.

[34] T. Hueckel and G. Baldi, "Thermoplasticity of Saturated Clays: Experimental Constitutive Study," *Journal of Geotechnical Engineering*, vol. 116, no. 12, pp. 1778–1796, Dec. 1990, doi: 10.1061/(ASCE)0733-9410(1990)116:12(1778).

[35] C. A. Hogentogler and E. A. Willis, "Stabilized Soil Roads," *Public Roads*, vol. 17, no. 3, pp. 45–65.

[36] I. Th. Rosenqvist, "Investigations in the Clay-Electrolyte-Water System," *Norwegian Geotechnical Institute, Publication*, no. 9, pp. 1–125, 1955.

[37] P. D. Trask and J. E. H. Close, "Effect of Clay Content on Strength of Soils," *Coastal Engineering Proceedings*, no. 6, p. 50, Jan. 1957, doi: 10.9753/icce.v6.50.

[38] G. A. Leonards, "Discussion of 'Leonards on Compacted Clay,'" *Transactions of the American Society of Civil Engineers*, vol. 125, no. 1, pp. 709–712, Jan. 1960, doi: 10.1061/TACEAT.0007847.

[39] C. C. Ladd, "Physico-Chemical Analysis of the Shear Strength of Saturated Clays," ScD dissertation, Massachusetts Institute of Technology, Cambridge, MA, 1961.

[40] J. K. Mitchell, "Shearing Resistance of Soils as a Rate Process," *Journal of the Soil Mechanics and Foundations Division*, vol. 90, no. 1, pp. 29–61, Jan. 1964, doi: 10.1061/JSFEAQ.0000593.

[41] J. M. Duncan and R. G. Campanella, *The effect of temperature changes during undrained tests*. Berkeley: Soil Mechanics and Bituminous Materials Laboratory, University of California, 1965.

[42] R. G. Campanella and J. K. Mitchell, "Influence of Temperature Variations on Soil Behavior," *Journal of the Soil Mechanics and Foundations Division*, vol. 94, no. 3, pp. 709–734, May 1968, doi: 10.1061/JSFEAQ.0001136.

[43] C. A. Noble and T. Demirel, "Effect of Temperature on the Strength Behavior of Cohesive Soil," in *Proceedings of International Conference on the Effects of Temperature and Heat on Engineering Behaviour of Soils: Highway Research Board, National Research Council, Special Report 103*, J. K. Mitchell, Ed., Washington, D.C., 1969, pp. 204–219.

[44] M. A. Sherif and Burrous C.M., "Temperature Effects on the Unconfined Shear Strength of Saturated, Cohesive Soil," in *Proceedings of International Conference on the Effects of Temperature and Heat on Engineering Behaviour of Soils: Highway Research Board, National Research Council, Special Report 103*, J. K. Mitchell, Ed., Washington, D.C., 1969, pp. 267–272.

[45] S. L. Houston, W. N. Houston, and N. D. Williams, "Thermo-Mechanical Behavior of Seafloor Sediments," *Journal of Geotechnical Engineering*, vol. 111, no. 11, pp. 1249–1263, Nov. 1985, doi: 10.1061/(ASCE)0733-9410(1985)111:11(1249).

[46] S. Leroueil and M. E. S. Marques, "State of the Art: Importance of Strain Rate and Temperature Effects in Geotechnical Engineering," in *Measuring and modeling time dependent soil behavior: Geotechnical Special Publication No. 61*, T. C. Sheahan and V. N. Kaliakin, Eds., ASCE, 1996, pp. 1–60.

[47] A. Casagrande and N. Carillo, "Shear failure of anisotropic materials," *Proceedings of the Boston Society of Civil Engineers*, vol. 31, no. 4, pp. 74–87, 1944.

[48] F. Tavenas and S. Leroueil, "Effects of Stress and Time on Yielding of Clays," in *Proceedings of the 9th ICSMFE*, Tokyo, 1977, pp. 319–326.

[49] V. N. Kaliakin, "Anisotropic Elasticity for Soils: A Synthesis of Some Key Issues," *BULLETIN of L.N. Gumilyov Eurasian National University. Technical Science and Technology Series*, vol. 127, no. 2, pp. 49–63, 2019, doi: 10.32523/2616-7263-2019-127-2-49-63.

[50] Y. F. Dafalias, "On elastoplastic-viscoplastic constitutive modelling of cohesive soils," in *Geomechanical Modelling in Engineering Practice*, R. Dungar and J. R. Studer, Eds., Amsterdam: Balkema, 1986, ch. 13, pp. 313–330.

[51] T. Hueckel and R. Pellegrini, "A note on thermomechanical anisotropy of clays," *Eng Geol*, vol. 41, no. 1–4, pp. 171–180, Jan. 1996, doi: 10.1016/0013-7952(95)00050-X.

[52] G. Baldi, T. Hueckel, A. Peano, and R. Pellegrini, "Developments in modelling of thermo-hydro-geomechanical behaviour of boom clay and clay-based buffer materials," *Report EUR 13365, Commission of the European Communities, Nuclear science and technology*, vol. 1, p. 134, 1991.

[53] C. Del Olmo, V. Fioravante, F. Gera, T. Hueckel, J. C. Mayor, and R. Pellegrini, "Thermomechanical properties of deep argillaceous formations," *Eng Geol*, vol. 41, no. 1–4, pp. 87–102, Jan. 1996, doi: 10.1016/0013-7952(95)00048-8.

[54] R. T. Martin and C. C. Ladd, "Fabric of Consolidated Kaolinite," *Clays Clay Miner*, vol. 23, no. 1, pp. 17–25, Feb. 1975, doi: 10.1346/CCMN.1975.0230103.

[55] R. J. Mitchell, "Some deviations from isotropy in a lightly overconsolidated clay," *Géotechnique*, vol. 22, no. 3, pp. 459–467, Sep. 1972, doi: 10.1680/geot.1972.22.3.459.

[56] S. P. S. Virdi and M. J. Keedwell, "Some observed effects of temperature variation on soil behaviour," in *International Conference on Rheology and Soil Mechanics*, M. J. Keedwell, Ed., London: Elsevier, 1988, pp. 336–354. doi: 10.1016/0148-9062(90)92838-6.

[57] C. J. Russell Coccia and J. S. McCartney, "A Thermo-Hydro-Mechanical True Triaxial Cell for Evaluation of the Impact of Anisotropy on Thermally Induced Volume Changes in Soils," *Geotechnical Testing Journal*, vol. 35, no. 2, pp. 227–237, Mar. 2012, doi: 10.1520/GTJ103803.

[58] H. Gray, "Progress Report on Research on the Consolidation of Fine-Grained Soils," in *Proceedings of the 1st ICSMFE*, Cambridge, MA, 1936, pp. 138–141.

[59] R. D. Charles, "Volume Changes in Isotropically Consolidated Soils Induced by Temperature Cycling," Master's thesis, University of Delaware, Delaware, 1988.

[60] K. R. Demars and R. D. Charles, "Soil volume changes induced by temperature cycling," *Canadian Geotechnical Journal*, vol. 19, no. 2, pp. 188–194, May 1982, doi: 10.1139/t82-021.

[61] G. Baldi, T. Hueckel, and R. Pellegrini, "Thermal volume changes of the mineral–water system in low-porosity clay soils," *Canadian Geotechnical Journal*, vol. 25, no. 4, pp. 807–825, Nov. 1988, doi: 10.1139/t88-089.

[62] R. G. Campanella, "Effect of Temperature and Stress on the Time-Deformation Behavior of Clays," PhD dissertation, University of California, Berkeley, 1965.

[63] R. L. Plum and M. I. Esrig, "Some Temperature Effects on Soil Compressibility and Pore Water Pressure," in *Proceedings of International Conference on the Effects of Temperature and Heat on Engineering Behaviour of Soils: Highway Research Board, National Research Council, Special Report 103*, J. K. Mitchell, Ed., Washington, D.C., 1969, pp. 231–242.

[64] I. Towhata, P. Kuntiwattanaku, I. Seko, and K. Ohishi, "Volume Change of Clays Induced by Heating as Observed in Consolidation Tests," *Soils and Foundations*, vol. 33, no. 4, pp. 170–183, Dec. 1993, doi: 10.3208/sandf1972.33.4_170.

[65] H. M. Abuel-Naga, D. T. Bergado, G. V. Ramana, L. Grino, P. Rujivipat, and Y. Thet, "Experimental Evaluation of Engineering Behavior of Soft Bangkok Clay under Elevated Temperature," *Journal of Geotechnical and*

*Geoenvironmental Engineering*, vol. 132, no. 7, pp. 902–910, Jul. 2006, doi: 10.1061/(ASCE)1090-0241(2006)132:7(902).

[66] R. E. Paaswell, "Temperature Effects on Clay Soil Consolidation," *Journal of the Soil Mechanics and Foundations Division*, vol. 93, no. 3, pp. 9–22, May 1967, doi: 10.1061/JSFEAQ.0000982.

[67] H. M. Abuel-Naga, D. T. Bergado, and B. F. Lim, "Effect of Temperature on Shear Strength and Yielding Behavior of Soft Bangkok Clay," *Soils and Foundations*, vol. 47, no. 3, pp. 423–436, Jun. 2007, doi: 10.3208/sandf.47.423.

[68] F. N. Finn, "The Effect of Temperature on the Consolidation Characteristics of Remolded Clay," in *Symposium on Consolidation Testing of Soils*, ASTM, 1952, pp. 65–71. doi: 10.1520/STP48297S.

[69] K. Habibaghi, "Influence of Temperature on Consolidation Behavior of Remolded Organic Paulding and Inorganic Paulding Soils," PhD dissertation, University of Illinois, Urbana, IL, 1969.

[70] K. Habibaghi, "Temperature effect on consolidation behaviour of overconsolidated soils," in *Proceedings of the 8th ICSMFE*, Moscow, USSR, 1973, pp. 159–163. doi: 10.1016/0148-9062(75)91842-2.

[71] S. Burghignoli, A., Desideri, A., & Miliziano, "Deformability of clays under non isothermal conditions," *Revista Italiana di Geotecnica*, vol. 25, no. 4, pp. 227–236, 1992.

[72] N. E. Simons, "Consolidation Investigation on Undisturbed Fornebu Clay," *Norwegian Geotechnical Institute Publication*, pp. 1–9, 1965.

[73] N. Tanaka, "Thermal elastic plastic behaviour and modelling of saturated clays," PhD dissertation, University of Manitoba, Winnipeg, Canada, 1995.

[74] C. Cekerevac and L. Laloui, "Experimental study of thermal effects on the mechanical behaviour of a clay," *Int J Numer Anal Methods Geomech*, vol. 28, no. 3, pp. 209–228, Mar. 2004, doi: 10.1002/nag.332.

[75] A. Burghignoli, A. Desideri, and S. Miliziano, "A laboratory study on the thermomechanical behaviour of clayey soils," *Canadian Geotechnical Journal*, vol. 37, no. 4, pp. 764–780, Aug. 2000, doi: 10.1139/t00-010.

[76] A. Sridharan and M. S. Jayadeva, "Double layer theory and compressibility of clays," *Géotechnique*, vol. 32, no. 2, pp. 133–144, Jun. 1982, doi: 10.1680/geot.1982.32.2.133.

[77] J. Graham, N. Tanaka, T. Crilly, and M. Alfaro, "Modified Cam-Clay modelling of temperature effects in clays," *Canadian Geotechnical Journal*, vol. 38, no. 3, pp. 608–621, 2001, doi: 10.1139/cgj-38-3-608.

[78] A. Burghignoli and A. Desideri, "Influenza della temperature sulla compressibilitia delle argille," in *Gruppo Nazionale di Coodinamento per gli Studi di Ingegneria Geotecnica*, Monselice, 1988, pp. 193–206.

[79] M. Boudali, S. Leroueil, and B. R. S. Murthy, "Viscous behaviour of natural soft clays," in *Proceedings of the 13th ICSMFE*, New Delhi, 1994, pp. 411–416.

[80] L. Moritz, "Geotechnical Properties of Clay at Elevated Temperatures," in *International Symposium on Compression and Consolidation of Clayey Soils - IS-Hiroshima 95*, Y. Hiroshi and O. Kusakabe, Eds., Amsterdam: Balkema, 1995, pp. 267–272.

[81] J. K. Mitchell and R. G. Campanella, "Creep Studies on Saturated Clays," in *ASTM-NRC Symposium on Laboratory Shear Testing of Soils, Special Technical Publication ASTM 361*, Ottawa, Canada: ASTM, 1964, pp. 90–103. doi: 10.1520/STP29986S.

[82] J. K. Mitchell, R. G. Campanella, and A. Singh, "Soil Creep As A Rate Process," *Journal of the Soil Mechanics and Foundations Division*, vol. 94, no. 1, pp. 231–253, Jan. 1968, doi: 10.1061/JSFEAQ.0001085.

[83] H. B. Seed, J. K. Mitchell, and C. K. Chan, "The Strength of Compacted Cohesive Soils," in *Proceedings of the ASCE Research Conference on the Shear Strength of Cohesive Soils*, Boulder, CO, 1960, pp. 877–964.

[84] V. A. Sowa, "A Comparison of the Effects of Isotropic and Anisotropic Consolidation on the Shear Behavior of a Clay," PhD dissertation, University of London, UK, 1963.

[85] D. J. Henkel and V. A. Sowa, "Discussion on Symposium on Laboratory Shear Testing of Soils," in *ASTM-NRC Symposium on Laboratory Shear Testing of Soils*, 1964.

[86] D. A. Sangrey, "The Behavior of Soils Subjected to Repeated Loading," PhD dissertation, Cornell University, Ithaca, NY, 1968.

[87] V. N. Kaliakin, "Bounding Surface Elastoplasticity-Viscoplasticity for Clays," PhD dissertation, University of California, Davis, 1985.

[88] K. Y. Lo, "Secondary Compression of Clays," *Journal of Soil Mechanics and Foundation Division*, vol. 87, no. SM4, pp. 61–88, 1961.

[89] R. L. Schiffman, C. C. Ladd, and A. T. Chen, "Secondary Consolidation of Clay," in *Proceedings of the Rheology and Soil Mechanics Symposium, IUTAM*, J. Kravtchenko and P. M. Sirieys, Eds., Springer-Verlag, 1966, pp. 273–304.

[90] T. Hueckel, B. François, and L. Laloui, "Explaining thermal failure in saturated clays," *Géotechnique*, vol. 59, no. 3, pp. 197–212, Apr. 2009, doi: 10.1680/geot.2009.59.3.197.

**Information about authors:**

*Victor N. Kaliakin* – PhD, Professor, Department of Civil, Construction, and Environmental Engineering, University of Delaware, Newark, Delaware, U.S.A., kaliakin@udel.edu

*Meysam Mashayekhi* – PhD, Assistant Professor, Department of Civil Engineering, University of Isfahan, Isfahan, 81744-73441, Iran, m.mashayekhi@cet.ui.ac.ir

**Author Contributions:**
*Victor N. Kaliakin* – data collection, interpretation, editing.
*Meysam Mashayekhi* – data collection, drafting, editing.

**Conflict of Interest:** The authors declare no conflict of interest.

**Use of Artificial Intelligence (AI):** The authors declare that AI was not used.

*Article*

# Rehabilitation of lengthy sewer pipelines by polymer-composite CIPP

Yerbol Zhumagaliyev, Assel Mukhamejanova, Akmaral Yeleussinova, Dana Bakirova, Aizhan Baketova*, Alizhan Kazkeyev, Tymarkul Muzdybayeva

[1]Department of Civil Engineering, L.N. Gumilyov Eurasian National University, Astana, Kazakhstan
*Correspondence: baketovaaizhan@mail.ru

**Abstract.** This study examines the feasibility of Cured-in-Place Pipe (CIPP) technology for trenchless rehabilitation of aging sewer pipelines, addressing the severe deterioration of Karaganda's sewer networks. A 3 km section was inspected using CCTV, ultrasonic, and shock-pulse methods to assess pipeline conditions, revealing structural defects with depreciation levels reaching 70-100%. The CIPP method was successfully applied to restore the integrity of 2.6 km pipelines while minimizing excavation, stabilizing the average flow rates and velocity of 0.8-1.2 m pipelines at 710 liter/s and 1.2 m/s, respectively. Hydraulic analysis confirmed that rehabilitated pipelines maintained sufficient flow velocity for self-cleaning and increased capacity, reducing blockage risks. The findings demonstrate that CIPP is a sustainable alternative to pipeline replacement, offering a viable solution for long-length sewer rehabilitation and supporting strategic urban infrastructure renewal.
**Keywords:** sewerage, rehabilitation, CIPP, ultraviolet curing, CCTV.

## 1. Introduction

Water is a key element of sustainable development, directly affecting life on Earth. As urban populations grow, urban functioning will depend on water management and water-related risks will be concentrated in cities [1]. Urban development increases impervious surfaces, intensifying the load on sewer systems through greater stormwater volume [2]. Sewer networks play an important role in protecting health and the environment, but aging pipelines can lead to leaks and malfunctions, creating environmental and health risks [3]. In this regard, the sewerage systems in Kazakhstan face many problems that require comprehensive solutions [4]. The majority of these systems were built in the 60s and require significant investment in rehabilitation and modernization [5]. In particular, the deterioration rate of Karaganda sewer networks had already reached 80% by 2006 [6]. Obviously, these networks have become even more dilapidated in the nearly 20 years that have passed and have accumulated so much stagnant household waste that they need either complete replacement or unconventional treatment approaches. Since the traditional systems, even pressurized ones [7], may not be able to handle the flushing of stagnation. Besides the friction of even small stagnations may disturb flow rate and quickly increase in size with clinging sludge and debris. Therefore, Karaganda sewer networks should be urgently inspected and rehabilitated using modern techniques considering the length of exhausted sections, to help reduce the risks and costs associated with their failure.

[25] presents a detailed analysis of design and rehabilitation methods for underground pipelines, including modern remediation technologies. The main attention is paid to engineering calculations and design, while rehabilitation issues are considered only superficially. The work does not fully take into account the complex mechanical stresses arising in real operating conditions. [8] reviews the various trenchless technologies used for pipeline repair and replacement, with a focus on modern remediation methods. The authors emphasize the reduced urban environmental impacts of trenchless methods, but the study does not analyze secondary effects. In particular, changes in soil permeability

can lead to land subsidence and localized increases in groundwater levels, which can have long-term consequences for the stability of buildings and utility infrastructure. [9] provides a comparative analysis of existing pipeline rehabilitation methods. However, this study does not include large-scale field tests with long-term monitoring of the condition of the rehabilitated pipes. This may lead to errors in predicting their operational durability since laboratory tests and theoretical models do not always reflect real operating conditions. [10] compares conventional (excavation) and trenchless technologies for the rehabilitation of sewer networks in terms of their carbon footprint. The study shows that trenchless methods reduce $CO_2$ emissions by 59.2% compared to excavation. However, the experimental data are derived from the example of the historical center of Brno, Czech Republic, where the infrastructure and building materials may differ significantly from other regions. Consequently, the results may vary in modern areas with different soil types, building densities, and hydrogeological conditions. [11] presented an innovative approach to trenchless rehabilitation of underground pipes using vacuum transfer molding of a resin combined with a fiberglass fabric blank. However, fiberglass composites can lose mechanical properties at high temperatures and cracks may appear in lower temperatures.

The considered studies make a significant contribution to the development of trenchless pipeline rehabilitation technologies but the solutions they propose appear costly, labor-intensive, and time-consuming making them unsuitable for the long-length exhausted pipelines of Karaganda sewer networks. To overcome these shortcomings, this study considers the adoption of Cured-in-place pipe (CIPP) technology [12] for trenchless rehabilitation. Since it enables pipeline restoration without replacement while minimizing associated costs [13]. The CIPP is poorly examined in local conditions due to its recency in the region. Therefore, this study aims to assess its performance for the long-length sewer pipelines of Karaganda.

## 2. Methods

The study area is represented by 3 km of sewerage pipelines located in the residential zone of Maikuduk in Karaganda, Kazakhstan, passing under the streets of Maylina, Orken, and Tsetkin. Unfortunately, no archival data for the site survived, but it was assumed that the networks had already operated for over 50 years. The study area was inspected according to [14]. The inspection aimed to determine the types of pipes, their burial depth, dimensions, materials, and defects. Visual inspection was performed by accessing sewer manholes. The instrumental inspection incorporated a Closed-circuit television inspection (CCTV) [15], ultrasonic [16] and shock-pulse [17] methods. The cleaning and washing of pipelines from the debris was performed mechanically and hydrodynamically under pressure. The rehabilitation of pipelines was carried out by the trenchless method [18] using polymer-composite CIPPs "Berolina-HF-Liner" [19] with wall thicknesses of 9.2 and 10.2 mm (Figure 1).
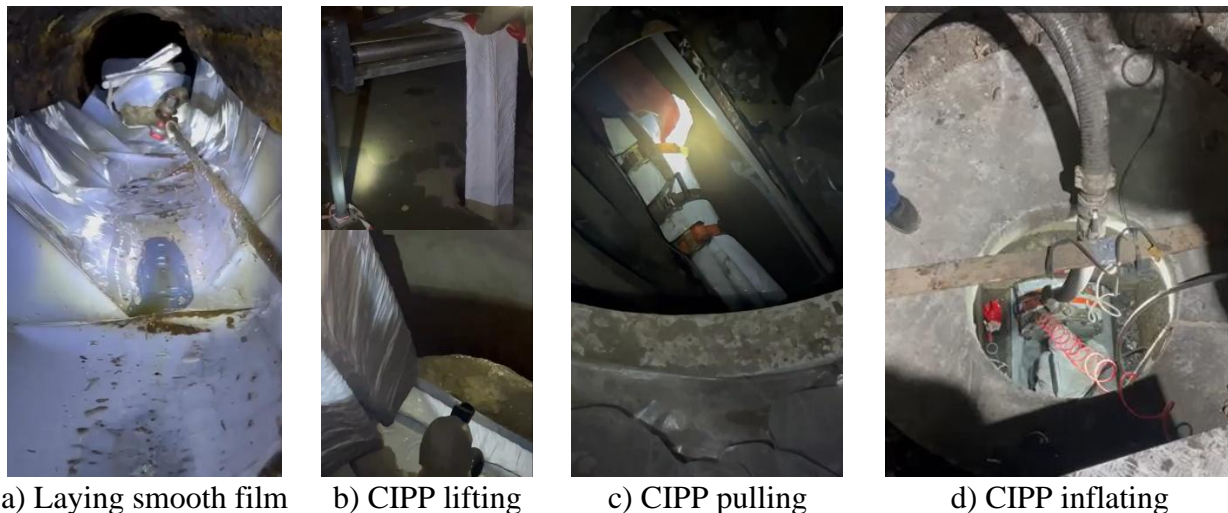


a) Laying smooth film   b) CIPP lifting   c) CIPP pulling   d) CIPP inflating
Figure 1 – Installation of polymer-composite CIPPs

Each CIPP was lifted through the manholes (Figure 1b) and pulled through the pipe to the next manhole using a winch (Figure 1c). A smooth film was pre-laid to protect the CIPP against damages (Figure 1a). The molding of CIPPs was conducted pneumatically (Figure 1d). The epoxy resin adhesive was used to bond CIPPs with existing pipes. Curing of the adhesive was carried out utilizing ultraviolet emission [20]. The hydraulic calculation of newly erected CIPPs were carried out according to [21].

## 3. Results and Discussion

Inspection of the study area revealed they are gravity sewers and that their pipelines were erected by 8 m pipes made of reinforced concrete according to [22] and embedded in depths of 3.5-6.5 m from the ground surface corresponding to the elevations of 530-545.5 m above sea level. Depending on the condition of the pipelines, some parts of the pipelines were rehabilitated with trenchless CIPP, and the other parts with the excavation method (Figure 2).
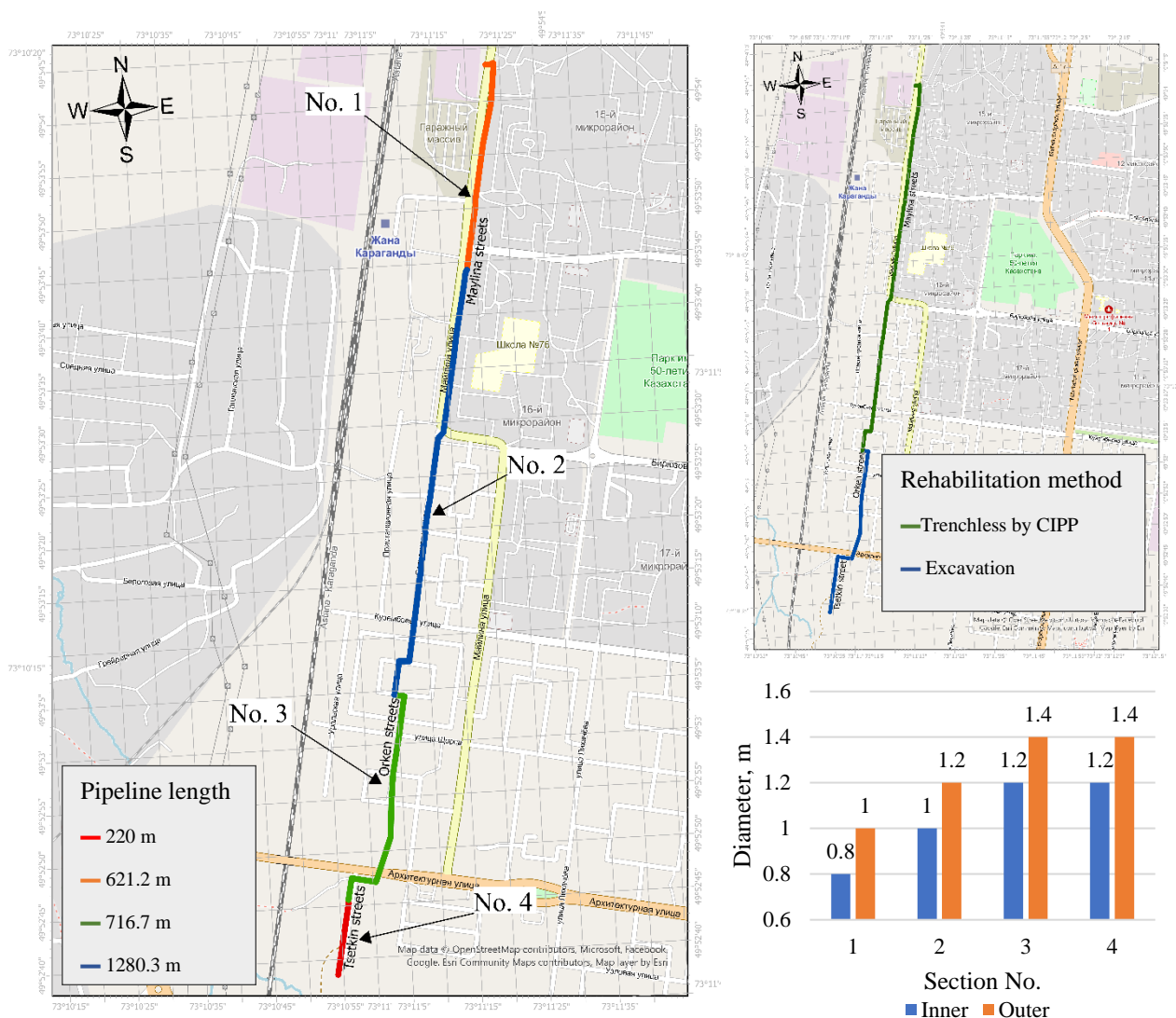


Figure 2 – Map of pipeline rehabilitation

Figure 2 above shows a rehabilitation map of pipelines, which are split into 4 sections and colored differently, with lengths of 621.2, 1280.3, 716.7, and 220.0 meters, respectively, altogether amounting to 2838.2 m, including 2618.2 m rehabilitated with the trenchless CIPP, and 220 m with the excavation method. It also shows the inner and outer diameters of the pipes, which range from 0.8 to 1.2 m for the inner diameter, and from 1.0 to 1.4 for the outer diameter.

Figure 2 below shows the results of instrumental inspection using the CCTV method.



Figure 2 – Pipelines condition before CIPP installation

As shown in Figure 4 above, the CCTV revealed and recorded distinct defects and debris in pipelines, which indicate their extensive deterioration, reduction in sewage flow rate, and expectance of failure. These issues include the cracking, splitting, and corrosion of pipe material, damage of reinforcement up to 70%, displacement of joints leading to groundwater infiltration, presence of silt and stagnations, coarse household wastes, and stones. The study revealed that the degree of depreciation of sections No. 1-3 of pipelines amounted to 70%. Section No. 4 of the pipelines encountered the worst damage with a deprecation degree of 100% indicating its unserviceability leading to soon subsidence of land above. Therefore, for this section, a decision was made to replace the pipes by excavation, which overcomes the [8] and [10] omissions.

The instrumental inspection by ultrasonic and shock-pulse methods revealed that the reinforced concrete elements of inspected pipes correspond to the strength class of B7.5. This indicates a fourfold loss of strength since it is supposed to be the class of B30 according to [22].

Figure 3 shows the reshoot images of CCTV representing the CIPP installation results after the careful treatment (cleaning and washing) of existing pipelines.
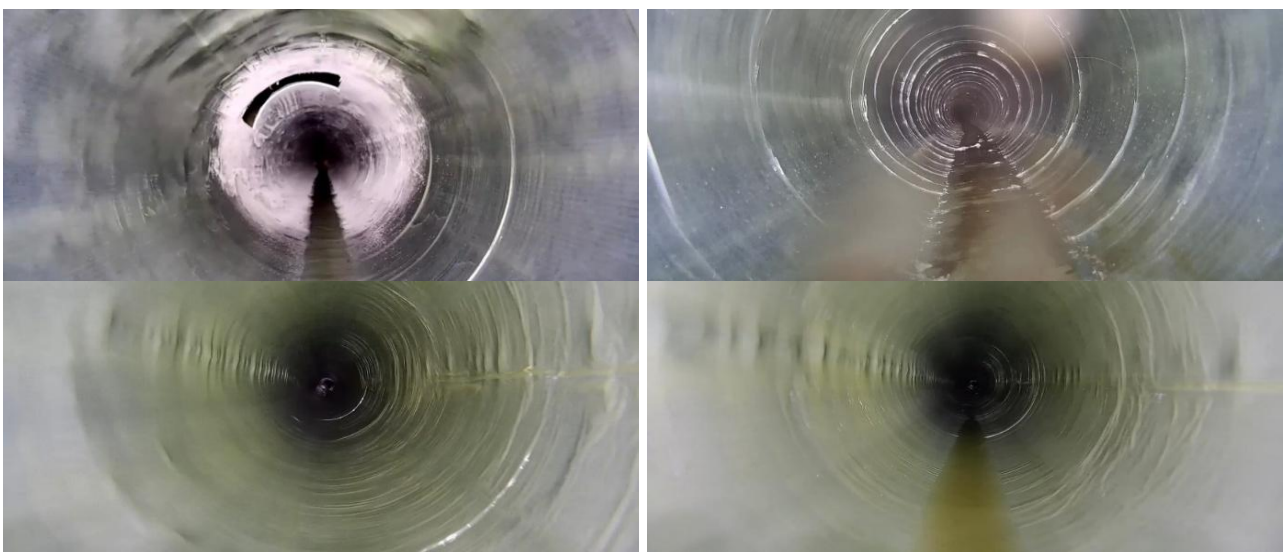


Figure 3 – Pipelines condition after CIPP installation

Figure 3 above clearly demonstrates how much the pipes were transformed after the cleaning, washing, and installation of CIPPs. It is possible to observe an increase in diameter, and consequently

stabilization of sewage flow. The post-installation CCTV images clearly show a significant improvement in the structural condition of the pipelines. The previously observed cracks, joint misalignments, and obstructions were eliminated after the cleaning and CIPP installation. The increase in pipeline smoothness is expected to enhance sewage flow and reduce the likelihood of further debris accumulation.

Figure 4 below presents the results of a hydraulic calculation for CIPPs of different diameters under sewage taking their 70%.
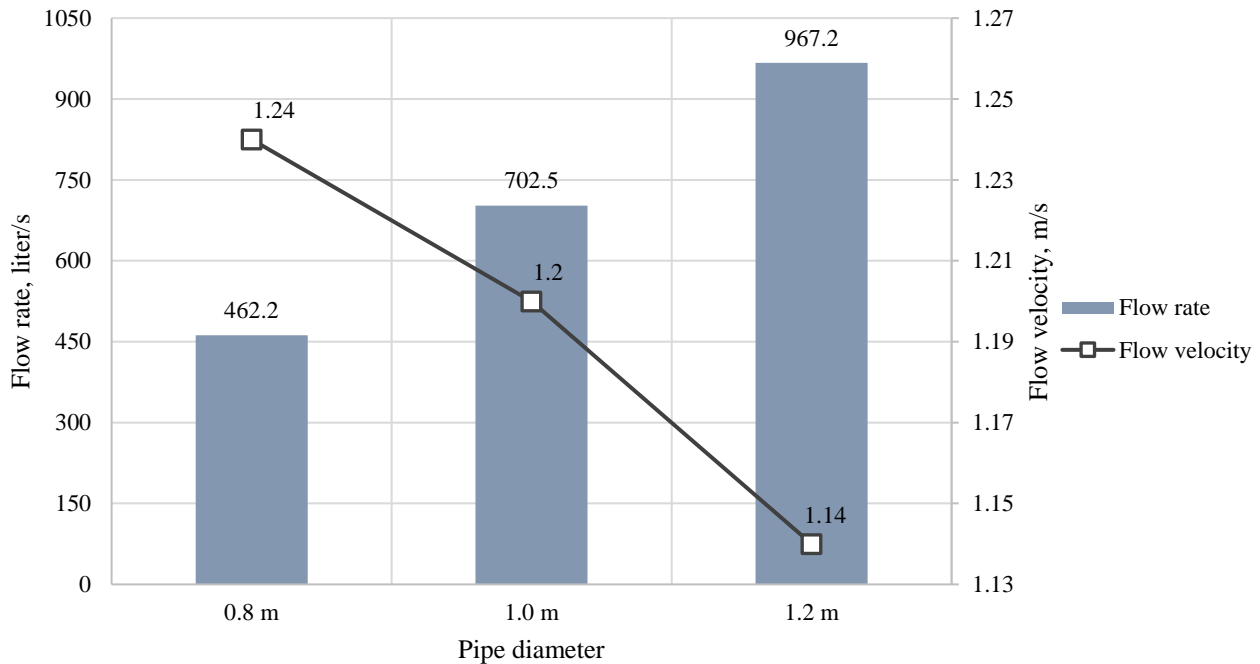


Figure 4 – Results of flow rate estimates

According to Figure 4 above, for a 0.8 m diameter pipe, the flow rate is 462.2 liter/s with a velocity of 1.24 m/s, for 1.0 m – 702.5 liter/s at 1.2 m/s, and 1.2 m – 967.2 liter/s at 1.14 m/s (710 liter/s and 1.2 m/s in average). A clear trend is observed: as the pipe diameter increases, the water flow rate rises, while the flow velocity decreases. This is explained by the fact that a larger diameter increases the cross-sectional area of the pipe, allowing a greater volume of water to pass through while simultaneously reducing the flow velocity under the same hydraulic conditions. These results suggest that the rehabilitated pipelines are better suited to handle peak flow conditions, minimizing risks of overflows and blockages.

## 4. Conclusions

The CIPP trenchless method effectively rehabilitates deteriorated sewer pipelines with a deprecation degree of up to 70%, restoring their structural integrity, improving sewage flow conditions, and minimizing excavation activities.

Based on the experience in Karaganda, the study confirms the feasibility of CIPP for long-length pipelines, providing a sustainable alternative to full pipeline replacement.

The hydraulic analysis demonstrates that rehabilitated pipelines with CIPP maintain sufficient flow velocity for self-cleaning while increasing flow capacity, reducing the risk of blockages, and improving long-term operational efficiency.

The study provides essential data on the types, materials, and condition of the 3 km sewer pipeline section in Karaganda, addressing the lack of archival records and offering a comprehensive assessment that supports future rehabilitation planning and maintenance strategies.

## References

[1] C. S. S. Ferreira, A. C. Duarte, M. Kasanin-Grubin, M. Kapovic-Solomun, and Z. Kalantari, "Hydrological challenges in urban areas," in *Advances in Chemical Pollution, Environmental Management and Protection*, vol. 8, no. 1, 2022, pp. 47–67. doi: 10.1016/bs.apmp.2022.09.001.

[2] W. Sohn, J. H. Kim, M. H. Li, R. D. Brown, and F. H. Jaber, "How does increasing impervious surfaces affect urban flooding in response to climate variability?," *Ecol Indic*, vol. 118, p. 106774, 2020, doi: 10.1016/j.ecolind.2020.106774.

[3] C. N. Damvergis, "Sewer systems: Failures and rehabilitation," *Water Utility Journal*, vol. 8, pp. 17–24, 2014.

[4] N. A. Ibragimova, O. V. Esyrev, Z. R. Zhantuarova, and Z. M. Biyasheva, "Comprehensive Assessment of Waste Water Pollution Rate in Almaty City, Kazakhstan," *International Journal of Environmental Science and Development*, vol. 7, no. 6, pp. 420–424, 2016, doi: 10.7763/IJESD.2016.V7.812.

[5] M. S. Kalmakhanova, J. L. Diaz de Tuesta, A. Malakar, H. T. Gomes, and D. D. Snow, "Wastewater Treatment in Central Asia: Treatment Alternatives for Safe Water Reuse," 2023. doi: 10.3390/su152014949.

[6] S. V. Zharov, S. S. Zharova, and A. A. Fesenko, "Istoriya razvitiya, sovremennoe sostoyanie i dalnejshaya ekspluataciya vodoprovodno-kanalizacionnogo hozyajstva g. Karagandy," *Trudy Universiteta*, vol. 23, no. 2, pp. 62–64, 2006.

[7] L. Yu, N. Li, X. Liu, Q. Yang, and J. Long, "Influence of flushing pressure, flushing frequency and flushing time on the service life of a labyrinth-channel emitter," *Biosyst Eng*, vol. 172, pp. 154–164, Aug. 2018, doi: 10.1016/j.biosystemseng.2018.06.010.

[8] F. Moser, A. P.; Steven, "Unearth the Secrets of Designing and Building High-Quality Buried Piping Systems," in *Buried Pipe Design*, 3rd ed., New York: McGraw Hill, 2008, p. 601.

[9] D.-H. Koo and S. T. Ariaratnam, "Innovative method for assessment of underground sewer pipe condition," *Autom Constr*, vol. 15, no. 4, pp. 479–488, Jul. 2006, doi: 10.1016/j.autcon.2005.06.007.

[10] T. Chorazy *et al.*, "Comparison of Trenchless and Excavation Technologies in the Restoration of a Sewage Network and Their Carbon Footprints," *Resources*, vol. 13, no. 1, p. 12, Jan. 2024, doi: 10.3390/resources13010012.

[11] W. S. Chin and D. G. Lee, "Development of the trenchless rehabilitation process for underground pipes based on RTM," *Compos Struct*, vol. 68, no. 3, pp. 267–283, May 2005, doi: 10.1016/j.compstruct.2004.03.019.

[12] F. A. Hoffstadt, "Cured-in-place composite pipe structures in infrastructure rehabilitation," *International SAMPE Symposium and Exhibition (Proceedings)*, vol. 45, p. I/, 2000.

[13] V. Kaushal, M. Najafi, R. Serajiantehrani, M. Malek Mohammadi, and S. Shirkhanloo, "Construction Cost Comparison between Trenchless Cured-in-Place Pipe (CIPP) Renewal and Open-Cut Replacement for Sanitary Sewer Applications," in *Pipelines 2022*, Reston, VA: American Society of Civil Engineers, Jul. 2022, pp. 171–177. doi: 10.1061/9780784484272.021.

[14] *SP RK 1.04-101-2012 Survey and assessment of the technical status of buildings and constructions*. 2012, p. 89.

[15] J. Myrans, R. Everson, and Z. Kapelan, "Automated detection of fault types in CCTV sewer surveys," *Journal of Hydroinformatics*, vol. 21, no. 1, pp. 153–163, Jan. 2019, doi: 10.2166/hydro.2018.073.

[16] *GOST 17624-2012 Concrete. Ultrasonic method of strength determination*. 2012.

[17] *GOST 22690-2015 Concretes. Determination of strength by mechanical methods of nondestructive testing*. 2015.

[18] *SN RK 4.01-04-2010 Instrukciya po vosstanovleniyu vodoprovodnyh i kanalizacionnyh setej metodom ustrojstva sploshnyh polimernyh rukavov*. 2010.

[19] BKP, "Berolina-Liner: Customised GRP tube liners with unique expansion behaviour." Accessed: Feb. 21, 2025. [Online]. Available: https://bkp-berolina.de/en/berolina-liner-system/berolina-liner/

[20] J. Majerová, J. Hodul, and R. Drochytka, "Properties and Structure of UV Light Cured CIPP Composites," *Key Eng Mater*, vol. 898, pp. 67–72, Aug. 2021, doi: 10.4028/www.scientific.net/KEM.898.67.

[21] A. A. Lukinyh and N. A. Lukinyh, *Tablicy dlya gidravlicheskogo raschyota kanalizacionnyh setej i dyukerov po formule akad. NN Pavlovskogo*, 4th ed. Moscow: Stroyizdat, 1974.

[22] *GOST 6482-2011 Reinforced concrete nonpressure pipes. Specifications*. 2011.

**Information about authors:**

*Yerbol Zhumagaliyev* – Master Student, Department of Civil Engineering, L.N. Gumilyov Eurasian National University, Astana, Kazakhstan, ek2023.info@gmail.com

*Assel Mukhamejanova* – PhD, Acting Associate Professor, Department of Civil Engineering, L.N. Gumilyov Eurasian National University, Astana, Kazakhstan, assel.84@list.ru

*Akmaral Yeleussinova* – Candidate of Technical Sciences, Head of the Department, Department of Civil Engineering, L.N. Gumilyov Eurasian National University, Astana, Kazakhstan, yeleussinova_aye@enu.kz

*Dana Bakirova* – Senior Lecturer, Department of Civil Engineering, L.N. Gumilyov Eurasian National University, Astana, Kazakhstan, strelec6767@mail.ru

*Aizhan Baketova* – PhD Student, Department of Civil Engineering, L.N. Gumilyov Eurasian National University, Astana, Kazakhstan, baketovaaizhan@mail.ru

*Alizhan Kazkeyev* – PhD Student, Department of Civil Engineering, L.N. Gumilyov Eurasian National University, Astana, Kazakhstan, alizhan7sk@gmail.com

*Tymarkul Muzdybayeva* – PhD, Senior Lecturer, Department of Civil Engineering, L. N. Gumilyov Eurasian National University, Astana, Kazakhstan, tumar2304@mail.ru

**Author Contributions:**
*Yerbol Zhumagaliyev* – methodology.
*Assel Mukhamejanova* – resources, data collection.
*Akmaral Yeleussinova* – visualization.
*Dana Bakirova* – analysis.
*Aizhan Baketova* – concept, drafting.
*Alizhan Kazkeyev* – interpretation.
*Tymarkul Muzdybayeva* – editing.

**Conflict of Interest:** The authors declare no conflict of interest.

**Use of Artificial Intelligence (AI):** The authors declare that AI was not used.

*Article*

# Field studies of frozen soils composed of alluvial Quaternary deposits

Ainur Montayeva[1], Abdulla Omarov[1,2,*], Gulshat Tleulenova[2], Assel Sarsembayeva[3], Yoshinori Iwasaki[4]

[1]Department of Research Coordination, Korkyt Ata Kyzylorda State University, Kyzylorda, Kazakhstan
[2]Department of Civil Engineering, L.N. Gumilyov Eurasian National University, Astana, Kazakhstan
[3]Department of Civil Engineering and Geodesy, Shakarim University, Semey, Kazakhstan
[4]Geo-Research Institute, Co., Ltd., Osaka, Japan
*Correspondence: omarov_01@bk.ru

**Abstract.** This study examines the behavior of frozen soils at a construction site in Astana, Kazakhstan. Field static load tests (SLT) and dynamic load tests (DLT), were conducted using driven piles embedded in alluvial Quaternary deposits overlying a 2.5 m permafrost layer. SLT results reveal settlements below 20 mm at a maximum load of 1400 kN, supporting a design capacity of 1167 kN after applying a safety factor of 1.2. Notably, creep behavior was observed in the upper soil layers, and lateral displacement patterns indicate complex interactions within the frozen soil. These findings highlight the need for further research into soil creep and lateral deformations in frozen environments.
**Keywords:** DLT, SLT, pile, frozen soils, soil creep.

## 1. Introduction

In cold climate construction applications, including Astana, Kazakhstan, pile foundations are crucial in ensuring the stability of buildings and infrastructure [1]. However, frozen soils present a complex geotechnical environment, subject to seasonal temperature fluctuations, frost heave, and permafrost degradation, all of which can significantly impact the bearing capacity (BC) and long-term durability of pile structures [2]. Previous studies [3] have shown that the strength of frozen soils increases as temperature decreases due to the reduction of unfrozen water content and the formation of ice bonds, while pile-soil interaction is governed by cohesion, internal friction, and pile surface roughness. In the context of global warming and permafrost degradation, the risks of excessive settlement [4] and reduced bearing capacity of pile foundations are increasing, as revealed by studies in Arctic regions [5]. This highlights the need for continuing studies on pile behavior in frozen soils.

[6] proposed a method and correction coefficient to determine the bearing capacity of piles in various permafrost soil conditions (i.e., different soil temperatures) based on static loading test (SLT) of piles installed in weak sites. However, the method was verified only in the loamy soils with temperatures ranging between -0.1 and -0.6 °C to a depth of 7 m. Therefore, considering a large possible variation of soil type and temperature ranges the method cannot be scaled widely, highlighting the necessity of continuous studies. [7] proposed a technique to obtain the pile-bearing capacity by testing it in a creep-relaxation regime in laboratory and field conditions on morainic loams. They argue that the technique should work well for permafrost soils if the bearing capacity is defined as the stabilized, relaxed pressure measured after a pile is loaded into the soil at a specific subzero temperature, the soil is then heated to a certain level, and sufficient time is allowed for pressure relaxation following unloading. Unfortunately, the authors did not provide evidence for

their hypothesis, which suggests the need for further tests at various temperature regimes and soil types. [8] conducted a series of accelerated SLTs of steel piles assuming their applicability for permafrost soils. However, the authors themselves experienced the unsuitability of such tests for permafrost soils due to their specific behavior. Because while such soils strengthen rapidly under fast loading, they creep under slow loading.

While many efforts were made to derive unified methods in existing studies, they all agree on the specificity of permafrost soils and their dissimilarity across sites, suggesting the need for continuous studies of their behavior, as well as the impracticality of unified approaches. Therefore, to broaden the knowledge and practice in this direction this study examines the permafrost soils in the case of Astana, Kazakhstan. Hence, the study aims to investigate the behavior of permafrost soils in a specific case and determine their bearing capacity by field tests and numerical analysis of a pile-base system. The field tests included both SLT and dynamic loading tests (DLT).

## 2. Methods

The study area is represented by the construction site of the Central Mosque of Astana city, Kazakhstan. According to the conducted survey [9], the site is located at the elevations of 348.33-348.74 meters above the sea at a sharply continental climate characterized by long and cold winters reaching -50 °C. The soil freezing depth in the region reaches 2.5 m on average. During the survey, the groundwater was found at a depth of 3-3.6 m. The geological structure of the survey site involves alluvial Quaternary deposits, including clay loams, medium-grained sands, gravelly sands, and gravel soils, as well as eluvial Lower Carboniferous soils, represented by loamy peat, peat soils, and stony soils (Table 1).

Table 1 – Properties of soil under natural/saturated state [9]

| No. | Soil type | Occurrence depth, m | Thickness, m | Normative values (n) | | | | | Estimated values based on: | | | | | | |
| | | | | | | | | | deformations (II) | | | bearing capacity (I) | | | |
| | | | | $\rho_n$, g/cm$^3$ | $c_n$, kPa | $\varphi_n$, ° | E, MPa | $E^*$, MPa | $\rho_{II}$, g/cm$^3$ | $c_{II}$, kPa | $\varphi_I$, ° | $\rho_I$, g/cm$^3$ | $c_I$, kPa | $\varphi_I$, ° | $R_0$, kPa |
| 1a | Loams | 0-6.7 | 5.1-6.7 | 1.94 | -/23 | -/28 | -/6.5 | - | 1.92 | -/15 | -/27 | 1.91 | -/11 | -/26 | - |
| 1b | Loams | | | 1.98 | -/42 | -/18 | -/6 | - | 1.95 | -/29 | -/15 | 1.93 | -/21 | -/13 | - |
| 2 | Medium sands | 5.7-7.0 | 0.5-2.6 | 1.92 | 2 | 35 | - | 17 | 1.92 | 1.6 | 32 | 1.92 | 1.33 | 30 | - |
| 3 | Gravelly sands | 4.5-9.0 | 1.0-6.5 | 1.92 | 1 | 38 | - | 35.7 | 1.92 | 0.8 | 35 | 1.92 | 0.67 | 33 | - |
| 4 | Gravel soils | 6.0-9.0 | 2.0-4.6 | 2 | - | - | 23 | 18 | - | - | - | - | - | - | 300 |
| 5 | Loamy peat | 10.7-12.0 | 0.7-16.0 | 2.06 | 80/44 | 22/30 | 12/9.5 | 20.9 | 2.05 | 64/30 | 20/27 | 2.04 | 53/21 | 19/25 | - |
| 6 | Peat soils | 11.0-23.5 | 0.5-14.5 | 2.2 | - | - | - | 36.4 | - | - | - | - | - | - | 400 |
| 7 | Stony soils | 17.0-26.0 | 1.0-2.0 | 2.4 | - | - | - | 36.4 | - | - | - | - | - | - | 450 |

*Plate loading test

The field tests were conducted using 0.3×0.3×8 m driven piles on 26 February 2019. The piles were installed with the Junttan PM-25 pile driving machine having a 7-ton hydraulic hammer, simultaneously measuring the dynamic parameters, such as the number of blows and height of the hammer per penetration depth. DLT was performed using 16 piles after their rest according to [10]. During testing, the falling height of the hammer's impact part was recorded at 10 cm intervals over the last meter of penetration, along with the number of hammer strikes required for each meter of pile penetration. Since the number of piles tested in a similar soil condition was more than 6, statistical processing of DLT results was performed according to [11]. When determining the bearing capacity of piles, a safety factor of 1.4 was applied according to [10].

SLT was conducted according to [10] using 4 piles at the site's weakest soils, incorporating a testing setup (Figure 1) consisting of primary and secondary beams, a hydraulic jack, a manometer, settlement gauges, and reinforced concrete blocks. The compressive load was subjected vertically with steps of 140 kN up to 1400 kN (design load accounting for the safety factor [12]). The bearing capacity estimates here incorporated a safety factor of 1.2 in line with [10].

Figure 1 – Testing setup for SLT

Additional analysis of the pile-base state and deformations was made by numerical simulation of SLT using Plaxis 2D as in [13]. A Mohr-Coulomb elastoplastic model was used to simulate the stress-strain state of the soil base. A linear elastic model was applied to simulate the pile. The calculations were performed in an axisymmetric setup. The loading procedure was similar to the field SLT.

## 3. Results and Discussion

Figure 2 demonstrates the change in dynamic parameters measured during the driving.



a) 1 m or 10 cm penetration      b) Total period      c) Hammer height
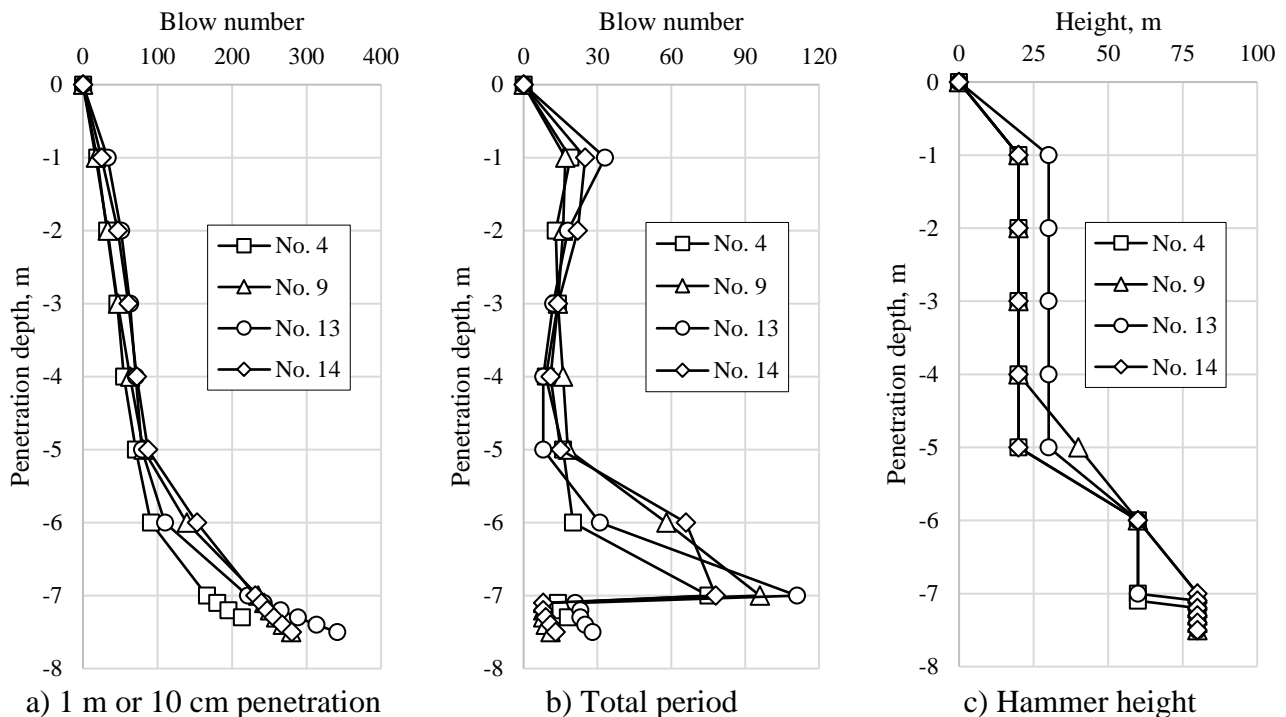
Figure 2 – DLT results

While the dynamic parameters were measured for all 16 piles, Figure 2 above shows their values for the most important ones, installed in the weak soils of the construction site, including the piles numbered 4, 9, 13, and 14. Thus, it took around 280 blows to penetrate the piles to a depth of 7.5 m (Figure 2a). It can be observed from Figure 2b that the hammer-blowing intensity at 1 m depth was 1.5 times higher than at the depths of 2-5 m. This can be explained by the fact that in February when the piles were installed, the freezing depth of local soils may still reach 1-2 m. Besides the upper layers of the soil-base of the site are comprised mostly of loams, which are rather

saturated and prone to icing that may create additional friction on the lateral surface of piles. Additionally, the hammer height stood steady in the depths of 1-5 m (Figure 2c), suggesting the existence of creep behavior of the soils at these depths. These results complement the thoughts about the omissions [8].

Table 2 below shows the results of DLT.

Table 2 – DLT results

| Pile No. | Driving depth, m | Hammer height, m | Refusal of driving, cm | Re-driving height, m | Refusals of re-driving, cm | Individual value of ultimate pile resistance, kN | Bearing capacity of piles, kN |
|---|---|---|---|---|---|---|---|
| 1 | 7.3 | 60 | 0.36 | 0.40 | 0.34 | 903 | |
| 2 | 7.5 | 60 | 0.53 | 0.50 | 0.36 | 986 | |
| 3 | 7.1 | 60 | 0.40 | 0.40 | 0.27 | 1021 | |
| 4 | 6.5 | 60 | 0.40 | 0.50 | 0.38 | 958 | |
| 5 | 6.8 | 60 | 0.40 | 0.40 | 0.30 | 965 | |
| 6 | 6.2 | 60 | 0.37 | 0.40 | 0.28 | 1001 | |
| 7 | 6.7 | 60 | 0.38 | 0.40 | 0.22 | 1138 | |
| 8 | 7.1 | 60 | 0.38 | 0.40 | 0.23 | 1111 | |
| 9 | 7.5 | 60 | 0.50 | 0.40 | 0.23 | 1111 | 960 |
| 10 | 5.9 | 60 | 0.36 | 0.40 | 0.28 | 1001 | |
| 11 | 5.9 | 60 | 0.36 | 0.50 | 0.40 | 932 | |
| 12 | 6.2 | 60 | 0.42 | 0.40 | 0.27 | 1021 | |
| 13 | 6.2 | 60 | 0.43 | 0.40 | 0.30 | 965 | |
| 14 | 6.5 | 60 | 0.36 | 0.40 | 0.34 | 903 | |
| 15 | 5.8 | 60 | 0.37 | 0.40 | 0.30 | 965 | |
| 16 | 6.4 | 70 | 0.36 | 0.50 | 0.43 | 897 | |

* Installed in weak soils of the site

DLT results presented in Table 2 above show that the piles were driven to depths ranging from 5.8 to 7.5 m with a constant driving height of 60 m (70 m in one case) and they showed low refusal rates (0.36 to 0.53 cm), while the re-driving heights were also stable at 0.40-0.50 m and refusals of 0.22-0.43 cm. Individual ultimate resistance ranged from 897 kN to 1138 kN, while the estimated by [10] bearing capacity of the piles was 960 kN. These trends reflect the heterogeneous soil profile at the site, where upper alluvial deposits consisting of loams and medium-grained sands with moderate density and lower strength are combined with underlying layers of gravelly sands and gravel soils that provide higher friction angles and stiffness. Consequently, the behavior of the composite soil is consistent with the results of the DLT.
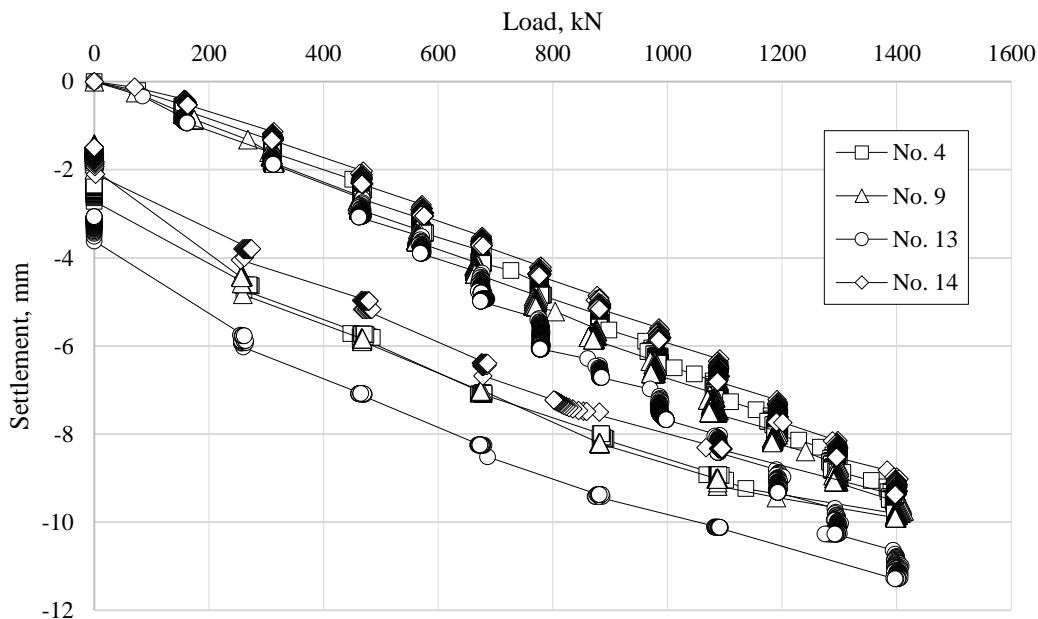
Figure 3 below shows the SLT results.



Figure 3 – SLT results

All four tested piles No. 4, 9, 13, and 14 showed similar trends in their SLTs, with settlement remaining minimal (often below 2 mm) at lower loads, then gradually increasing but still staying under 10–11 mm at the maximum applied load of around 1400 kN, which is way below the 20 mm threshold mandated by [12]. This indicates that, although the shallow soil may include permafrost to a depth of about 2.5 m, the deeper alluvial layers (loams, sands, and gravelly soils) effectively limit overall deformation. Consequently, none of the piles exhibited signs of bearing failure or excessive settlement, and each can safely be assigned a bearing capacity of 1167 kN, derived by applying a 1.2 safety factor to the maximum test load of 1400 kN.

Figure 4 below shows the results of numerical simulations of SLT in Plaxis 2D.



a) Vertical displacements                     b) Horizontal displacements
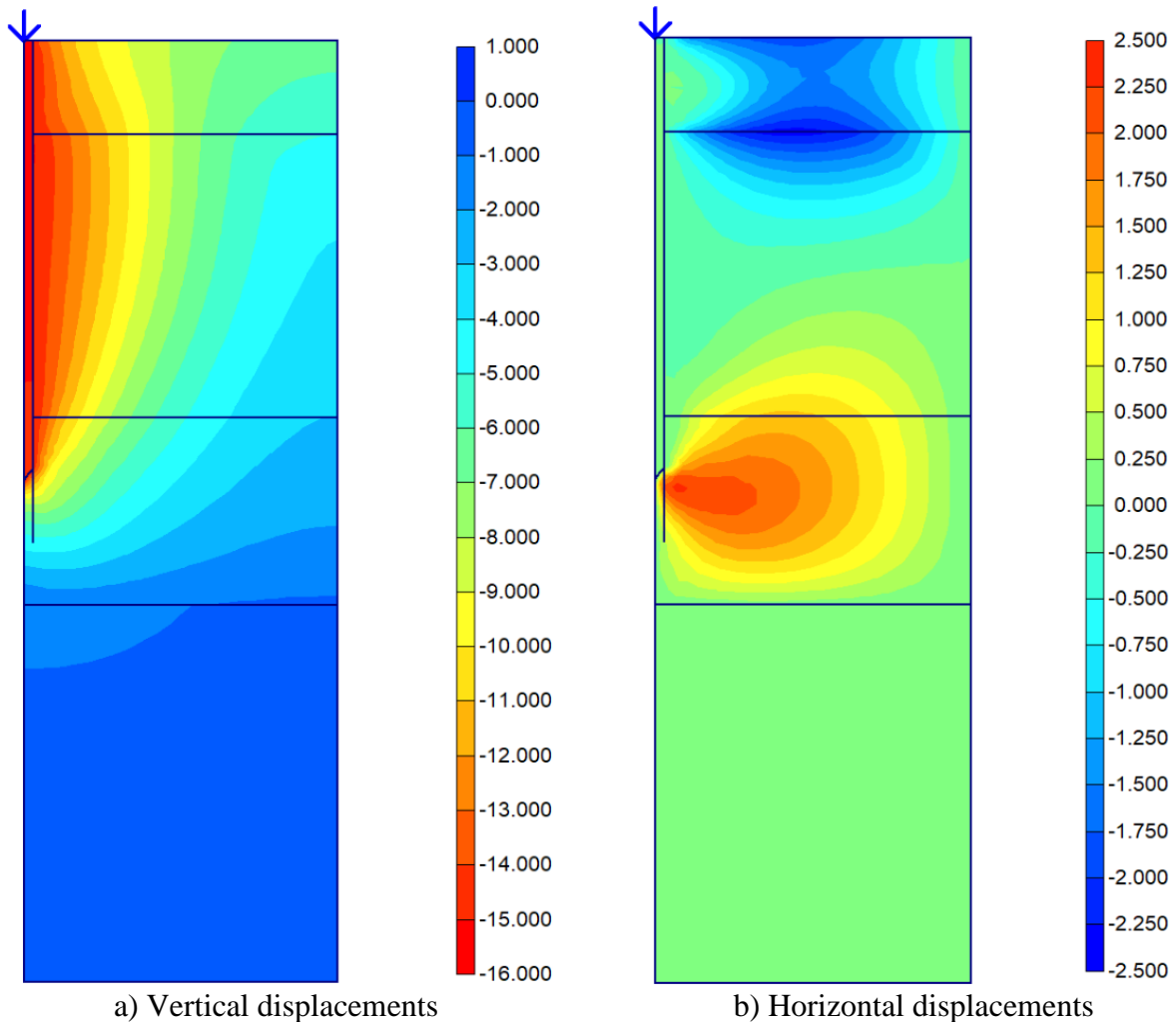
Figure 4 – Results of numerical simulations

The heatmaps from Figure 4 demonstrate that the simulation of SLT using a pile subjected to the load of 1400 kN with steps of 140 kN resulted in both vertical and lateral displacements of the soils to some extent. The values of displacements are reflected by the legend with gradient colors from blue to red for the vertical (Figure 4a), and vice-versa for the horizontal displacements (Figure 4b), corresponding to the positivity and negativity of the values, respectively. As is seen from a failure pattern in Figure 4a, the loading process initiated the pulling of the part of the soil base so that the closer it was to the pile the more its vertical displacement, suggesting the logical behavior of such a process. Unlike the vertical one, the lateral displacement created two dissimilar failure patterns. The pattern appeared close to the pile tip represented by a lateral movement, likely due to the resting of the pile on hard soils. Another pattern, somewhere in the depths of 1-2 m took a concave shape. This most likely is evidence of the creep behavior of soils due to permafrost at those depths, which coincides with [8], suggesting the necessity for future work in this direction.

Nevertheless, the highest values of vertical and horizontal displacements amounted to 15.17 mm and 2.38 mm, respectively, which are lower than the threshold of 20 mm [12]. This advocates that the bearing capacity of piles may be derived similarly to the field SLT using a safety factor of 1.2 and the highest load of 1400 kN, which results in 1167 kN as above.

## 4. Conclusions

The field tests demonstrate that the driven piles exhibit positive performance in frozen soils at the construction site of Central Mosque in Astana, Kazakhstan, with settlements remaining significantly below the 20 mm limit under a maximum load of 1400 kN. After applying a 1.2 safety factor, a bearing capacity of 1167 kN is achieved.

Due to the inherent variability and unique characteristics of permafrost soils from site to site, the findings of this study are pivotal in expanding our knowledge of frozen soil properties and behavior.

Observations of creep behavior in the upper, partially frozen soils and emerging patterns of lateral displacements underscore the complexity of soil-pile interactions in such environments. Further investigations into soil creep and lateral displacement behavior are essential to optimize foundation design and ensure long-term performance under variable temperature regimes.

## Acknowledgments

## References

[1] A. Zhussupbekov, A. Omarov, N. Shakirova, and D. Razueva, "Complex Analysis of Bored Piles on LRT Construction Site in Astana," in *Lecture Notes in Civil Engineering*, vol. 49, 2020, pp. 461–471. doi: 10.1007/978-981-15-0450-1_48.

[2] A. I. Potapov, A. I. Shikhov, and E. N. Dunaeva, "Geotechnical monitoring of frozen soils: problems and possible solutions," *IOP Conf Ser Mater Sci Eng*, vol. 1064, no. 1, p. 012038, Feb. 2021, doi: 10.1088/1757-899X/1064/1/012038.

[3] G. Xu, J. Qi, and W. Wu, "Temperature Effect on the Compressive Strength of Frozen Soils: A Review," in *Springer Series in Geomechanics and Geoengineering*, Cham: Springer, 2019, pp. 227–236. doi: 10.1007/978-3-319-89671-7_19.

[4] L. Tang *et al.*, "Numerical analysis of frost heave and thawing settlement of the pile–soil system in degraded permafrost region," *Environ Earth Sci*, vol. 80, no. 20, p. 693, Oct. 2021, doi: 10.1007/s12665-021-09999-4.

[5] J. B. de O. L. Dourado, L. Deng, Y. Chen, and Y.-H. Chui, "Foundations in Permafrost of Northern Canada: Review of Geotechnical Considerations in Current Practice and Design Examples," *Geotechnics*, vol. 4, no. 1, pp. 285–308, Mar. 2024, doi: 10.3390/geotechnics4010015.

[6] V. N. Eroshenko, "Determination of the loading capacity of piles in permafrost by means of static tests," *Soil Mechanics and Foundation Engineering*, vol. 13, no. 3, pp. 174–176, May 1976, doi: 10.1007/BF01705314.

[7] P. Korolev and M. Korolev, "Tests of piles in melted and frozen soils in creep mode: relaxation conditions," *IOP Conf Ser Mater Sci Eng*, vol. 365, p. 042052, Jun. 2018, doi: 10.1088/1757-899X/365/4/042052.

[8] I. A. Nikolenko, A. P. Kuleshov, and L. A. Strokova, "Comparative analysis of the results of standard and accelerated field tests of pile foundations in permafrost soils," *Bulletin of the Tomsk Polytechnic University Geo Assets Engineering*, vol. 334, no. 3, pp. 40–50, Feb. 2023, doi: 10.18799/24131830/2023/3/3905.

[9] V. N. Popov, *Technical report on engineering-geological surveys on the project: "Mosque at the address of Astana, Esil district, between Kabanbai Batyr and Mangilik El avenues."* Karaganda: KaragandaGIIZ and K* LLP, 2019.

[10] *GOST 5686-2012 Soils. Field test methods by piles*. 2012.

[11] *GOST 20522-2012 Soils. Methods of statistical treatment of test results*. 2012.

[12] *SN RK 5.01-03-2013 Pile foundations*. 2013.

[13] V. Ghiasi and S. Eskandari, "Comparing a single pile's axial bearing capacity using numerical modeling and analytical techniques," *Results in Engineering*, vol. 17, p. 100893, Mar. 2023, doi: 10.1016/j.rineng.2023.100893.

**Information about authors:**

*Ainur Montayeva* – PhD, Associate Professor, Department of Research Coordination, Korkyt Ata Kyzylorda State University, Kyzylorda, Kazakhstan, montayeva_ainur@mail.ru

*Abdulla Omarov* – PhD, Senior Lecturer, Department of Civil Engineering, L.N. Gumilyov Eurasian National University, Astana, Kazakhstan, omarov_01@bk.ru

*Gulshat Tleulenova* – PhD, Acting Associate Professor, Department of Civil Engineering, L.N. Gumilyov Eurasian National University, Astana, Kazakhstan, gulshattleulenova23@mail.ru

*Assel Sarsembayeva* – Candidate of Technical Sciences, PhD, Science Professor, Department of Civil Engineering and Geodesy, Shakarim University, Semey, Kazakhstan, assel_enu@mail.ru

*Yoshinori Iwasaki* – PhD, Doctor of Technical Sciences, Professor, Geo-Research Institute, Co., Ltd., Osaka, Japan, yoshi-iw@geor.or.jp

**Author Contributions:**
*Ainur Montayeva* – concept, methodology, funding acquisition.
*Abdulla Omarov* – drafting, data collection, testing, modeling, analysis.
*Gulshat Tleulenova* – visualization.
*Assel Sarsembayeva* – editing.
*Yoshinori Iwasaki* – interpretation.

**Conflict of Interest:** The authors declare no conflict of interest.

**Use of Artificial Intelligence (AI):** The authors declare that AI was not used.

*Article*

# Prediction of compressive strength and density of aerated ash concrete

Darya Anop[1], Olga Rudenko[1], Vladimir Shevlyakov[1], Zulfiya Aubakirova[2], Nikolai Soshnikov[1], Meiram Begentayev[3]

[1]D. Serikbayev East Kazakhstan Technical University, Ust-Kamenogorsk, Kazakhstan
[2]Abylkas Saginov Karaganda Technical University, Karaganda, Kazakhstan
[3]Satbayev University, Almaty, Kazakhstan
*Correspondence: o_rudenko_vkgtu@mail.ru

**Abstract.** The article presents the results of studies on forecasting the compressive strength and density of aerated ash concrete. A theoretical review was conducted on the variability of strength and density of cellular concretes when selecting their compositions. A series of experiments was conducted to study the dynamics of changes in the compressive strength and density of non-autoclaved gas-ash concrete during the initial stages of hardening under natural conditions and after thermal treatment to select a composition of the specified quality. It was revealed that it is possible to control both the strength and the density at the early stages of hardening to forecast these parameters at the design age of 28 days. It was established that the compressive strength of aerated ash concrete samples hardening under natural conditions increased by an average of 42.62% at the design age compared to the strength at 7 days, while the density decreased on average by 19.19%. For aerated ash concrete samples that underwent thermal treatment (steaming), the increase in strength averaged 34.67%, and the decrease in density was 11.07%. The obtained results are of practical value for scientists and engineers engaged in the development of cellular concrete compositions.
**Keywords:** cellular concrete, aerated concrete tests, ash and slag waste, compressive strength, density.

## 1. Introduction

The use of cellular concrete in construction, both in monolithic housing construction and for the manufacture of individual products, does not lose its relevance, including due to several advantages in contrast to other types of concrete and such a traditional material as ceramic brick [1], [2]. Cellular concrete has excellent heat and sound insulation properties, and products made from it are easy to process. At the same time, cellular concrete is more "capricious" when selecting a composition of a certain specified quality. The structure formation of cellular concrete is influenced by such factors as the type of raw material, the ratio between the components, the water-solid ratio (W/S), the type and amount of foaming agent, the mode of heat and moisture treatment, and others [2].

The main standardized characteristics of cellular concrete are the concrete grade by average density and the corresponding values of concrete classes by compressive strength [3]. Therefore, when developing compositions for cellular concretes and blocks made from them, it is important to monitor both the strength and density of the concrete [4].

Many studies are devoted to the development of cellular concrete compositions, both foam and aerated concrete of autoclaved and non-autoclaved hardening, including the use of industrial waste.

In the work [5], the authors investigated the effect of a complex modifier based on graphene oxide and lignosulfonate on the physical and mechanical properties of non-autoclaved aerated concrete, such as compressive and flexural strength. Portland cement M500, sand, slaked construction carbonate-lime flour, and aluminum powder were used as raw materials. It was found that the complex additive of graphene oxide provides the greatest increase in compressive strength by 54% and flexural strength

by 45%. The disadvantage of this study is that density control was not carried out.

The authors of the study [6] determined the effect of various components, such as the water-cement ratio, NaOH content, polycarboxylate superplasticizer, aluminum powder, and calcium stearate, on the strength and density of non-autoclaved aerated concrete based on sulfoaluminate cement. The strength of the samples was determined at the ages of 7 and 28 days, and the density only at the design age of 28 days. At the same time, the values of compressive strength at the age of 28 days were consistently higher than the values of compressive strength at the age of 7 days for all the studied components in different percentage ratios. The dynamics of density in samples with different curing periods were not studied.

A literature review [7] examines the use of additives such as fly ash, crushed granulated blast-furnace slag, and waste such as quarry dust, rubber particles, rice husk ash, plastic waste, glass powder, and others on the properties of aerated and foam concrete. Their influence was assessed based on such properties as workability, elastic modulus, compressive strength, flexural strength, and microstructural characteristics. Unfortunately, the study missed the data on the dynamics of density for samples with different curing periods.

The study [8] related to the selection of autoclaved cellular concrete compositions focused on replacing part of the sand with waste from its production; there is also a lack of data on the dynamics of changes in strength and density at different curing periods.

The work [9] was devoted to the selection and optimization of the composition of non-autoclaved aerated concrete. The study compared the properties of autoclaved and non-autoclaved aerated concrete with the introduction of metakaolinite, microsilica, and rice husk in the amount of 7% into the mixture. The comparison was carried out according to compressive strength, flexural strength, and splitting strength. The results of the study confirmed the classical patterns of strength gain for autoclaved and non-autoclaved aerated concrete. For non-autoclaved concrete, there was a significant increase in all types of strength from 7 to 180 days, while for autoclaved concrete, such an increase is practically not observed. In this study, the humidity of samples at the age of 3, 7, 14, 21, 28, and 180 days was also determined. At the same time, the humidity of autoclaved aerated concrete remained practically unchanged from 3 to 28 days and then decreased to 3...5% and became slightly lower than that of non-autoclaved concrete. However, at the age of 3 days, it was 1.5 times lower than that of non-autoclaved aerated concrete. This is due to the conditions of concrete hardening in an autoclave and the end of the Portland cement hydration process, when water is chemically bound into calcium hydrosilicates and other hydration products. The study also lacks data on monitoring the density of samples at different hardening periods, which is important for the selection of cellular concrete compositions when developing it with a given density. The solution to this problem will make a certain contribution to scientists and engineers involved in the development of cellular concrete recipes and would significantly save their time.

Our previous study [10] was devoted to experiments with aerated ash concrete. In continuation of this initiative and considering the gaps in the existing studies, this study aims to investigate the dynamics of changes in the strength and density of non-autoclaved aerated concrete.

To achieve the goal, the following tasks were solved:

1. To conduct a theoretical review of data on the variability of strength and density of cellular concrete in the selection of their compositions, including the use of industrial waste.

2. To conduct an experiment to study the dynamics of strength and density of non-autoclave curing aerated ash concrete to select the composition of a given quality.

## 2. Methods

The experiments were performed in cooperation with an enterprise of the East Kazakhstan region, which specializes in the production of gas blocks according to [4]. The composition of aerated ash concrete from which the samples were prepared in that enterprise was taken from [10] and incorporated the following components: the ash-slag waste from the coal-fired thermal power plant in

Ust-Kamenogorsk, East Kazakhstan region, was used as the main filler; Portland cement of grade SEM I 52.5N served as the binder; aluminum powder of grade PAP-1, activated with caustic soda, was employed as the pore-forming (gas-forming) agent. Figure 1 shows the experimental procedures.
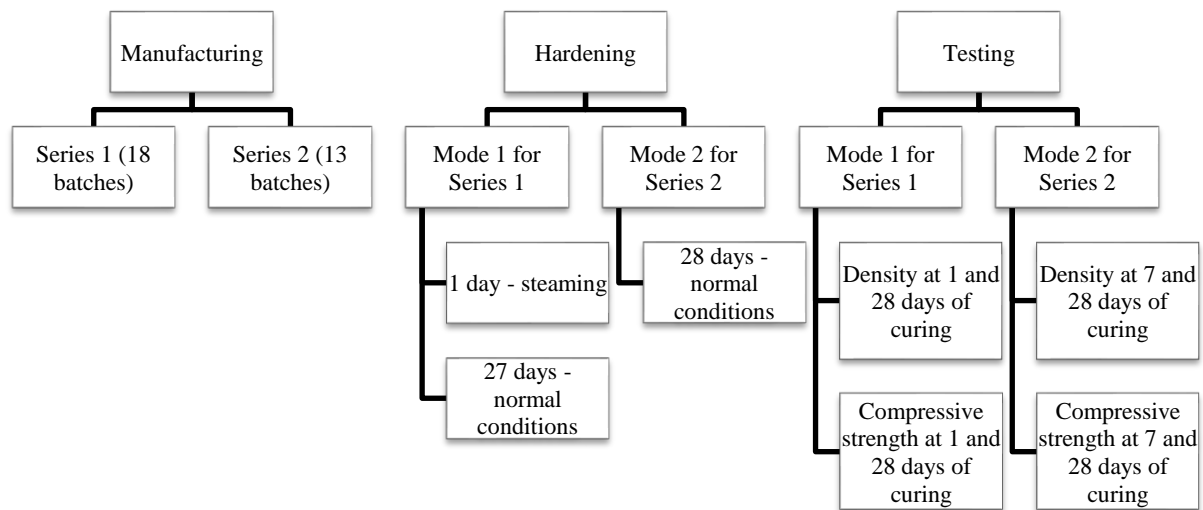
Figure 1 – Experimental procedures

As shown in Figure 1 above, for predicting the strength and density of aerated ash concrete, two series of batches were manufactured, cured in two modes, and tested for density and compressive strength. Density was estimated following [11] based on moisture content, which was determined using a moisture meter of MG4B brand (Figure 2a). Strength tests were carried out according to [12] on a hydraulic press 2PG-10 with two ranges of gauges 0-5 tons and 0-10 tons (Figure 2b).

|                    |                        |
|--------------------|------------------------|
| a) Moisture content | b) Compressive strength |

Figure 2 – Determination of moisture content and compressive strength of aerated concrete

Each batch comprised 6 samples. Each sample was made in a cubic shape of 15×15×15 cm in size. After production, the samples were set in the air for 40-60 minutes at a temperature of 18-20°C. Series 1 and 2 comprised 18 and 13 batches, respectively, so altogether, 186 samples were manufactured, including 108 for series 1 and 78 for series 2. Each series was hardened at its mode of curing. In mode 1, the samples of series 1 were cured for 1 day in steaming and 27 days in normal conditions. The samples were steamed in a steaming chamber KUP-1 in the following mode: temperature increase to the required parameters – within 60 minutes from 20 to 90 °C and humidity of 90%; steaming – within 6 hours at a temperature of 90 °C and humidity of 90%; cooling to 20 °C. After that, half of the samples within each batch were tested (54 samples), and the rest were placed in normal conditions in a KNT-120 chamber for further strength gain. In mode 2, the samples of series 2 were cured for 28 days in normal conditions in the same chamber. Besides, half of them (39 samples) were tested after 7 days of curing. After 28 days of curing, the samples from each mode (54 samples from series 1 and 39 samples from series 2) were also tested.

To predict the strength and density of aerated ash concrete, this study uses the Statistica 10 software package as in [13]. The software enabled the development of mathematical dependencies between strength, density, and the values of increase in strength and decrease in the density of the samples throughout the curing period.

## 3. Results and Discussion

The results of testing the samples of the first series are presented in Table 1 below.

Table 1 – Test results of the first series of samples

| Batch No. | Additives [10] | Compressive strength, MPa | | Density, kg/m³ | | Increase in strength, MPa | Decrease in density, kg/m³ | Density reduction, % | Reduction in density, % |
|---|---|---|---|---|---|---|---|---|---|
| | | 1 day | 28 days | 1 day | 28 days | | | | |
| 1 | Zeolite | 1.28 | 2.03 | 691 | 610 | 0.75 | 81 | 37.04 | 13.28 |
| 2 | Zeolite | 1.46 | 2.18 | 717 | 663 | 0.72 | 54 | 33.08 | 8.14 |
| 3 | - | 1.42 | 2.23 | 772 | 677 | 0.81 | 95 | 36.30 | 14.03 |
| 4 | - | 1.56 | 2.42 | 761 | 683 | 0.86 | 78 | 35.60 | 11.42 |
| 5 | - | 1.54 | 2.45 | 766 | 692 | 0.91 | 74 | 37.23 | 10.69 |
| 6 | - | 1.73 | 2.66 | 766 | 705 | 0.93 | 61 | 35.00 | 8.65 |
| 7 | Anhydrite | 1.92 | 2.83 | 785 | 712 | 0.91 | 73 | 32.23 | 10.25 |
| 8 | Anhydrite | 1.98 | 3.00 | 828 | 730 | 1.02 | 98 | 33.97 | 13.42 |
| 9 | Gypsum | 1.88 | 3.04 | 826 | 741 | 1.16 | 85 | 38.21 | 11.47 |
| 10 | Fullerenol | 2.03 | 3.12 | 817 | 748 | 1.09 | 69 | 34.94 | 9.22 |
| 11 | Fullerenol | 2.23 | 3.21 | 870 | 758 | 0.98 | 112 | 30.52 | 14.78 |
| 12 | Fullerenol | 2.19 | 3.46 | 856 | 778 | 1.27 | 78 | 36.72 | 10.07 |
| 13 | Fullerenol | 2.29 | 3.49 | 862 | 796 | 1.20 | 66 | 34.38 | 8.25 |
| 14 | Quicklime | 2.23 | 3.55 | 935 | 808 | 1.32 | 126 | 37.27 | 15.65 |
| 15 | Quicklime | 2.58 | 3.66 | 904 | 812 | 1.08 | 92 | 29.49 | 11.33 |
| 16 | Quicklime | 2.51 | 3.70 | 903 | 820 | 1.19 | 83 | 32.07 | 10.12 |
| 17 | Quicklime | 2.50 | 3.85 | 909 | 828 | 1.35 | 81 | 35.00 | 9.78 |
| 18 | Quicklime | 2.51 | 3.87 | 902 | 830 | 1.36 | 72 | 35.07 | 8.67 |

Table 1 above shows the values of compressive strength and density of the samples from 18 batches at the curing ages of 1 and 28 days. The table also shows the estimated values of the increase in strength and decrease in density of the samples, along with their ratios. These tables show that regardless of the composition of the ash concrete in batches, there is an increase in strength at the design age of 28 days compared to the strength at the reference period of 1 day, as well as a decrease in density. For visual analysis of changes in strength and density dynamics, a histogram of strength increase and a density graph are plotted in Figure 3, a histogram of density change and a strength graph in Figure 4, and a graph of the dependence of strength, density, and change in strength in Figure 5.
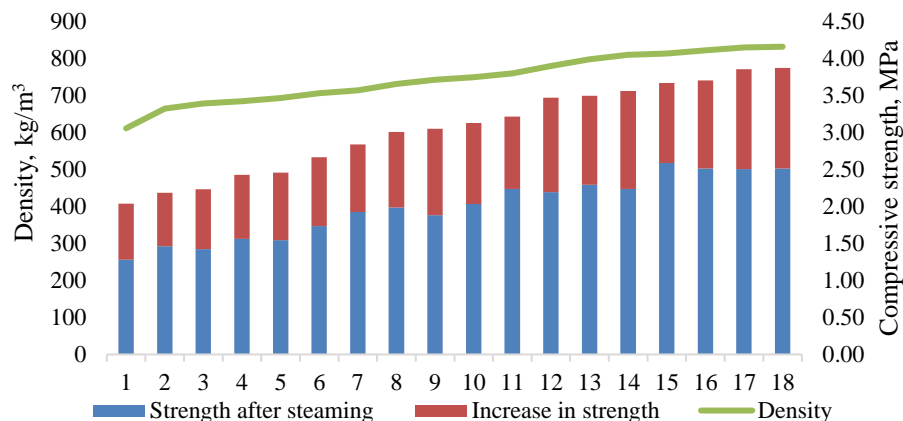


Figure 3 – Histogram of strength increase and density plot

Analysis of the obtained results showed that in samples that were subjected to heat treatment, the strength at the design age of 28 days compared to the strength immediately after steaming (at the age of 1 day) increased by an average of 34.67%. The minimum increase in strength was 29.49%, and the compressive strength changed from 2.58 to 3.66 MPa. The maximum increase in strength was 37.23%, i.e., from 1.54 to 2.45 MPa in batch No. 5.

The increase in the strength of cellular concretes due to the use of various additives is consistent with the previously conducted studies on the selection of compositions of non-autoclave concretes [5], [6]. The slightly smaller increase in strength is due to the use of other additives.

At the same time, there was a decrease in density (Figure 4).
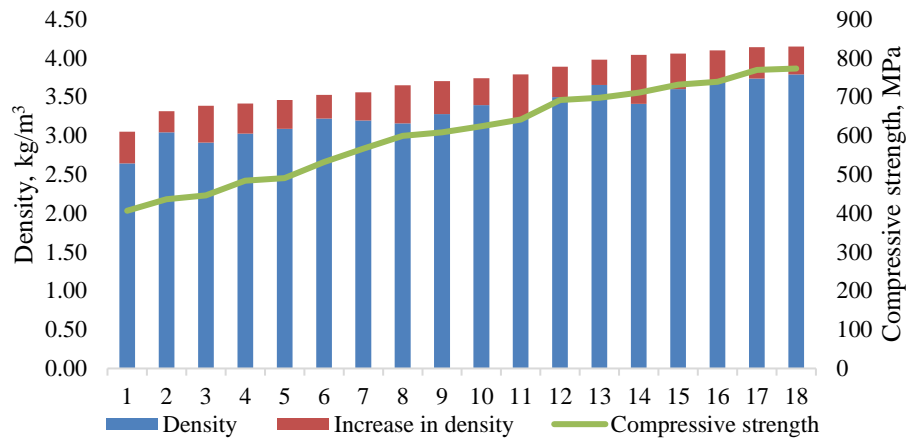


Figure 4 - Histogram of density variation and strength plot

The density reduction in the samples after 28 days compared to the samples after steaming averaged 11.07%. The minimum density reduction was 8.14% and amounted from 717 to 663 kg/cm$^3$, i.e., the density class of aerated ash concrete decreased from D750 to D700. The maximum density reduction of 15.65% from 935 to 808 kg/cm$^3$ gave a reduction in density class from D950 to D850.

The obtained results on density reduction extend the previous studies on the selection of cellular concrete compositions [5], [6], [8].

The results of predicting the strength and density of cellular ash concrete of the first series of samples using the Statistica 10 software package are shown in Figure 5.
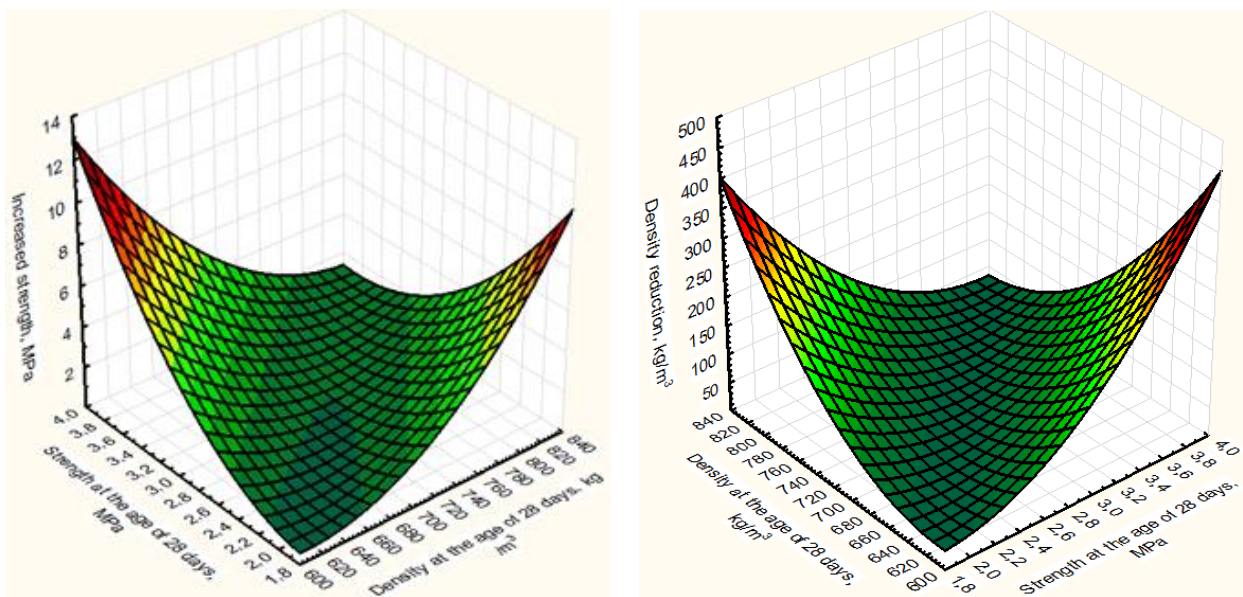


a) Graph of dependence of strength, density, and strength increase

b) Graph of dependence of strength, density, and density reduction

Figure 5 – Dependency graphs for heat-treated aerated concrete

Analysis of the obtained results showed that the increase in strength and decrease in density at the design age of 28 days compared to the strength immediately after steaming (at the age of 1 day) occurs evenly proportionally.

The average strength gain of 34.67% is quite consistent with previous studies that showed the dynamics of increasing the strength of cellular concrete of non-autoclave hardening. The results on the dynamics of density of cellular concretes of non-autoclave hardening (density decrease by 11.07% on average) are new and expand the studies [5], [6], [7], [9].

The results of testing the samples of the second series are presented in Table 2 below.

Table 2 – Results of testing samples of the second series

| Batch No. | Additives [10] | Compressive strength, MPa | | Density, kg/m³ | | Increase in strength, MPa | Decrease in density, kg/m³ | Increase in strength, % | Reducing density, % |
|---|---|---|---|---|---|---|---|---|---|
| | | 7 days | 28 days | 7 days | 28 days | | | | |
| 1 | Zeolite | 0.88 | 1.80 | 762 | 142.03 | 620 | 0.92 | 51.01 | 22.91 |
| 2 | Zeolite | 1.29 | 2.23 | 802 | 121.83 | 680 | 0.94 | 42.27 | 17.92 |
| 3 | - | 1.68 | 2.36 | 1082 | 241.37 | 841 | 0.68 | 28.70 | 28.70 |
| 4 | - | 1.18 | 2.37 | 871 | 180.94 | 690 | 1.19 | 50.12 | 26.24 |
| 5 | Anhydrite | 1.55 | 2.47 | 898 | 187.36 | 711 | 0.92 | 37.25 | 26.35 |
| 6 | Anhydrite | 1.53 | 2.89 | 1049 | 225.10 | 824 | 1.36 | 47.14 | 27.32 |
| 7 | Fullerenol | 1.76 | 2.89 | 1063 | 212.50 | 850 | 1.13 | 39.00 | 25.00 |
| 8 | Fullerenol | 1.94 | 3.09 | 945 | 166.74 | 778 | 1.15 | 37.31 | 21.43 |
| 9 | Fullerenol | 1.78 | 3.48 | 995 | 155.91 | 839 | 1.70 | 48.90 | 18.58 |
| 10 | Quicklime | 2.06 | 3.51 | 1026 | 224.63 | 801 | 1.45 | 41.35 | 28.04 |
| 11 | Quicklime | 2.03 | 3.67 | 982 | 168.21 | 814 | 1.64 | 44.69 | 20.66 |
| 12 | Quicklime | 2.35 | 4.45 | 1028 | 167.92 | 861 | 2.10 | 47.23 | 19.51 |
| 13 | Quicklime | 2.55 | 4.61 | 1090 | 192.04 | 898 | 2.06 | 44.76 | 21.38 |

Table 2 above shows the compressive strength and density values of samples from 13 batches at the curing ages of 7 and 28 days. The table also shows the estimated values of the increase in strength and decrease in density of the samples, along with their ratios. Just as in the first series of samples, the test results of the second series presented in table 2 indicate that, regardless of the gas-ash concrete composition, there is an increase in strength at the design age of 28 days compared to the strength at the reference period of 7 day, as well as a decrease in density.

For visual analysis of changes in strength and density dynamics, a histogram of strength increase and a density graph are plotted in Figure 6, a histogram of density change and a strength graph in Figure 7, and a graph of the dependence of strength, density, and change in strength in Figure 8.
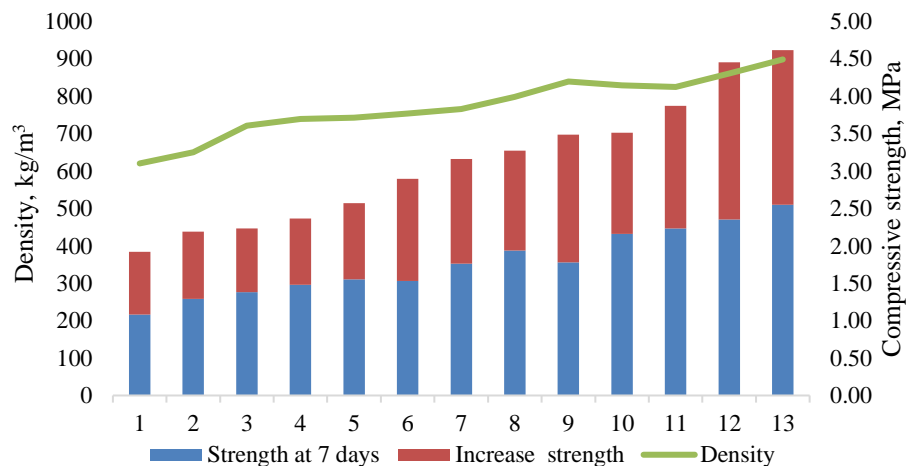


Figure 6 – Strength change histogram and density graph

Analysis of the obtained results showed that in the samples that gained strength under natural conditions, the strength at the design age of 28 days compared to the strength at the age of 7 days

increased by an average of 42.62%. The minimum increase in strength was 37.44%, and the compressive strength changed from 1.48 to 2.37 MPa. The maximum increase in strength was 48.90%, i.e., from 1.78 to 3.48 MPa in batch No. 9.

Increasing the strength of cellular concretes through the use of various additives is consistent with previous studies [5] and [6]. The slightly smaller increase in strength compared to [5] is due to the use of other additives.

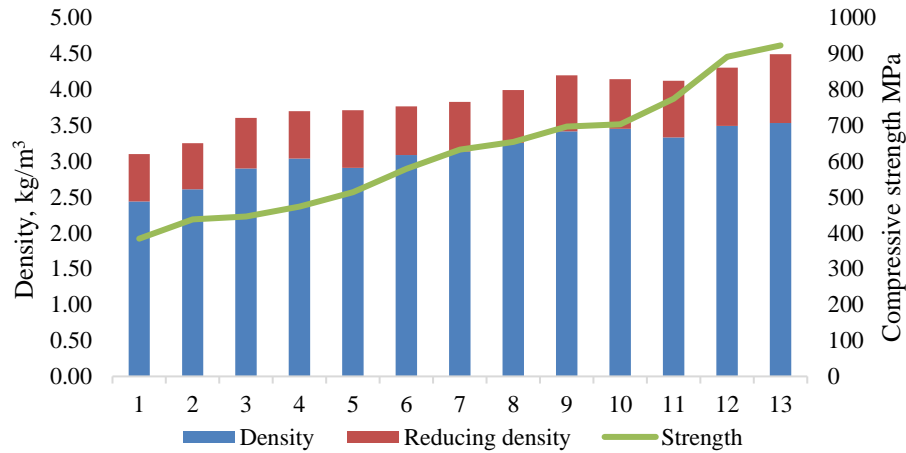At the same time, there was a decrease in density (Figure 7).



Figure 7 – Histogram of density change and strength graph

In the samples gaining strength under natural conditions, a decrease in density was also observed. The decrease in density in the samples after 28 days compared to the samples at the age of 7 days averaged 19.19%. The minimum density decrease was 16.77% – from 968 to 829 kg/cm$^3$, which corresponds to a change in the density class of gas-reinforced concrete from D1000 to D850. The maximum density reduction is 21.70% from 903 to 765 kg/cm$^3$, i.e., from D950 to D800.

The obtained results on density reduction also extend the previous studies on the selection of cellular concrete compositions [5], [6], [7].

The results of predicting the strength and density of the cellular ash concrete of the second series of samples using the Statistica 10 software package are shown in Figure 8.
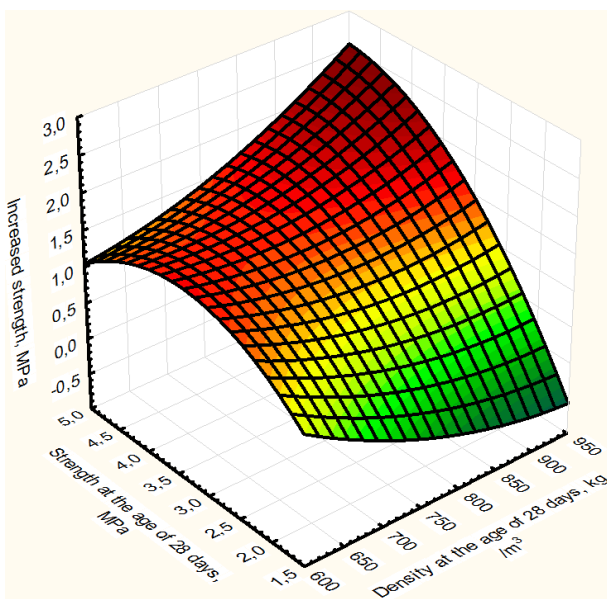


a) Graph of the dependence of strength, density, and strength increase
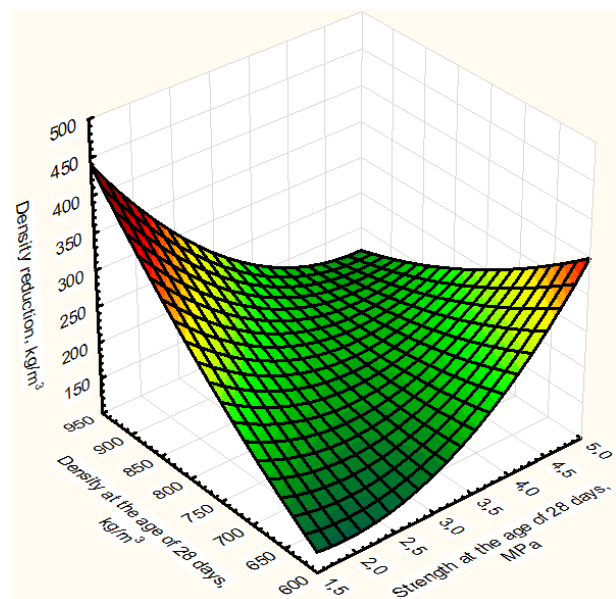
b) Graph of the dependence of strength, density, and density reduction

Figure 8 – Dependency graphs for aerated concrete hardened under normal conditions

Analysis of the obtained results showed that as in series 1, the observed increase in strength and decrease in density at the design age of 28 days compared to the strength at the age of 7 days during the strength gain under natural conditions occurs evenly proportionally.

The average strength gain of 42.62% is quite consistent with previous studies that showed the dynamics of increasing the strength of cellular concrete of non-autoclave hardening at the ages of 7 and 28 days. The results on the dynamics of density of cellular concrete of non-autoclave hardening at the age of 7 and 28 days (density decrease by 19.19% on average) are new and expand the studies [5], [6], [7], [9].

## 4. Conclusions

This study proves that it is possible to predict both the compressive strength and the density of ash concrete.

It was found that the strength at the design age increased by 34.67% compared to the strength at the age of 1 day during heat treatment of samples and by 42.62% compared to the strength at the age of 7 days without heat treatment of samples.

Changes in the density of aerated ash concrete at different hardening periods have been established. It was revealed that the density at the design age decreased by 11.07% compared to the density at the age of 1 day during heat treatment of samples and by 19.19% compared to the density at the age of 7 days without heat treatment of samples.

The results obtained have practical significance for scientists and engineers involved in the development of cellular concrete formulations.

## Acknowledgments

## References

[1] R. Suryanita, "Experimental study on performance of cellular lightweight concrete due to exposure high temperature," *International Journal of GEOMATE*, vol. 21, no. 83, Jul. 2021, doi: 10.21660/2021.83.6287.

[2] O. V. Rudenko, D. K. Anop, A. O. Lutai, N. V. Soshnikov, Z. A. Aubakirova, and E. I. Kuldeyev, "Global and Domestic Experience of Aerated Concrete Production and the Possibility of Using Local Materials," *Bulletin D. Serikbayev of EKTU*, no. 4, pp. 324–334, Dec. 2023, doi: 10.51885/1561-4212_2023_4_324.

[3] *GOST 25485-89. Cellular concretes. Specifications*. 1990, p. 15.

[4] *GOST 21520-89 Small-sized wall blocks of cellular cancrete. Specifications*. 1990, p. 7.

[5] D. Aljaboobi, I. Burakova, A. Burakov, R. Sldozian, and A. Tkachev, "Production of non-autoclaved aerated concrete with graphene oxide and plasticizer additives," *News of higher educational institutions. Construction*, no. 3 (771), pp. 52–60, Mar. 2023, doi: 10.32683/0536-1052-2023-771-3-52-60.

[6] F. Peng, C. Chen, S. Jiu, Q. Song, and Y. Chen, "Preparation and Characterization of Novel Sulfoaluminate-Cement-Based Nonautoclaved Aerated Concrete," *Materials*, vol. 17, no. 4, p. 836, Feb. 2024, doi: 10.3390/ma17040836.

[7] I. S. Raj and K. Somasundaram, "Sustainable Usage of Waste Materials in Aerated and Foam Concrete: A Review," *Civil Engineering and Architecture*, vol. 9, no. 4, pp. 1144–1155, Jul. 2021, doi: 10.13189/cea.2021.090416.

[8] N. N. Lam, "Recycling of AAC waste in the manufacture of autoclaved aerated concrete in Vietnam," *International Journal of GEOMATE*, vol. 20, no. 78, Feb. 2021, doi: 10.21660/2021.78.j2048.

[9] T. T. Nguen and D. V. Oreshkin, "Selection and optimization of composition of non-autoclaved aerated concrete mixture for conditions in Vietnam," *Internet-Vestnik VolgGASU*, no. 2(33), pp. 1–7, 2014.

[10] O. V. Rudenko, N. A. Charykov, N. A. Kulenova, M. A. Sadenova, D. K. Anop, and E. Kuldeyev, "Aerated Concrete, Based on the Ash of Thermal Power Plants, Nanostructured with Water-Soluble Fullerenols," *Processes*, vol. 12, no. 10, p. 2139, Oct. 2024, doi: 10.3390/pr12102139.

[11] *GOST 12730.0-2020 Concretes. General requirements for methods of determination of density, moisture content, water absorption, porosity and water tightness*. 2021, p. 3.

[12] *GOST 10180-2012 Concretes. Methods for strength determination using reference specimens*. 2013, p. 36.

[13] A. M. Grjibovski, S. V. Ivanov, and M. A. Gorbatova, "Descriptive statistics using statistica and spss software," *Science & Healthcare*, no. 1(18), pp. 7–23, Mar. 2016, doi: 10.34689/SH.2016.18.1.001.

**Information about authors:**

*Darya Anop* – Candidate of Technical Sciences, D. Serikbaev East Kazakhstan Technical University, Ust-Kamenogorsk, Kazakhstan, darjagalkina@mail.ru

*Olga Rudenko* – Candidate of Technical Sciences, D. Serikbaev East Kazakhstan Technical University, Ust-Kamenogorsk, Kazakhstan, o_rudenko_vkqtu@mail.ru

*Vladimir Shevlyakov* – Candidate of Technical Sciences, D. Serikbaev East Kazakhstan Technical University, Ust-Kamenogorsk, Kazakhstan, shevlyakovvf08@mail.ru

*Zulfiya Aubakirova* – PhD Student, Abylkas Saginov Karaganda Technical University, Department of Construction Materials and Technologies, Karaganda, Kazakhstan, aubakirova.zulfiya@mail.ru

*Nikolai Soshnikov* – Technician, D. Serikbaev East Kazakhstan Technical University, Ust-Kamenogorsk, Kazakhstan, nik.soshnikov.66@mail.ru

*Meiram Begentayev* – Rector, Satbayev University, Almaty, Kazakhstan, m.begentayev@satbayev.university

**Author Contributions:**
*Darya Anop* – modeling, analysis.
*Olga Rudenko* – drafting, editing.
*Vladimir Shevlyakov* – concept, methodology.
*Zulfiya Aubakirova* – resources, interpretation.
*Nikolai Soshnikov* – data collection, testing.
*Meiram Begentayev* – funding acquisition, visualization.

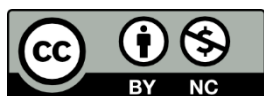**Conflict of Interest:** The authors declare no conflict of interest.

**Use of Artificial Intelligence (AI):** The authors declare that AI was not used.

*Article*

# Effect of glass waste on ceramics and concrete production

Danara Mazhit, Zhanar Kaliyeva, Daniyar Bazarbayev

Department of Technology of Industrial and Civil Engineering, L.N. Gumilyov Eurasian National University, Astana, Kazakhstan
*Correspondence: zhanna-080477@mail.ru

**Abstract.** The article is devoted to the study of using glass waste for ceramics and concretes production. The results of the spectral analysis of glass composition are presented, and phase changes and their impact on the microstructure and strength properties of ceramics and concrete are studied. Scanning electron microscopy and energy dispersive X-ray spectroscopy of the final material are discussed. As a result, it was revealed that after 28 days, concrete with added glass powder delayed the strength rise, but by day 112, the strength had considerably grown to 76.36 MPa. This results from pozzolanic reactions, where calcium hydroxide and glass combine to generate more hydration products that boost strength. Glass-based ceramic shows 13.20 MPa compressive strength, which satisfies construction material criteria, and was achieved by adding glass waste at a level of 10% of the clay mass. In addition to lowering the demand for natural mineral resources, the use of glass in ceramic blends promotes sustainable development and lessens the environmental load. Both the ceramic and concrete samples had a high content of $SiO_2$ and $Al_2O_3$ oxides. These are the main components that provide the material with high mechanical strength and chemical resistance. In the Spectral analysis of glass, in all the graphs, we see a high tendency for silicon dioxide (silica). This is explained by the fact that $SiO_2$ belongs to the group of glass-forming oxides, i.e., it is prone to the formation of supercooled melt-glass.

**Keywords:** production waste, concretes, ceramics, recycling, physical and mechanical properties.

## 1. Introduction

One of the top concerns for construction materials research is the development of efficient thermal and structural insulation materials, which is a difficult procedure. It is worth noting that the rational obtain of unprocessed materials and the full involvement of man-made waste in production are paramount in this area. Experience both domestically and internationally demonstrates that one of the most promising uses for industrial waste processing is the creation of construction materials, which makes it possible to meet the need of developed countries for raw materials up to 40% [1].

The use of industrial wastes in concrete products has certain benefits [2]. The combined use of fuel-containing waste and chemical compounds that prevent water evaporation can compensate for the shrinkage deformation of monolithic concrete and increase its crack resistance [3].

[4] used waste containing saponite in the production of fine-grained concrete with high levels of strength, frost resistance, and workability. In experimental models of vibrating reinforced concrete columns, the type of technology used in [4] had a major impact on the physical, mechanical, and structural features of concrete. According to [5], [6], the slag and fly ash are useful supplementary materials for enhancing the qualities of cement-concrete. These works show that an increase in cement consumption and the amount of filler in self-compacting concrete causes the concrete mixture's viscosity to drop. They found that if the amount of filler exceeds 15% by weight of cement, the viscosity is practically independent of cement consumption. Additional cementitious materials (ACMs) such as fly ash, ground blast furnace slag, fumed silica, and metakaolin are being utilized more frequently as binders for high-strength and high-performance concretes [7]. [8] created research

and technical bases to produce and use the concrete based on ash-slag mixtures of thermal power plants. They divided the ash and slag combination into a fine-grained fraction with slag passing through a 5 mm sieve. Next, the fine-grained fraction, slag, cement, and mixing water are dosed in the mixer individually based on the concrete's composition. It was discovered that this technological advancement enables concrete to be strengthened by 20–30% while consuming 15.20% less cement in the concrete production with the same strength. [9] attempted to fully substitute the coarse aggregate with a broken concrete and a portion of a fine aggregate with crushed glass, obtaining compositions replacing these aggregates by 20%, 25%, and 30%. The primary findings of this study demonstrated that the maximum compressive strength, which considerably surpasses the strength of concrete grade B35 and approaches the strength of concrete grade B40 and B45, is achieved when glass is used as a fine aggregate replacing sand by 30%. This suggests that glass is suitable for use in a variety of structures. In addition, they showed that strength growth does not occur linearly as the amount of glass in concrete samples increases, but instead, the rate of strength growth slows down with time. [10] developed a technology for producing high-strength concrete based on industrial and household glass waste. Glass as a filler for concrete compositions usually reduces the strength of the material due to the chemical interaction of glass and cement. Therefore, the researchers presented a new approach to create composite glass concrete, crushing broken glass. Glass particles of about 50-60 micrometers in size, obtained in a ball mill, were used as a filler. Glass was also used as a binder, but crushed finer up to one micrometer. As a result of a series of experiments, they managed to increase the strength of the glass concrete composition by 2.5 times.

Ceramic manufacturing is one of the industries that utilize the materials the most. The loss of natural resources used as raw materials for the ceramic industry is a serious problem for this sector of the economy and affects the price and quality of ceramic products. In this regard, [11] took into consideration the possibilities of employing mine waste in the form of ultramafic rocks (wehrlites and dunite) as an additive in the manufacturing of building ceramics. [12] investigated the prospect of creating facing ceramics from the waste of the metallurgical and glass sectors. According to the findings of the study, a batch of 40% clay and 60% cullet must be fired at 1050°C to produce laboratory samples of facing ceramics having a density of 2064 kg/m$^3$, a compressive strength of 42.24 MPa, and closed-pore formation. The impact of partially replacing the basic mix of ceramic floor tiles with waste urban glass is covered in [13]. Because of the high percentage of fluxing oxides in the waste, which promotes the formation of the glassy phase, increasing the waste addition to 20% results in an increase in linear shrinkage during firing, which subsequently gradually decreases to less than 3%. Bulk density rises as temperature and waste addition percentage increase. Water absorption diminishes as temperature and waste addition rise, with temperature having a greater impact than waste addition. [14] considered the prospect of producing facing ceramics and clinker based on brick clays utilizing large-tonnage waste glass products. The study selected a composite additive based on glass waste as a salt mineralizer required for sintering the clay-glass batch. The crystalline and amorphous phase is derived from sodium aluminosilicates. The X-ray phase analysis of the sintered ceramic composition revealed the presence of approximately 40% glass phases, which are uniformly distributed over the crystalline substance based on the composite's microphotography. [15] proposed to utilize waste in the form of finely ground slag, which is added to the raw material mixture to create wall ceramics that are stronger and have better thermal insulation properties. For wall-building materials, including ceramics, thermal conductivity remains a pressing issue. Therefore, as one of the particular solutions to this problem, the study suggested the use of porous ceramics in enclosing structures. Thus, while burnable additives added to the clay mass of ceramic wall materials effectively increase their porosity, they also control the firing temperature and encourage consistent sintering [16]. To enhance the thermal characteristics of ceramic products, the initial batch is commonly modified by incorporating a porous additive. For example, the use of a cullet clay - sodium hydroxide system (in a clay-glass cullet component ratio of 50:50, sodium hydroxide 4-6%) and a 2% additive of anthracite, limestone or a gas-forming agent allows expanding the scope of application of glass-ceramics as a structural heat-insulating material [17], [18], [19]. [20] studied the chemical composition of various wastes applicable to partially replace natural components in ceramics. The

waste from galvanic manufacture is a paste-like material with a moisture content of 65–85% and a density of 1160–1240 kg/m$^3$. The sludge's composition and moisture content determine whether or not it can be used in a ceramic charge. The characteristics of ceramic products are mostly influenced by the bulk content of calcium carbonate in the sludge. In this regard, [21], [22] studied the effect of galvanic slurries on ceramic materials. They revealed on test samples that as the sludge content increases above 9%, substances such as calcium carbonate and iron oxides increase, which leads to an increase in the melt and intensive sintering of the shard. Thus, the introduction of up to 9% galvanic sludge into the batch helps preserve the porous structure and can be used as an additive for ceramic materials used in construction. To create ceramics, [23] proposed compositions based on red clay, including cullet and waste from the pulp and paper industries. The study showed that when burnt at 1050 °C and 1100 °C, ceramic materials based on cullet and additives from the pulp and paper sector showed superior mechanical and physical qualities than materials made entirely of clay. [24] supports the possibility of using large-scale, widely distributed scrap brick waste produced when replacing outdated brickwork or crushing waste to increase the raw material base for the production of ceramic bricks with good mechanical and physical qualities as well as a low thermal conductivity coefficient. They investigated the effect of waste on the technological characteristics of clayey raw materials. [25] proposed the addition of red or bauxite mud to clay. They showed that bricks made only of clay have a lower compressive strength than bricks made with 50% red mud added to clay and sintering at 950°C for an hour. Eventually, they obtained a clayey material with compressive strength of 52.54 MPa, water absorption of 21%, and linear shrinkage of 0.46%. [26] made in-depth research of the sludge from titanium and ilmenite pigment manufacturing. They concluded that leftover brick wastes can be used as a technogenic raw material to manufacture ceramic bricks. Ceramic stone, made with the addition of crushed brick powder, is characterized by fairly high mechanical strength and is graded M100 and M150, which meets the regulatory requirements of [27]. The optimal content of crushed broken ceramic bricks is 10-30 wt. %. When it increases to more than 30 wt. %, the compressive strength is significantly reduced, and the samples' water absorption rate increases, and when its content decreases to less than 10 wt. %, properties remain virtually unchanged [28]. [29] performed X-ray diffraction (XRD) of glass, and differential thermal analysis (DTA) and scanning electron microscopy (SEM) of samples containing 10-15% glass, obtaining an improvement in mechanical and thermal properties but a deterioration in the appearance of samples containing 25% or more glass.

Previous studies showed numerous possibilities of using waste for various purposes. However, the constant increase of industrial waste in the world suggests the need for further improvements in this direction. Besides, the large amounts of silicon oxide found in glass can react with calcium hydroxide in concrete to produce an alkali-silicate reaction that reduces the material's durability. If the proportions of adding glass powder are not correctly selected, a decrease in the strength and frost resistance of ceramic and concrete products can be observed. Due to the addition of glass to the composition of building materials, new technological processes are added, including grinding, heat treatment, etc., and accordingly, they require significant costs. The lack of knowledge in the aforementioned aspects suggests that it is necessary to continue research, improving the composition and properties of the final material, and develop more effective methods incorporating glass waste for concrete and ceramic production. To overcome these issues and to make further attempts to utilize the waste and supplement the existing knowledge, this study aims to study the potential of glass wastes for concretes and ceramics.

## 2. Methods

Concrete and ceramic samples were prepared in laboratory conditions incorporating glass as an industrial waste.

The mixture for the concrete samples was prepared according to [30] using M400-graded cement from Heidelberg [31], sand and gravel from a quarry deposit 15 km from Astana, tap water, and glass. The sand was cleaned of foreign matter and sieved through a 0.63 mm sieve. It was

dehydrated in a drying chamber at a temperature of 100 °C. The gravel was washed thoroughly to remove various impurities and dried in similar conditions. The glass was taken from the remains of bottles crushed to a size of 1-2 mm and turned into powder (Figure 1a). The chemical composition of the powder glass was preliminarily revealed by XRD spectral analysis using a 5EDX9000B spectrometer [32]. Chemical element concentrations were assessed in relation to reference samples. Table 1 below shows the composition of the prepared concrete mixtures.

Table 1 – Composition of concrete samples, %

| No. | Cement | Sand | Gravel | Water | Glass waste |
|---|---|---|---|---|---|
| 1 | 10.20 | 23.49 | 50.02 | 9.16 | 7.12 |
| 2 | 10.20 | 20.43 | 50.02 | 9.16 | 10.18 |
| 3 | 10.2 | 17.42 | 50.02 | 9.16 | 13.2 |
| 4 | 10.2 | 14.51 | 50.02 | 9.16 | 16.11 |
| 5 | 10.2 | 10.73 | 50.02 | 9.16 | 19.89 |

The concrete samples were prepared in 10×10×10 cm cubic forms (Figure 2b) and were kept for 28 and 112 days, after which tests were carried out for compressive strength according to [33].



a) Crushed glass



Figure 2 – Concrete samples

Figure 1 – Preparation of concrete samples

The mixture for the ceramic samples was prepared using the crushed bottle glass as above and clay from a quarry deposit owned by the SG Brick factory [34] in Astana. The selected clay belongs to the group of medium-dispersed clays and is technologically characterized as moderately plastic and insensitive to drying and firing processes. The clay was preliminarily crushed using a jaw crusher before being mixed with glass powder. Several compositions of clay-glass mixtures were prepared with a glass fraction of 5%, 10%, 15%, and 25%. The ceramic samples were molded in a cylindrical shape with a diameter of 5 cm and a height of 10 cm. The samples were placed in a drying chamber and fired in a kiln at 1000-1200 °C, according to [35]. After that, the samples were tested for compressive strength according to [36] (Figure 2).



Figure 2 – Ceramic sample tested for compressive strength

Next, we selected the crushed particles of both concrete and ceramic samples and subjected them to SEM likewise [29] using a Hitachi TM4000Plus microscope in magnifications ranging from 25 to 2000 times to examine the microstructural characteristics of materials. The research on phase distribution and the characteristics of the concrete surface received the most attention. SEM analysis assisted in determining the surface's morphology and structure; the existence of cracks and other flaws, which can impact the strength and resistance to additional impacts; and the size and distribution of the materials particles. Additionally, we conducted an energy-dispersive spectroscopy (EDS) to reveal the composition of the concrete and ceramic materials measured in mass and atomic fractions of each element detected. This analysis helped identify the main chemical elements and see how they are distributed across the material at different points, and how the material looks from the inside at different magnifications.

## 3. Results and Discussion

The test results of the glass spectroscopy showed a high tendency of silicon dioxide (silica). Most of the types of glass mentioned in the literature contain significant amounts of $SiO_2$ (>70%). This is explained by the fact that $SiO_2$ belongs to the group of glass-forming oxides, and it is prone to the formation of supercooled melt-glass. The glass with such a percentage of $SiO_2$ has high strength, hardness, heat resistance, and chemical inertness. Thus, the chemical composition of glass relative to cement is presented in Table 2.

Table 2 – Chemical composition of glass relative to cement, %

| $Na_2O$ | MgO | $Al_2O_3$ | $SiO_2$ | $SO_3$ | Cl | $K_2O$ | CaO | $TiO_2$ | $Fe_2O_3$ |
|---|---|---|---|---|---|---|---|---|---|
| 0.136 | 0.61 | 2.4981 | 90.124 | 0.0401 | 0.0028 | 0.1674 | 12.7689 | 0.1418 | 1.0772 |

Table 2 above shows that the glass contains a significant amount of silica. High $SiO_2$ content usually ensures high chemical inertness and thermal stability of the material. As noted in [37], $Al_2O_3$ and CaO play a key role in the closure of hydrate phases in the cement paste. The presence of $Al_2O_3$ (about 4.3%) can ensure the formation of additional aluminate phases that increase early strength. A small amount of alkali oxides ($Na_2O$, $K_2O$) can, on the one hand, hinder hydration and, on the other hand, increase the risk of alkali-acid filling reaction. However, in this case, their content is relatively small.

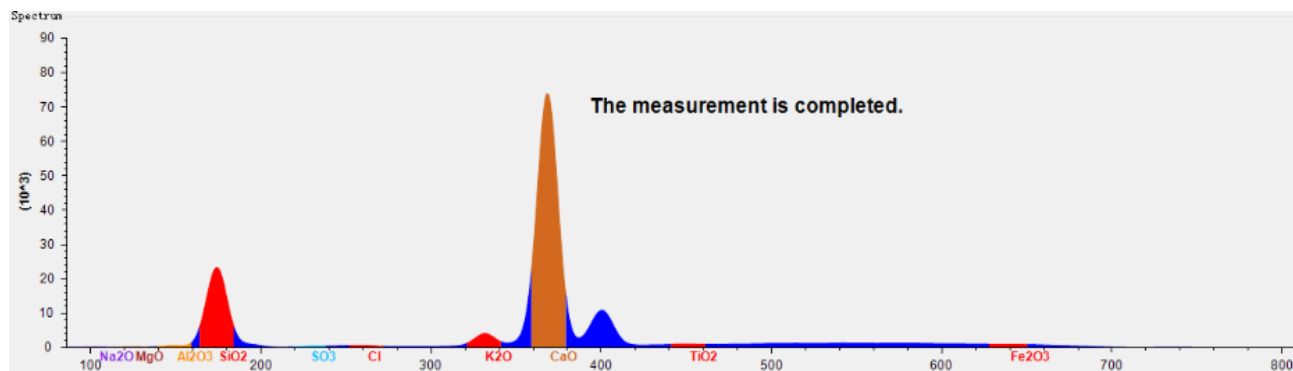Figure 3 shows spectra of glass compared to cement.



Figure 3 – Spectra of glass compared to cement

The high $SiO_2$ content in glass (around 70%) promotes a pozzolanic reaction when interacting with the cement matrix, which can lead to improved mechanical properties of concrete due to the additional formation of cement compounds [38]. High CaO content in cement promotes intensive hydration, which ensures the formation of a strong cement matrix. A slight decrease in CaO (our 62% compared to 64–66% in the literature) can slow down hydration reactions and affect early strength gain [39]. The lowest Cl content may indicate high chemical purity. Chlorine is usually added to glass

as a flux to improve fusibility and remove gas bubbles during melting. The presence of 2.5% $Al_2O_3$ in the glass composition shows improved mechanical and thermal properties of the glass.

The compressive strength of concrete was 20.50 MPa after 28 days, but after 112 days, it was 76.36 MPa. The maximum compressive strength in this concrete is achieved by using glass as a fine aggregate instead of sand at 20% replacement, while in [9], it reached 30%. Several studies suggest that a longer curing time is beneficial for strength growth and that a higher specific surface area of recycled and broken glass may lead to a bigger increase in compressive strength [37]. Because the "alkali-silicate reaction" is negligible and may even result in a decrease in strength because of the initial weak bond between the glass and the cement matrix, adding glass powder to concrete can slow down the strength gain process in the early stages while simultaneously contributing to an increase in strength later on. Due to the hydration of cement, concrete becomes stronger over time, and the effect is enhanced in later stages when glass particles containing amorphous silica are present. This helps to generate other hydration products, including hydrated calcium silicates (C-S-H), which boost strength. Pozzolanic reaction: Glass acts as a pozzolanic additive since it is an amorphous substance with a high silica content. This indicates that it can generate more C-S-H gels by interacting with calcium hydroxide that is released during cement hydration.

The compressive strength of the ceramic material was 13.14 MPa. This was achieved with the addition of glass in the amount of 15% of the total mass of clay. Since the typical strength values for wall materials are between 10 and 15 MPa, a result of 13.14 MPa might suggest reduced porosity and efficient compaction. Ceramic materials with a strength of 13.14 MPa are used as heat-insulating blocks, decorative wall panels, cladding for buildings, and load-bearing walls.

To make the material more appealing for a range of climates, thorough research must be carried out to ascertain its resilience to cold, durability, and aggressive environment behavior.

Figure 4 shows concrete's microstructure analysis report by Scanning electron microscope.


a) Magnification of 25x


c) Magnification of 1000x


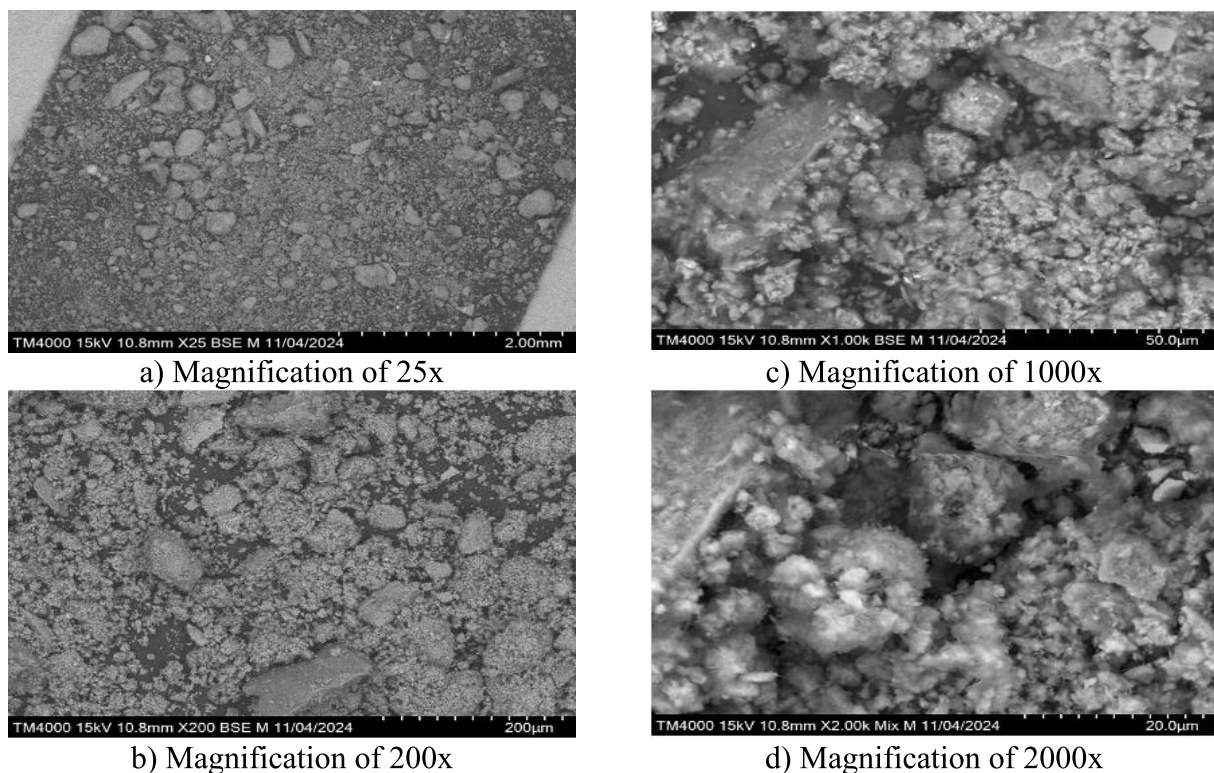b) Magnification of 200x


d) Magnification of 2000x

Figure 4 – Micrograph of concrete material surface

The above microphotograph of the concrete surface at different magnifications allows us to see the structure of the material. Individual particle detection, measurement, and analysis were made feasible by the capacity to extend to various sizes: a) The material's heterogeneity and porosity are demonstrated by 1 mm-sized particles. b) A more intricate structure is seen here, with individual filler

and cement matrix grains ranging in size from 50 to 200 microns. c) Particles range in size from 5 to 50 microns, and hydration products are apparent. d) The hydrated calcium silicate phases that give C-S-H gel its mechanical strength are apparent as crystalline structures with particle sizes ranging from 1 to 5 microns.

Compared to classic concrete, capillary pores can reach several micrometers, while in concrete with glass their number and size are reduced. This is confirmed by studies where glass acts as a microfiller, reducing porosity [40]. The area between the filler and the cement paste is usually more porous and vulnerable to moisture and ion penetration, and the addition of glass can result in a more even distribution of fine particles in the cement matrix [41]. The use of glass as an additive to the concrete mix has a positive effect on its microstructure. Compared to classic concrete, concrete with glass has a denser structure of cement stone, reduced capillary porosity, and potentially higher strength and durability. However, it is necessary to take into account the possible alkali-silicate reaction with an excessive amount of alkaline components, therefore, it is necessary to observe the optimal proportions of the glass additive to eliminate negative effects.

Figure 5 illustrates various elements found in the concrete with the peaks in the spectrum.
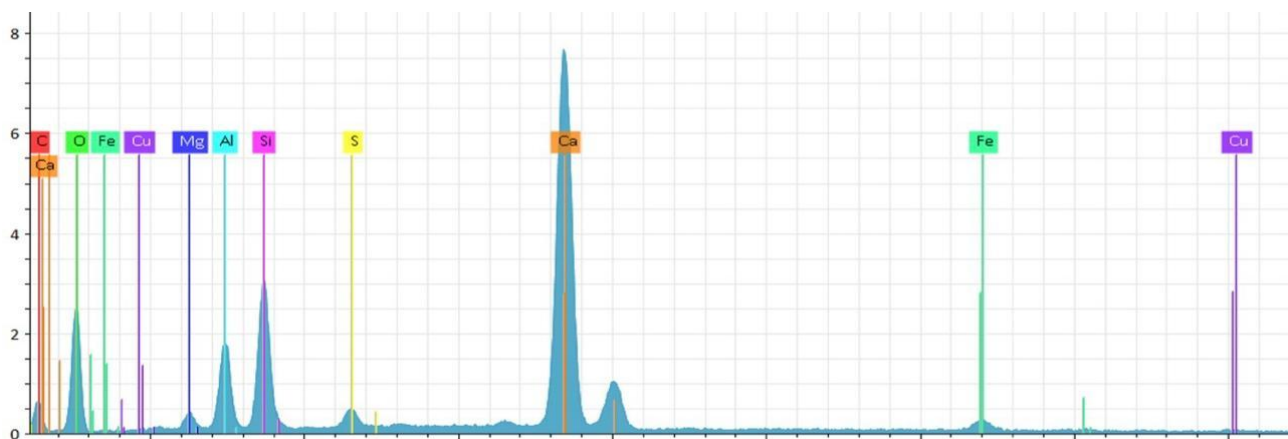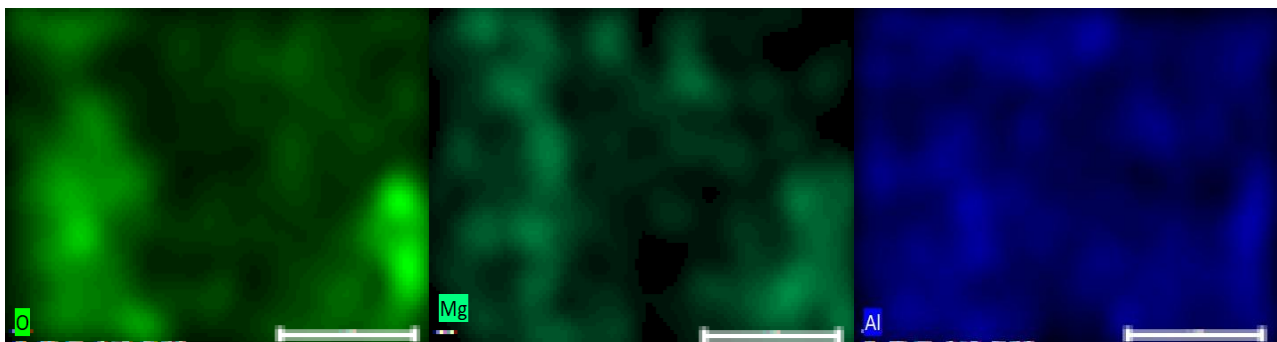


Figure 5 – Energy dispersion spectrum of concrete by elements

Based on the EDS results above, the percentage of elements found in concrete are as follows: O – 38.04%, Mg – 1.51%, Al – 6.95%, Si – 11.35%, S – 1.6%, Ca – 37.04%, Fe – 2.59%, and Cu – 0.92%. The oxygen is the primary ingredient of concrete's oxides and silicates. It contributes to the creation of oxide compounds (silicates and aluminosilicates), which make up the majority of concrete's structure and provide it with stability, mechanical strength, and water resistance. The primary ingredient in cement is calcium, which also helps to generate calcium hydrates (C-S-H) and portlandite ($Ca(OH)_2$), which give concrete its resilience. Because magnesia compounds are formed, magnesium has an impact on frost resistance. Iron, copper, sulfur, and aluminum all speed up the cement's hardening process and offer resistance against chemical impacts.

The element distribution map in Figure 6 shows how the elements are distributed in the concrete, with each color representing a different element: O, Mg, Si, Fe, Al, and C.
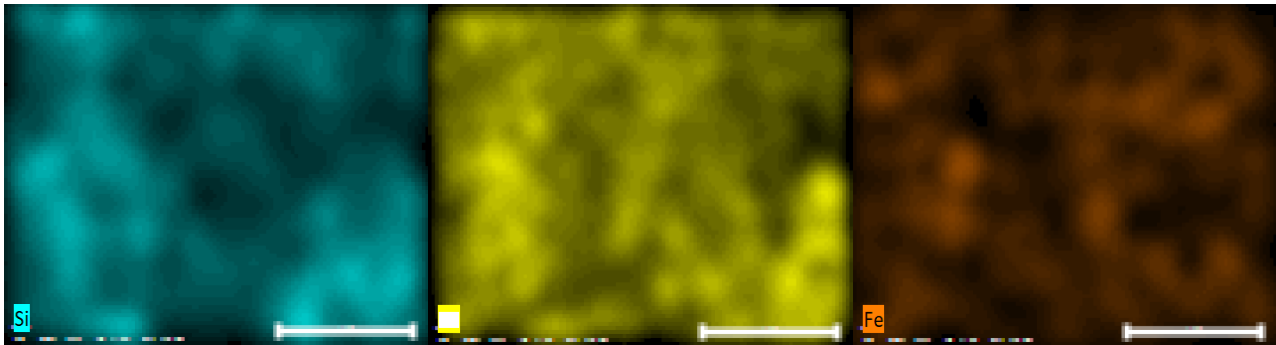
Figure 6 – Energy dispersive spectroscopy elements indicated in colors

Table 3 provides information about the chemical composition of concrete by oxides.

Table 3 – Oxide chemical composition in concrete, %

| MgO | $Al_2O_3$ | $SiO_2$ | $SO_3$ | CaO | FeO |
|---|---|---|---|---|---|
| 10.17 | 13.66 | 33.07 | 1.96 | 29.71 | 4.40 |

The decrease in CaO (29.71%) compared to conventional concrete (60-67%) confirms the presence of pozzolanic materials such as glass. The increased content of $Al_2O_3$ (13.66%) improves the thermal resistance of concrete, it exceeds the values of the classic composition of concrete on Portland cement (4-8%). MgO (10.17%) in this composition is also higher (1-5%), which affects swelling and shrinkage. $SiO_2$ is the main component of the pozzolanic reaction, which increases the density of the cement stone structure [40].
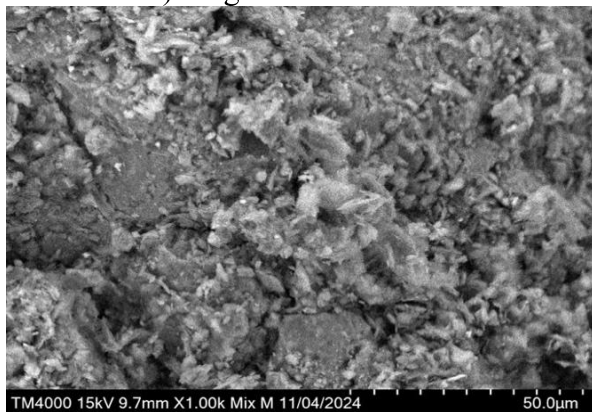
Figure 7 shows micrographs of deep (BSE) and mixed (Mix) surfaces of ceramic material burned at 1000 °C with 15% waste addition, in 4 different magnifications.
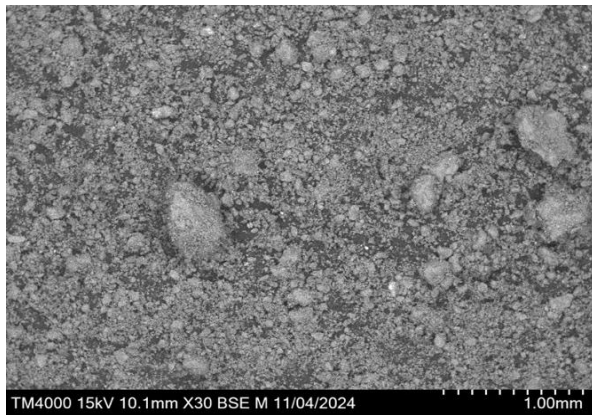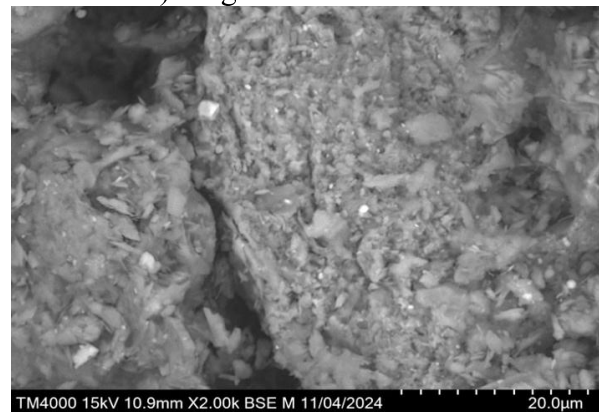


a) Magnification of 30x
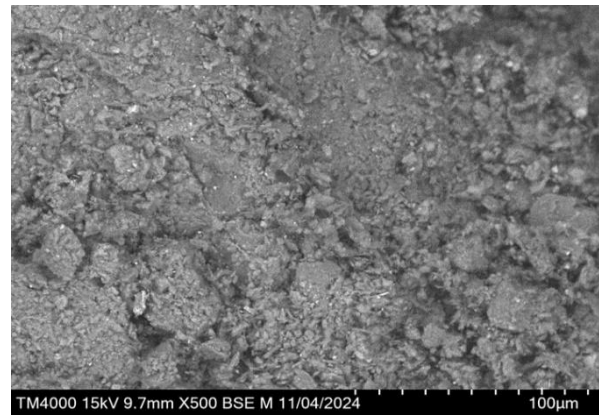


c) Magnification of 500x



b) Magnification of 1000x



d) Magnification of 2000x

Figure 7 – Micrograph of ceramic material surface

In Figure 7a, particles are large, angular, and ranging in size from 500 microns to 1 mm. In Figure 7b, particles range in size from 1 micron to 50 microns with fine grains and thin lamellar formations. In Figure 7c, particle size varies from 50 microns to 100 microns. We see a porous structure and heterogeneity in the distribution of the material. In Figure 7d, particles range in size from 0.5 microns to 20 microns. Here, we can see fine structures, microcracks, and areas of dense particle accumulation. Sizes from 0.5 microns to 1 mm affect its mechanical properties, such as strength and resistance to external influences.

It can be assumed that the appearance of microcracks and pores is associated with the addition of glass components, which leads to a change in the structure of the material during sintering. Probably, glass helps to reduce porosity and increase the strength of the material.

Comparing the obtained results with other studies, it can be noted that the addition of glass components similarly affected the microstructure of ceramic materials in the works of other authors [14]. With an increase in the cullet content from 0% to 10%, water absorption decreased from 15.67% to 15.10%, porosity decreased from 28.77% to 28.29%, and the maximum strength of 31.68 MPa was achieved with a cullet content of 7.5%, which is associated with the formation of a glassy phase filling the pores and microcracks in the ceramic structure. Studies conducted using spectral analysis also showed a decrease in porosity and an improvement in mechanical properties with the addition of a glass phase [42].

The sintered body displays the liquid phase as a result of the glass waste melting, which closes holes and reduces porosity, reducing water absorption and enhancing the mechanical properties of fired samples [43].

Mapping the surface of the ceramic sample is in view at Figure 8.
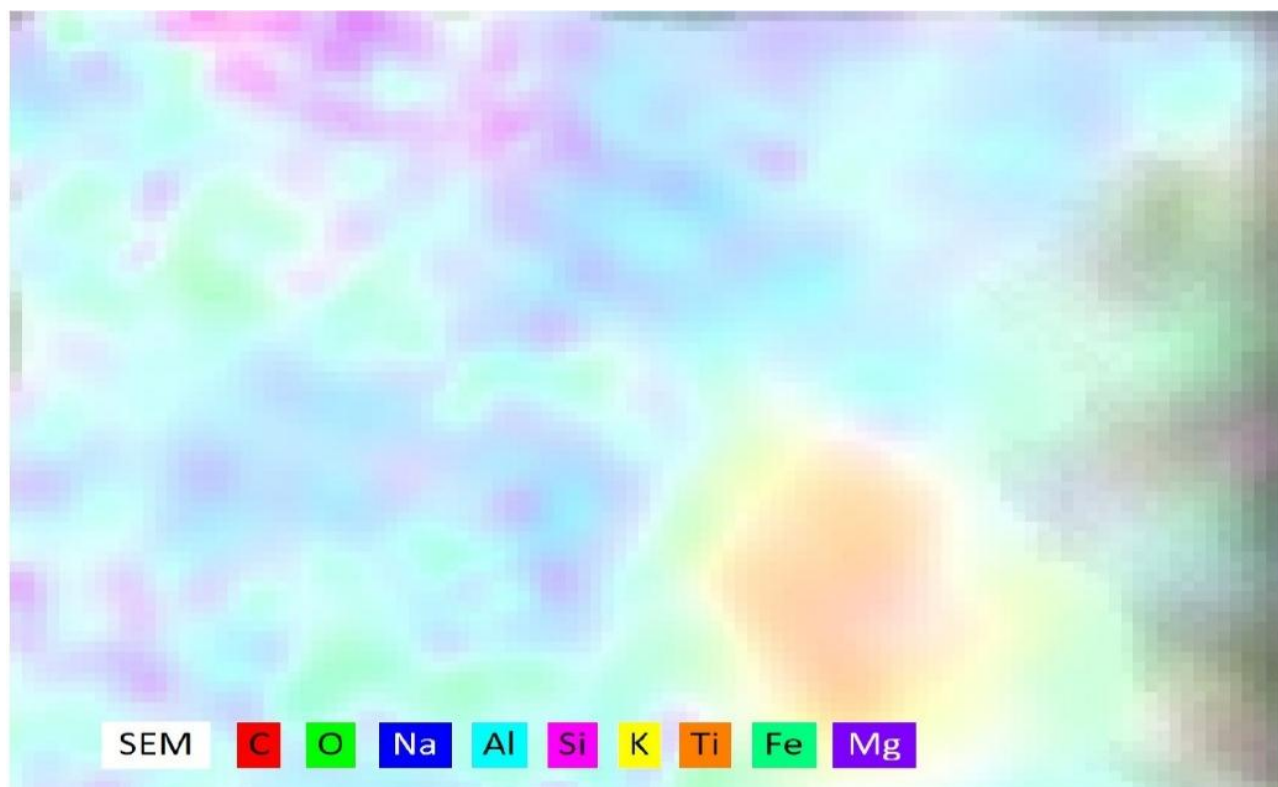


Figure 8 – Energy dispersive spectroscopy elements are indicated in colors

The elements of the ceramic sample presented on the map with magnification 4000x are highlighted in different colors, and we also see the designation of each element in a specific color. The predominance of green, blue and pink colors is evident, which corresponds to the high O, Al, Si content. We see this in the table below.

Table 4 shows the chemical composition of ceramic material by elements.

Table 4 – Element-by-element composition of ceramic material, %

| O | Na | Mg | Al | Si | K | Ti | Fe |
|---|---|---|---|---|---|---|---|
| 46.03 | 1.01 | 0.51 | 12.83 | 21.54 | 2.85 | 11.62 | 3.61 |

In Table 4 above, the high Si (21.54) and Al (12.83) content confirms the presence of the main ceramic phases, such as quartz and alumina, which is consistent with the data presented in many studies. The presence of K and Na in small quantities (2.85% and 1.01%, respectively) promotes sintering and the formation of a glassy phase. This improves the structural integrity of the material and facilitates the production process. Similar observations are given in works on the optimization of the composition of ceramic mixtures [44]. This ratio is important for ensuring the thermal stability and strength of ceramic products. The Ti percentage of 11.62% may suggest the presence of phases that boost the material's strength. Research suggests that some titanium-containing phases might aid in enhancing mechanical properties. More study is necessary to determine whether much titanium might lead to the production of undesirable pollutants. Although the Fe level is quite modest (3.61%), its presence can influence the final product's color and, in some situations, aid in the production of particular crystalline phases. According to the research, even trace levels of iron can alter ceramics' mechanical and optical properties [42].

Table 5 shows the chemical composition of ceramic material by oxides.

Table 5 – Oxide chemical composition of ceramic material, %

| MgO | $Al_2O_3$ | $SiO_2$ | K2O | $TiO_2$ | FeO | $Na_2O$ |
|---|---|---|---|---|---|---|
| 0.77 | 22.14 | 42.09 | 3.14 | 17.70 | 4.24 | 1.24 |

As can be seen from Table 5 above, the next oxides are responsible for the strength characteristics: $Al_2O_3$, $SiO_2$, $TiO_2$, $SiO_2$, $Al_2O_3$, and $Na_2O$. Aluminum provides mechanical strength and chemical resistance, especially at high temperatures, and silicon indicates resistance to acids. Titanium and iron oxide improve the corrosion properties of the material, and potassium oxide chemical resistance. The presence of alkaline oxides ($K_2O$, $Na_2O$) and MgO in small concentrations allows the reduction of the baking temperature, improves the process of glassy phase formation, and increases the illumination of the finished product [45].

## 4. Conclusions

The study's findings support the potential applications of cullet in the manufacturing of concrete and ceramic construction materials. The implementation of these technologies not only lessens the environmental impact of waste disposal but also enhances the end goods' performance attributes. However, the following crucial factors must be considered for successful industrial implementation:

1. Taking into consideration the existence of cullet, technological parameters for hardening concrete and firing ceramic goods are adjusted.

2. Production cost estimation that accounts for the substitution of glass waste for conventional raw materials.

3. Carrying out experimental studies at already-existing businesses to evaluate the true properties of materials.

4. Develop a scheme for the delivery of glass waste to building materials manufacturers, calculate all costs associated with transportation, etc.

4. It is necessary to develop appropriate technological schemes for the production of ceramic and concrete products using waste glass for various purposes.

5. Conduct experiments to define mechanical load resistance, moisture resistance, and frost resistance.

6. Try mixing glass waste with other industrial waste in certain proportions and see their effect on the properties of ceramic and concrete materials.

# References

[1] J. Pranckevičienė and I. Pundienė, "Effect of Mechanically Activated Nepheline-Syenite Additive on the Physical–Mechanical Properties and Frost Resistance of Ceramic Materials Composed of Illite Clay and Mineral Wool Waste," *Materials*, vol. 16, no. 14, p. 4943, Jul. 2023, doi: 10.3390/ma16144943.

[2] K. Khonjo, Y. Toleuov, A. Azbergenova, and A. Urumbayeva, "Study of cement binders applicable for modified cast-in-place concrete," *Technobius*, vol. 2, no. 3, p. 0022, Sep. 2022, doi: 10.54355/tbus/2.3.2022.0022.

[3] J. Plank, E. Sakai, C. W. Miao, C. Yu, and J. X. Hong, "Chemical admixtures — Chemistry, applications and their impact on concrete microstructure and durability," *Cem Concr Res*, vol. 78, pp. 81–99, Dec. 2015, doi: 10.1016/j.cemconres.2015.05.016.

[4] M. V. Morozova, "The effect of temperature and humidity treatment on the strength set of fine-grained concrete with the addition of saponite-containing material," *Nanotechnologies in Construction A Scientific Internet-Journal*, vol. 16, no. 3, pp. 227–234, Jun. 2024, doi: 10.15828/2075-8545-2024-16-3-227-234.

[5] A. Teara, D. S. Ing, and V. W. Tam, "The use of waste materials for concrete production in construction applications," *IOP Conf Ser Mater Sci Eng*, vol. 342, p. 012062, Apr. 2018, doi: 10.1088/1757-899X/342/1/012062.

[6] M. L. Berndt, "Properties of sustainable concrete containing fly ash, slag and recycled concrete aggregate," *Constr Build Mater*, vol. 23, no. 7, pp. 2606–2613, Jul. 2009, doi: 10.1016/j.conbuildmat.2009.02.011.

[7] I. Brás, P. C. Silva, R. M. S. F. Almeida, and M. E. Silva, "Recycling Wastes in Concrete Production: Performance and Eco-toxicity Assessment," *Waste Biomass Valorization*, vol. 11, no. 3, pp. 1169–1180, Mar. 2020, doi: 10.1007/s12649-018-0382-y.

[8] D. S. Smirnov, L. F. Mavliev, K. R. Khuziakhmetova, and I. R. Motygullin, "Effect of mineral additive based on ground blast furnace slag on the properties of concrete and concrete mixtures," *Известия Казанского государственного архитектурно-строительного университета*, no. 4, pp. 61–69, 2022, doi: 10.52409/20731523_2022_4_61.

[9] A. V. Shcherban, "Use of Crushed Concrete and Broken Glass in Secondary Concrete Production," *Young researcher of the Don*, vol. 8, no. 6, pp. 42–48, 2023.

[10] S. S. Dobrosmyslov *et al.*, "High-Strength Building Material Based on a Glass Concrete Binder Obtained by Mechanical Activation," *Buildings*, vol. 13, no. 8, p. 1992, Aug. 2023, doi: 10.3390/buildings13081992.

[11] V. A. Solonina, "Possibilities of using industrial waste to produce building ceramics," *Architecture, Construction, Transport*, no. 4(102), pp. 73–81, 2022, doi: 10.31660/2782-232X-2022-4-73-81.

[12] N. K. Skripnikova, O. A. Kunts, and , A. B. Ulmasov, "Glass and metallurgical wastes in facing ceramics production," *Vestnik Tomskogo gosudarstvennogo arkhitekturno-stroitel'nogo universiteta. JOURNAL of Construction and Architecture*, vol. 23, no. 6, pp. 165–171, Dec. 2021, doi: 10.31675/1607-1859-2021-23-6-165-171.

[13] E. M. A. Hamid *et al.*, "Recycling of urban glass waste in ceramic floor tiles toward sustainability," *Vietnam Journal of Chemistry*, vol. 62, no. 3, pp. 316–327, Jun. 2024, doi: 10.1002/vjch.202300237.

[14] I. A. Zhenzhurist, V. G. Khozin, and R. K. Nizamov, "The Use of Industrial Waste of Glass Products in the Technology of Construction Ceramics," *Stroitel'nye Materialy*, vol. 777, no. 12, pp. 34–36, 2019, doi: 10.31659/0585-430X-2019-777-12-34-36.

[15] J. Pizoń, J. Gołaszewski, M. Alwaeli, and P. Szwan, "Properties of Concrete with Recycled Concrete Aggregate Containing Metallurgical Sludge Waste," *Materials*, vol. 13, no. 6, p. 1448, Mar. 2020, doi: 10.3390/ma13061448.

[16] V. A. Solonina and M. D. Butakova, "Producing ceramic wall material using industrial waste," *IOP Conf Ser Earth Environ Sci*, vol. 1061, no. 1, p. 012048, Jul. 2022, doi: 10.1088/1755-1315/1061/1/012048.

[17] D. R. Damdinova, N. N. Anchiloev, and V. E. Pavlov, "Foam Glasses of Cullet – Clay – Sodium Hydroxide System: Compositions, Structures and Properties," *Building materials*, no. 8, pp. 38–40, 2014.

[18] T. K. Pavlushkina and Kisilenko N.G., "Using of the glass cut in the manufacture of building materials," *Glass and Ceramics*, vol. 84, no. 5, pp. 27–34, 2011.

[19] N. F. Zhernova, E. A. Doroganov, F. E. Zhernova, and I. N. Stepina, "Issledovanie materialov, poluchennyh spekaniem v sisteme «Glina - stekloboj»," *Bulletin of Belgorod State Technological University named after. V. G. Shukhov*, no. 1, pp. 20–23, 2013.

[20] I. A. Levitskii and A. I. Poznyak, "Thermophysical Characteristics of Furnace Tiles Obtained Using Galvanic Production Wastes," *Glass and Ceramics*, vol. 72, no. 3–4, pp. 130–134, Jul. 2015, doi: 10.1007/s10717-015-9740-4.

[21] M. A. Sukharnikova, E. S. Pikalov, O. G. Selivanov, É. P. Sysoev, and V. Yu. Chukhlanov, "Development of a Batch Composition for the Production of Construction Ceramic Based on Raw Material from Vladimir Oblast: Clays and Galvanic Sludge," *Glass and Ceramics*, vol. 73, no. 3–4, pp. 100–102, Jul. 2016, doi: 10.1007/s10717-016-9834-7.

[22] V. Mymrin *et al.*, "Red clay application in the utilization of paper production sludge and scrap glass to fabricate ceramic materials," *Appl Clay Sci*, vol. 107, pp. 28–35, Apr. 2015, doi: 10.1016/j.clay.2015.01.031.

[23] A. I. Fomenko, Kaptushina A.G., and Gryzlov V.S., "Expansion of raw material resources base for construction ceramics," *Construction Materials*, no. 12, pp. 25–27, 2015.

[24] L. Pérez-Villarejo, F. A. Corpas-Iglesias, S. Martínez-Martínez, R. Artiaga, and J. Pascual-Cosp, "Manufacturing new ceramic materials from clay and red mud derived from the aluminium industry," *Constr Build Mater*, vol. 35, pp. 656–665, Oct. 2012, doi: 10.1016/j.conbuildmat.2012.04.133.

[25] P. Santos, C. Martins, and E. Júlio, "Enhancement of the thermal performance of perforated clay brick walls through the addition of industrial nano-crystalline aluminium sludge," *Constr Build Mater*, vol. 101, pp. 227–238, Dec. 2015, doi: 10.1016/j.conbuildmat.2015.10.058.

[26] D. V. Makarov, O. V. Suvorova, and V. A. Masloboev, *Prospects of processing the mining and mineral processing waste in Murmansk Region into ceramic building materials*. Apatity: FRC KSC RAS, 2019. doi: 10.25702/KSC.978-5-91137-403-7.

[27] *GOST 530-2012 Ceramic brick and stone. General technical conditions*. 2012.

[28] G. Ascensão, M. P. Seabra, J. B. Aguiar, and J. A. Labrincha, "Red mud-based geopolymers with tailored alkali diffusion properties and pH buffering ability," *J Clean Prod*, vol. 148, pp. 23–30, Apr. 2017, doi: 10.1016/j.jclepro.2017.01.150.

[29] H. Darweesh, "Recycling of Glass Waste in Ceramics-Part II: Microstructure of Ceramic Products using XRD, DTA and SEM Techniques," *Research & Development in Material Science*, vol. 13, no. 4, May 2020, doi: 10.31031/RDMS.2020.13.000817.

[30] *GOST 27006-2019 Concrete. Rules for selection of composition*. 2019.

[31] C. Schlienkamp, "Heidelberg Cement AG," *Die Aktiengesellschaft*, vol. 66, no. 18, pp. r271–r272, Sep. 2021, doi: 10.9785/ag-2021-661827.

[32] ESI, "XRF spectrometer EDX9000B detects the content of residual elements Cu, Pb, Zn, As, Sn and K2O in sinter pellets." Accessed: Mar. 01, 2025. [Online]. Available: https://www.esi-xrf.com/info/xrf-spectrometer-edx9000b-detects-the-content-89964537.html

[33] *GOST 10180-2012 Concretes. Methods for strength determination using reference specimens*. 2012.

[34] G-Park, "SG Brick." Accessed: Mar. 01, 2025. [Online]. Available: https://gpark.kz/zavody/sg-brick/

[35] *GOST 21216-2014 Clay raw materials. Test methods*. 2014.

[36] *GOST 57606-2017 Ceramic composites. Compression test method at normal temperature*. 2017.

[37] C. Shi and K. Zheng, "A review on the use of waste glasses in the production of cement and concrete," *Resour Conserv Recycl*, vol. 52, no. 2, pp. 234–247, Dec. 2007, doi: 10.1016/j.resconrec.2007.01.013.

[38] I. D. Konorov and A. M. M. Ibrahim, "Using waste glass as a partial replacement for binder in concrete," *Economics of construction*, no. 11, pp. 183–190, 2023, doi: 10.24412/0131-7768-2023-11-183-190.

[39] H. F. W. Taylor, *Cement chemistry*, vol. 2. London: Thomas Telford Publishing, 1997. doi: 10.1680/cc.25929.

[40] P. K. Mehta and P. J. M. Monteiro, *Concrete: Microstructure, Properties, and Materials, 4th Edition*. McGraw-Hill Companies, Inc, 2006.

[41] R. Siddique, J. Khatib, and I. Kaur, "Use of recycled plastic in concrete: A review," *Waste Management*, vol. 28, no. 10, pp. 1835–1852, 2008, doi: 10.1016/j.wasman.2007.09.011.

[42] A. Salakhov, V. Morozov, N. Boltakova, R. Salakhova, and G. Faseeva, "Sovremennye metody issledovaniya dlya razrabotki tehnologii innovacionnyh keramicheskih materialov," *Herald of Technological University*, vol. 16, no. 21, pp. 95–97, 2013.

[43] R. Xiao, B. Huang, H. Zhou, Y. Ma, and X. Jiang, "A state-of-the-art review of crushed urban waste glass used in OPC and AAMs (geopolymer): Progress and challenges," *Cleaner Materials*, vol. 4, p. 100083, Jun. 2022, doi: 10.1016/j.clema.2022.100083.

[44] A. V. Khorina and T. I. Shelkovnikova, "INTERCONNECTION OF HIGH-STRENGTH CERAMIC PROPERTIES WITH MICROSTRUCTURE AND PHASE COMPOSITION," *Bulletin of the East Siberian State University of Technology and Management*, vol. 94, no. 3, pp. 74–89, 2024, doi: 10.53980/24131997_2024_3_74.

[45] Y.-H. Choi, Y.-W. Kim, I.-S. Han, and S.-K. Woo, "Effect of alkaline earth metal oxide addition on flexural strength of porous mullite-bonded silicon carbide ceramics," *J Mater Sci*, vol. 45, no. 24, pp. 6841–6844, Dec. 2010, doi: 10.1007/s10853-010-4939-9.

**Information about authors:**
*Danara Mazhit* – PhD Student, Department of Technology of Industrial and Civil Engineering, L.N. Gumilyov Eurasian National University, Astana, Kazakhstan, danara.08.1998@mail.ru
*Zhanar Kaliyeva* – Candidate of Technical Sciences, Associate Professor, Department of Technology of Industrial and Civil Engineering, L.N. Gumilyov Eurasian National University, Astana, Kazakhstan, zhanna-080477@mail.ru
*Daniyar Bazarbayev* – PhD, Associate Professor, Department of Technology of Industrial and Civil Engineering, L.N. Gumilyov Eurasian National University, Astana, Kazakhstan, phdd84@mail.ru

**Author Contributions:**
*Danara Mazhit* – concept, data collection, resources, drafting, interpretation.
*Zhanar Kaliyeva* – methodology, testing, visualization, editing, analysis.
*Daniyar Bazarbayev* – validation, review, specialized technical input, modeling.

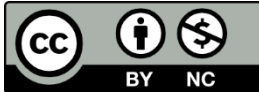**Conflict of Interest:** The authors declare no conflict of interest.

**Use of Artificial Intelligence (AI):** The authors declare that AI was not used.

*Article*

# Physicochemical properties of silica fume and fly ash from Tau-Ken Temir LLP and Pavlodar CHP for potential use in self-compacting concrete

[ID]Erzhan Kuldeyev[1], [ID]Zhanar Zhumadilova[1], [ID]Adlet Zhagifarov[1], [ID]Aigerim Tolegenova[1,*] [ID]Mussa Kuttybay[2], [ID]Abzal Alikhan[1]

[1]Satbayev University, Almaty, Kazakhstan
[2]Auezov University, Shymkent, Kazakhstan
*Correspondence: a.tolegenova@satbayev.university

**Abstract.** This article presents the results of a study on the structural and chemical properties of silica fume and fly ash from local plants, focusing on their potential as mineral additives in self-compacting concrete. Scanning electron microscopy (SEM) and X-ray fluorescence (XRF) analysis were used to investigate particle morphology, microstructure, and elemental composition. Silica fume was characterized by a high $SiO_2$ content (>75%), spherical particle morphology, and a smooth surface, which promotes the formation of a dense cement matrix. Fly ash exhibited a complex chemical composition dominated by $SiO_2$ and $Al_2O_3$ oxides, with spherical particles and surface roughness enhancing adhesion to the cement paste. The results demonstrated that the combined use of silica fume and fly ash has the potential to improve concrete workability, increase strength, reduce the water-cement ratio, and enhance durability due to microstructure densification. Partial cement replacement with these additives may not only optimize concrete performance but also reduce the environmental footprint of cement production. The findings highlight the efficiency of silica fume and fly ash as pozzolanic components for developing high-performance and sustainable self-compacting concrete.

**Keywords:** silica fume, fly ash, self-compacting concrete, mineral additives, pozzolanic materials, physical properties, microstructure, durability, sustainable construction.

## 1. Introduction

Cement production is accompanied by high $CO_2$ emissions, accounting for about 6-8% of global anthropogenic greenhouse gas emissions [1]. In addition, concrete mixtures often face problems of increased water consumption, shrinkage, porosity, and insufficient durability, especially under conditions of exposure to moisture and freeze-thaw [2]. The solution to these problems may be the partial replacement of cement with secondary cementitious materials such as silica fume and fly ash, which can improve the density, strength and rheological properties of cement compositions, as well as reduce the negative impact on the environment [3-4]. The combined application of cement, silica fume, and fly ash can significantly enhance the properties of self-compacting concrete while reducing cement consumption. Silica fume, due to its pozzolanic activity and tiny particle size, promotes and enhances the cohesion and strength of the concrete [5]. Fly ash, having the ability to fill pores and enhance the granulometric composition, promotes reduced water consumption in the mixture and increases its plasticity. By reducing cement consumption when using these mineral additives, $CO_2$ emissions are reduced during production, and general properties are improved, such as strength, shrinkage resistance, durability, and resistance to aggressive environments [6-7].

Numerous studies have shown that the application of silica fume and fly ash has a significant effect on the microstructure and properties of concrete. [9] found that the combined application of these additives enhances compressive and bending strength, as well as the microstructure of cement stone. At the same time, [10] confirmed similar results, noting a synergistic effect associated with

increasing the packing density and pozzolanic activity of cement. Studies by [11] have shown that the application of fly ash and silica fume increases concrete's resistance to aggressive media, reducing permeability and improving its microstructure. Using machine learning techniques to analyze additive compositions [12] could accurately predict concrete strength, emphasizing optimizing their content.

In addition, the binary additive systems studied by [13] contribute to reducing the water-cement ratio, improving rheological properties, and increasing strength. The effect of fly ash on the micro- and macro-level properties of concrete was investigated by [14], who noted the uniform distribution of aggregate and reduction of microcracks.

[15] confirmed that using fly ash and silica fume increases the strength of concrete, especially in high-performance compositions. [16] emphasized the importance of these additives to increase the resistance of concrete to chloride penetration and its durability. These achievements are supported by the conclusions of [17], who demonstrated that using fly ash and silica fume additives in combination with reinforcement with plastic fibers enhances fiber adhesion to the matrix and reduces concrete shrinkage.

A study by [18] showed that various substrate hardening modes with fly ash and silica fume additives contribute to high strength, even during wet hardening. [19] confirmed that the combination of fly ash and silica fume reduces the sensitivity of concrete to hardening conditions and provides high strength even under unfavorable care conditions.

[20] studied the substrate's resistance to chloride corrosion. They showed that using fly ash and silica fume reduces the permeability of concrete, significantly increasing its durability. These results highlight the prospects of using pozzolan additives to modify concrete properties.

Based on the analysis of existing studies, it has been established that the properties of region-specific mineral additives, such as silica fume produced by Tau-Ken Temir LLP and fly ash from Pavlodar CHP, remain insufficiently studied. There is a lack of comprehensive data on their effect on the properties of self-compacting concrete, particularly regarding their influence on rheology, hydration processes, microstructure formation, and durability. Therefore, this research aims to fill this gap by investigating the effect of silica fume and fly ash on the properties of self-compacting concrete, including its mechanical characteristics, microstructure, and durability.

The primary purpose of the study is to develop approaches for partially replacing cement in concrete mixtures with these locally produced mineral additives to enhance both the environmental sustainability and performance of concrete. The objectives of the work include determining the optimal dosages of silica fume and fly ash, evaluating their influence on the rheological, strength, and durability properties of concrete, and analyzing microstructural changes associated with their use.

## 2. Methods

As a reactive pozzolanic additive, we used silica fume MKU-95, produced by «Tau-Ken Temir» LLP (Karaganda, Kazakhstan), corresponding to [21]. The physical and chemical properties of silica fume were assessed based on the provided technical documentation of «QAZAQ INNOTEC» LLP and verified using standard laboratory techniques where necessary.

To modify the cement mortar, we used fly ash obtained at the Pavlodar CHP. Fly ash is a by-product of coal combustion and has pozzolan properties, which allows it to be used as an active mineral additive in cement systems [22]. Its chemical composition includes a high percentage of silica fume ($SiO_2$), which enhances the durability and mechanical properties of the cement mortar [23].

For experimental analysis, samples of silica fume and fly ash were analyzed in their raw state without incorporating them into cement pastes or mortars using scanning electron microscopy (SEM) and X-ray fluorescence (XRF). To determine the elemental composition of the material, an energy-dispersive X-ray spectroscopy (EDS) analysis was conducted. The primary focus was to evaluate their physical, chemical, and microstructural properties. For SEM and XRF analysis, a small amount of finely ground silica fume and fly ash samples were prepared by sieving with a 200-mesh to obtain a powder with a particle size of 74 microns (µm) (i.e., 0.074 mm). The microstructure of the materials

during SEM was analyzed using a Jeol JCM-7000 scanning electron microscope (Japan). The XRF analysis was carried out using a NEX CG II Series energy-dispersive X-ray fluorescence (EDXRF) spectrometer to determine the elemental composition of the material.

## 3. Results and Discussion

Table 1 presents the chemical composition of silica fume and fly ash.

Table 1 – Chemical composition of silica fume and fly ash

| Material | Chemical composition element ($\omega$, mass %) | | | | | |
|---|---|---|---|---|---|---|
| | C | O | Al | Si | Ca | Fe |
| Silica fume | - | 48.77 | - | 51.23 | - | - |
| Fly ash | 18.4 | 48.3 | 7.6 | 18 | 5 | 6.4 |

Table 1 shows that the chemical composition of silica fume consists primarily of silicon (Si) and oxygen (O), with mass fractions of 51.23% and 48.77%, respectively. This composition confirms the high purity of silica fume, which is mainly composed of silicon dioxide ($SiO_2$). The dominance of $SiO_2$ in silica fume is known to contribute to pozzolanic reactions in cementitious systems, enhancing concrete's overall durability and mechanical performance [24]. The chemical composition of fly ash contains multiple elements, including oxygen (48.3%), carbon (18.4%), silicon (18%), aluminum (7.6%), calcium (5%), and iron (6.4%). The presence of silicon and aluminum oxides indicates the pozzolanic nature of fly ash, which can react with calcium hydroxide in cement to form additional binding compounds, improving the long-term strength and durability of concrete [25]. The presence of carbon in fly ash suggests a certain level of unburned residue, which may influence its performance in cementitious mixtures [26].

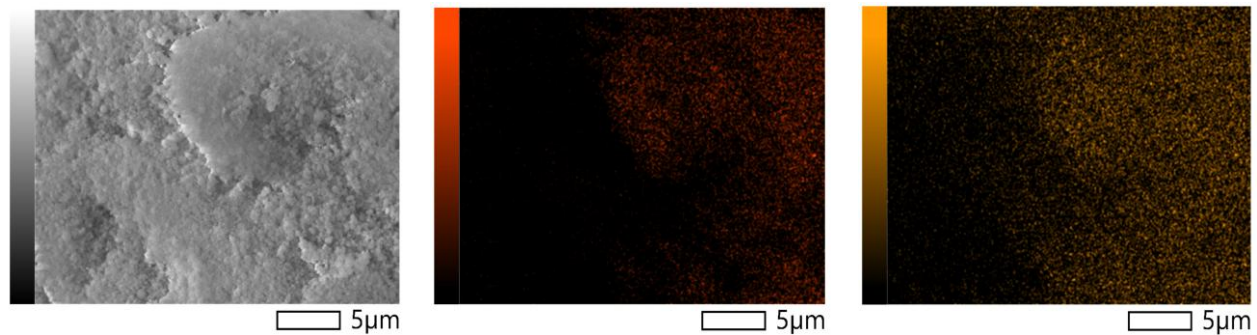Figures 1 and 2 below show the results of the SEM analysis of the silica fume.
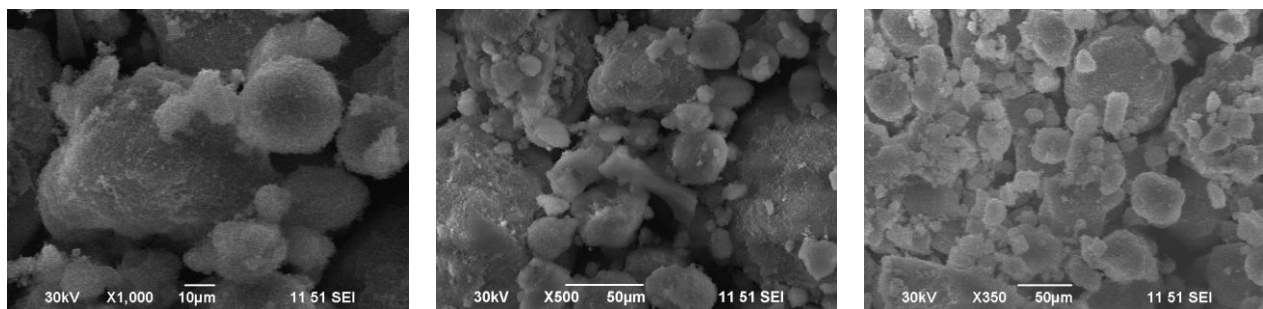


a) Magnification of ×1000       b) Magnification of ×500       c) Magnification of ×350

Figure 1 – Microstructure of silica fume from SEM



a) Image of silica fume particles       b) Carbon (C)       c) Aluminum (Al)

Figure 2 – Elemental mapping characterization of silica fume

SEM images at ×1000 magnification (Figure 1a) demonstrate that silica fume particles are predominantly spherical, which is characteristic of materials formed during the condensation of silica oxide vapors. The particle size ranges from approximately 100 nm to 1–2 μm, indicating a high degree of dispersion and homogeneity. The images in Figures 1b and 1c at lower magnifications (×500 and ×350) reveal that individual particles tend to form agglomerates of various sizes due to interparticle forces, such as van der Waals interactions [27]. These agglomerates significantly exceed the size of individual particles, which should be considered when using silica fume in cementitious materials. Additional dispersion techniques may be required to ensure uniform particle distribution within the cement matrix. Higher magnification SEM images indicate that the surface of silica fume particles is smooth, with minimal defects. This smooth surface enhances particle adhesion to the cement matrix, which is expected to influence the mechanical properties of concrete composites positively. Elemental mapping performed on silica fume samples in Figure 2 confirms the uniform distribution of silicon and oxygen, with no visible impurities. The observed spherical morphology and fine particle size are consistent with the results reported by [28], who emphasized the role of silica fume in enhancing particle packing and reducing porosity in cement composites. The tendency for agglomeration was also noted in the work of [29], highlighting the need for proper dispersion methods when incorporating silica fume into concrete.

Figures 3 and 4 below show the results of the SEM analysis of the fly ash, with Figure 4 demonstrating the concentration of individual elements of fly ash at the micro level, where color gradients reflect the intensity of the presence of a particular element.
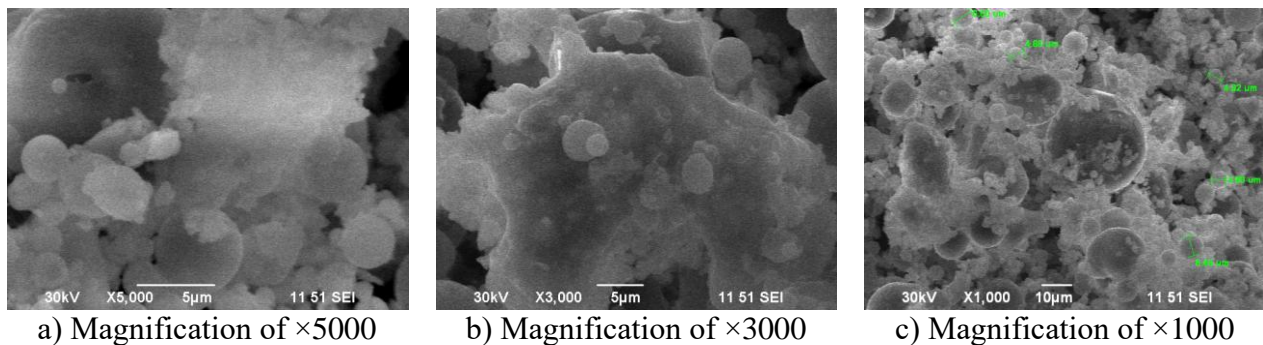


| a) Magnification of ×5000 | b) Magnification of ×3000 | c) Magnification of ×1000 |

Figure 3 – Microstructure of fly ash from SEM



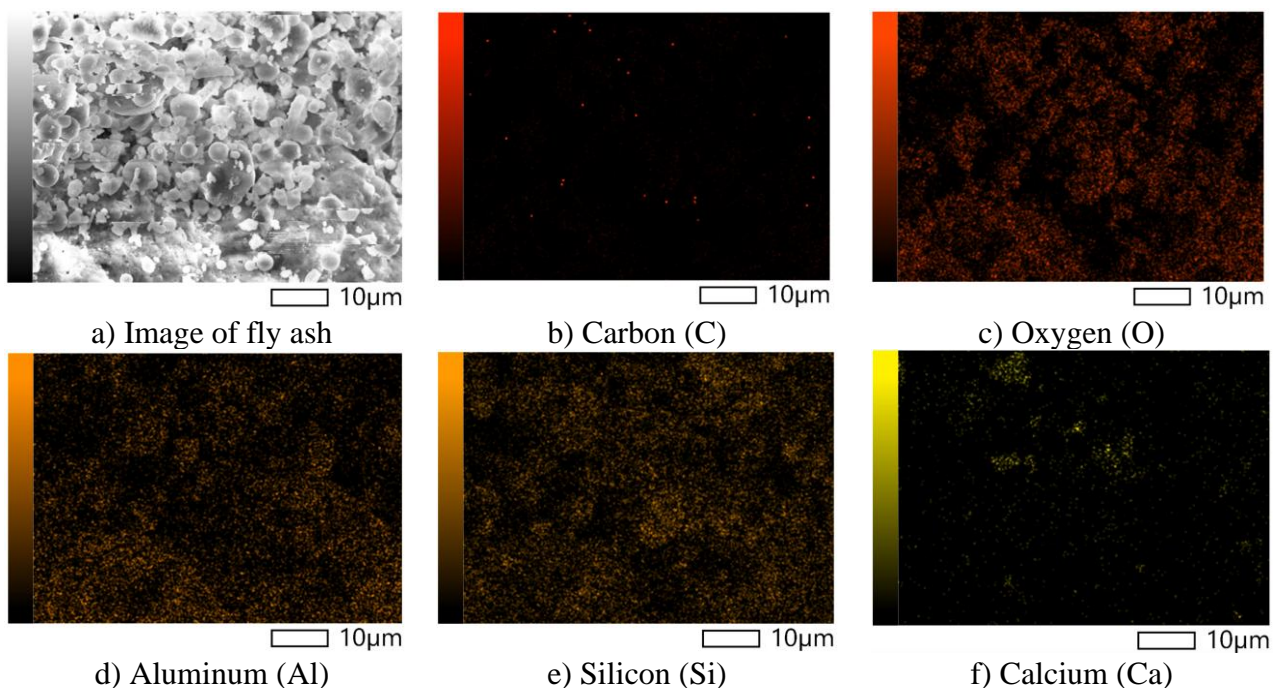| a) Image of fly ash | b) Carbon (C) | c) Oxygen (O) |
| d) Aluminum (Al) | e) Silicon (Si) | f) Calcium (Ca) |

Figure 4 – Elemental mapping characterization of fly ash

Figure 3a, which demonstrates SEM images at ×5000 magnification, shows that fly ash particles predominantly have a spherical or near-spherical shape, which is typical for materials obtained from high-temperature combustion processes. The particle sizes vary from approximately 0.5 to 10 μm. Certain particles exhibit rough or irregular surfaces with small, embedded inclusions, indicative of the heterogeneous chemical nature of fly ash. These inclusions are likely associated with the presence of silica, alumina, and iron oxides, which may provide additional pozzolanic and binding properties. SEM image at ×1000 magnification (Figure 3c) shows that fly ash particles tend to form agglomerates, reaching sizes up to 20 μm. This agglomeration is attributed to physicochemical interactions between the particles. As with silica fume, the agglomeration may require additional dispersion measures during concrete preparation to ensure uniform particle distribution. The spherical shape of fly ash particles aligns with the findings of [30] and [31], who noted that this morphology improves workability and reduces water demand in concrete.

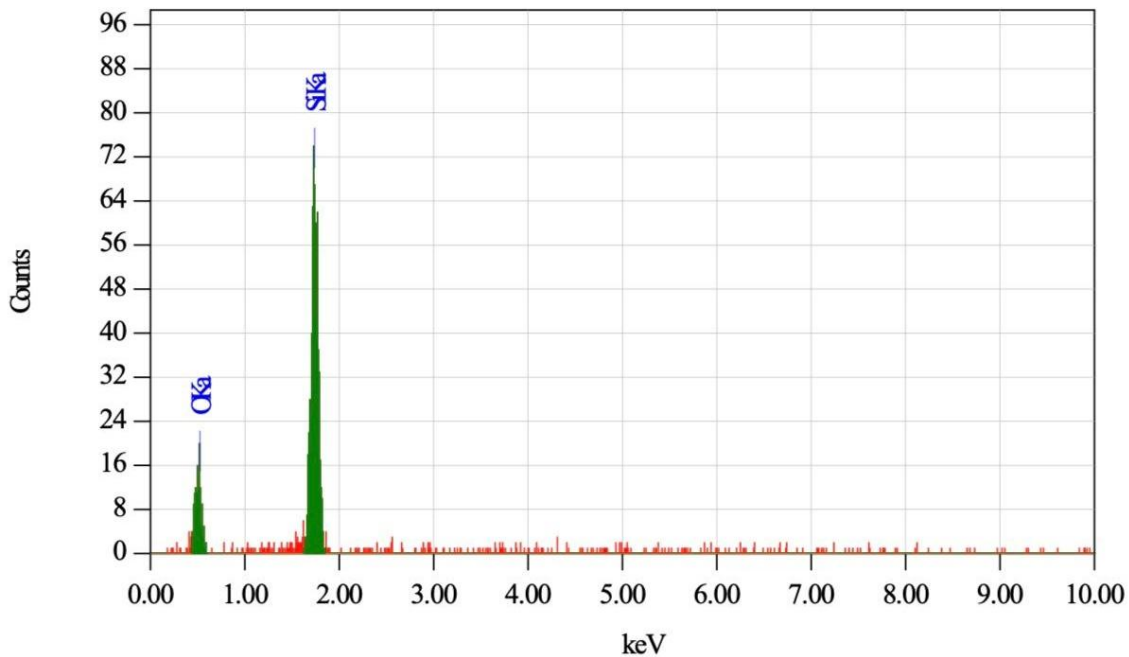Figure 5 below shows the results of the XRF analysis of silica fume.



Figure 5 – XRF spectrum of silica fume

XRF analysis from Figure 5 confirmed that silica fume is characterized by a high content of silicon dioxide ($SiO_2$), which is consistent with its standard chemical composition. The XRF spectrum clearly shows a dominant $SiK\alpha$ peak, indicating that $SiO_2$ accounts for more than 75% of the material's composition, almost coinciding with [32]. The presence of the oxygen ($OK\alpha$) peak further confirms that silica is in oxide form, which reflects the high purity of the material. The XRF data also revealed an absence or minimal presence of other elements, indicating a low level of impurities. This confirms the high quality of the silica fume, making it a particularly valuable pozzolanic material for high-performance concrete and cement composites. The high $SiO_2$ content is a key factor contributing to the pozzolanic activity of silica fume, enabling it to effectively interact with calcium hydroxide ($Ca(OH)_2$), which forms during cement hydration. This interaction results in the formation of additional calcium silicate hydrates (C-S-H), leading to the densification of the cement matrix and improvement in the mechanical strength and durability of concrete, as noted in [33]. Based on the XRF analysis, silica fume from the Tau-Ken Temir plant can be classified as a high-purity pozzolanic material suitable for applications in high-strength and self-compacting concrete, providing improved strength, reduced permeability, and enhanced durability.

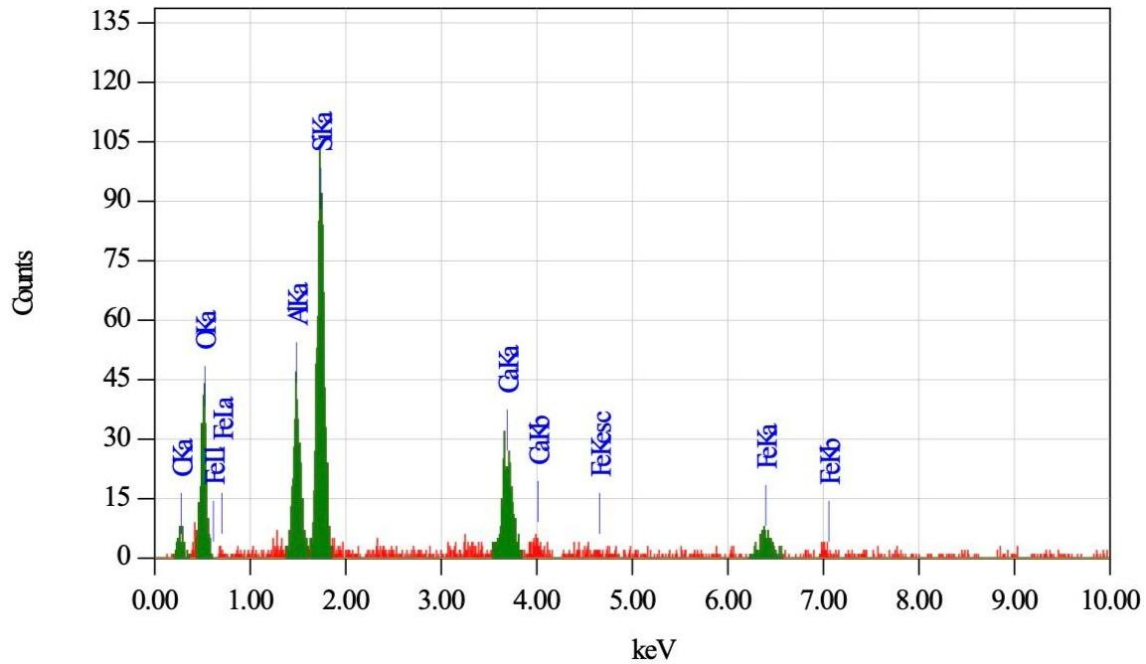Figure 6 below shows the results of the XRF analysis of fly ash.

Figure 6 – XRF spectrum of fly ash

As shown in Figure 6 above, the XRF analysis of fly ash allowed for the determination of its elemental composition and confirmed the presence of the primary oxides responsible for the material's pozzolanic activity. The XRF spectrum reveals the presence of strong SiKα and AlKα peaks, indicating a high content of silicon dioxide ($SiO_2$) and aluminum oxide ($Al_2O_3$), which form the primary matrix of fly ash. These oxides play a crucial role in the pozzolanic reactivity of the material, contributing to the strength and durability of cementitious composites [34]. The XRF spectrum also shows the presence of oxygen (OKα), confirming that the detected elements are present in oxide form. A calcium (CaKα) peak was recorded, indicating the presence of calcium oxide (CaO), which can participate in hydration reactions, improving the binding properties of fly ash. Iron peaks (FeKα and FeLα) were detected as well, corresponding to iron oxides ($Fe_2O_3$), which can influence the density, color, and certain physicochemical characteristics of the material. Additionally, trace amounts of potassium (Kα) and titanium (TiKα) were observed, indicating the complex chemical composition of fly ash. Although their concentrations are low, these elements may still indirectly affect the reactivity and performance of fly ash in cement systems. The XRF results demonstrate that fly ash is a multi-component oxide material with a high content of $SiO_2$ and $Al_2O_3$, confirming its suitability as a pozzolanic additive in cement and concrete. The presence of CaO and $Fe_2O_3$ suggests that the material can actively participate in cement hydration processes, while its pozzolanic properties contribute to improving strength and durability. These findings support the use of fly ash from the Pavlodar CHP to partially replace cement or use it as an active mineral additive in concrete, especially in alkaline environments. Earlier, in a study by [35], it was found that fly ash formed during the combustion of coal in thermal power plants contains significant amounts of silicon $SiO_2$ and aluminum $Al_2O_3$ oxides, which make up the bulk of its chemical composition. Besides, iron $Fe_2O_3$ and calcium CaO oxides are present in smaller amounts. Our results correspond to these data, confirming that the investigated fly ash has the acceptable properties required for pozzolan materials.

## 4. Conclusions

The study revealed key patterns in the behavior and properties of silica fume and fly ash as mineral additives for self-compacting concrete.

1. XRF analysis confirmed the high content of $SiO_2$ in silica fume (over 75%), which determines its pronounced pozzolanic activity. SEM images demonstrated that silica fume particles have a spherical shape, smooth surface, and a tendency to form agglomerates. The high dispersion

and purity of silica fume ensure its effective interaction with calcium hydroxide during hydration, which contributes to the densification of the cement matrix and an increase in strength and durability.

2. XRF analysis of fly ash showed that its composition is dominated by $SiO_2$ and $Al_2O_3$ oxides, which are responsible for its pozzolanic properties. SEM analysis confirmed that fly ash particles are predominantly spherical, with surface roughness and occasional agglomerates, characteristic of materials obtained from high-temperature coal combustion. The complex surface morphology of fly ash promotes adhesion to the cement matrix, improving the microstructure and mechanical properties of concrete.

3. The combined use of silica fume and fly ash allows for optimizing the composition of self-compacting concrete mixtures. Their simultaneous application contributes to reducing the water-cement ratio, increasing compressive and flexural strength, and enhancing resistance to aggressive environments. The synergy between the high dispersion of silica fume and the pozzolanic activity of fly ash leads to improved hydration processes and denser structure formation, which is especially important in the development of high-performance self-compacting concretes.

4. The results confirm the potential of silica fume and fly ash as effective mineral additives for the production of self-compacting concrete. Their partial replacement of cement not only improves the operational properties of concrete but also reduces its environmental impact, supporting the transition to more sustainable construction practices.

The findings of this study can serve as a basis for developing new high-performance concrete composites with improved strength, durability, and resistance to aggressive environments.

## Acknowledgments

## References

[1] R. M. Andrew, "Global CO $_2$ emissions from cement production, 1928–2018," *Earth System Science Data*, vol. 11, no. 4, pp. 1675–1710, Nov. 2019, doi: 10.5194/essd-11-1675-2019.

[2] P. K. Mehta and P. J. M. Monteiro, Concrete: microstructure, properties, and materials, Fourth edition. New York: McGraw-Hill Education, 2014.

[3] G. Sua-iam and B. Chatveera, "A study on workability and mechanical properties of eco-sustainable self-compacting concrete incorporating PCB waste and fly ash," *Journal of Cleaner Production*, vol. 329, p. 129523, Dec. 2021, doi: 10.1016/j.jclepro.2021.129523.

[4] D. P. Bentz and C. F. Ferraris, "Rheology and setting of high volume fly ash mixtures," *Cement and Concrete Composites*, vol. 32, no. 4, pp. 265–270, Apr. 2010, doi: 10.1016/j.cemconcomp.2010.01.008.

[5] W. Yuan, L. Ji, L. Meng, M. Fang, and X. Zhang, "Influence of Mineral Admixtures on the Performance of Pervious Concrete and Microscopic Research," *Buildings*, vol. 14, no. 2, p. 533, Feb. 2024, doi: 10.3390/buildings14020533.

[6] A. R. Lashari, A. Kumar, R. Kumar, and S. H. Rizvi, "Combined effect of silica fume and fly ash as cementitious material on strength characteristics, embodied carbon, and cost of autoclave aerated concrete," *Environmental Science and Pollution Research*, vol. 30, no. 10, pp. 27875–27883, Nov. 2022, doi: 10.1007/s11356-022-24217-9.

[7] M. Şahin Yön, "Mechanical, durability and microstructure properties of eco-friendly self-compacting mortars with addition of volcanic scoria, silica fume and boron waste as cement replacement," *Construction and Building Materials*, vol. 462, p. 139894, Feb. 2025, doi: 10.1016/j.conbuildmat.2025.139894.

[8] M. Murtaza, J. Zhang, C. Yang, X. Cui, C. Su, and A. N. Ramadan, "Performance analysis of self compacting concrete by incorporating fly ash, coal gangue powder, cement kiln dust and recycled concrete powder by absolute volume method," *Construction and Building Materials*, vol. 431, p. 136601, Jun. 2024, doi: 10.1016/j.conbuildmat.2024.136601.

[9] F. A. Mustapha, A. Sulaiman, R. N. Mohamed, and S. A. Umara, "The effect of fly ash and silica fume on self-compacting high-performance concrete," *Materials Today: Proceedings*, vol. 39, pp. 965–969, 2021, doi: 10.1016/j.matpr.2020.04.493.

[10] M. T. Arshad, S. Ahmad, A. Khitab, and A. Hanif, "Synergistic Use of Fly Ash and Silica Fume to Produce High-Strength Self-Compacting Cementitious Composites," *Crystals*, vol. 11, no. 8, p. 915, Aug. 2021, doi: 10.3390/cryst11080915.

[11] A. Singh, P. K. Mehta, and R. Kumar, "Strength and microstructure analysis of sustainable self-compacting concrete with fly ash, silica fume, and recycled minerals," *Materials Today: Proceedings*, vol. 78, pp. 86–98, 2023, doi: 10.1016/j.matpr.2022.11.282.

[12] S. Kumar, R. Kumar, B. Rai, and P. Samui, "Prediction of compressive strength of high-volume fly ash self-compacting concrete with silica fume using machine learning techniques," *Construction and Building Materials*, vol. 438, p. 136933, Aug. 2024, doi: 10.1016/j.conbuildmat.2024.136933.

[13] A. Singh, P. K. Mehta, and R. Kumar, "Performance of binary admixtures (Fly Ash and Silica Fume) on Self Compacting concrete," *Materials Today: Proceedings*, vol. 58, pp. 970–977, 2022, doi: 10.1016/j.matpr.2022.02.489.

[14] J. Guru Jawahar, C. Sashidhar, I. V. Ramana Reddy, and J. Annie Peter, "Micro and macrolevel properties of fly ash blended self compacting concrete," *Materials & Design (1980-2015)*, vol. 46, pp. 696–705, Apr. 2013, doi: 10.1016/j.matdes.2012.11.027.

[15] A. M. Falmata, A. Sulaiman, R. N. Mohamed, and A. U. Shettima, "Mechanical properties of self-compacting high-performance concrete with fly ash and silica fume," *SN Applied Sciences*, vol. 2, no. 1, p. 33, Jan. 2020, doi: 10.1007/s42452-019-1746-z.

[16] W. Wongkeo, P. Thongsanitgarn, A. Ngamjarurojana, and A. Chaipanich, "Compressive strength and chloride resistance of self-compacting concrete containing high level fly ash and silica fume," *Materials & Design*, vol. 64, pp. 261–269, Dec. 2014, doi: 10.1016/j.matdes.2014.07.042.

[17] C. Dong *et al.*, "Fresh and hardened properties of recycled plastic fiber reinforced self-compacting concrete made with recycled concrete aggregate and fly ash, slag, silica fume," *Journal of Building Engineering*, vol. 62, p. 105384, Dec. 2022, doi: 10.1016/j.jobe.2022.105384.

[18] A. F. Bingöl and İ. Tohumcu, "Effects of different curing regimes on the compressive strength properties of self compacting concrete incorporating fly ash and silica fume," *Materials & Design*, vol. 51, pp. 12–18, Oct. 2013, doi: 10.1016/j.matdes.2013.03.106.

[19] H. A. Mohamed, "Effect of fly ash and silica fume on compressive strength of self-compacting concrete under different curing conditions," *Ain Shams Engineering Journal*, vol. 2, no. 2, pp. 79–86, Jun. 2011, doi: 10.1016/j.asej.2011.06.001.

[20] A. Sadr Momtazi, B. Tahmouresi, and R. Kohani Khoshkbijari, "An Investigation on Mechanical Properties and Durability of Concrete Containing Silica Fume and Fly Ash," *Civil Engineering Journal*, vol. 2, no. 5, pp. 189–196, May 2016, doi: 10.28991/cej-2016-00000025.

[21] *STRK EN 13263-2:2014. Silica fume for concrete. Part 2: Conformity evaluation*.

[22] K. Akmalaiuly, N. Berdikul, I. Pundienė, and J. Pranckevičienė, "The Effect of Mechanical Activation of Fly Ash on Cement-Based Materials Hydration and Hardened State Properties," *Materials*, vol. 16, no. 8, p. 2959, Apr. 2023, doi: 10.3390/ma16082959.

[23] M. I. Khan, Y. M. Abbas, and G. Fares, "Enhancing Cementitious Concrete Durability and Mechanical Properties through Silica Fume and Micro-Quartz," *Sustainability*, vol. 15, no. 22, p. 15913, Nov. 2023, doi: 10.3390/su152215913.

[24] H. M. Hamada *et al.*, "Effect of silica fume on the properties of sustainable cement concrete," *Journal of Materials Research and Technology*, vol. 24, pp. 8887–8908, May 2023, doi: 10.1016/j.jmrt.2023.05.147.

[25] R. V. de la Villa, I. S. de Soto, R. García-Giménez, and M. Frías, "Thermodynamic Evaluation of Pozzolanic Reactions between Activated Pozzolan Mix of Clay Waste/Fly Ash and Calcium Hydroxide," *Journal of Materials in Civil Engineering*, vol. 29, no. 8, Aug. 2017, doi: 10.1061/(ASCE)MT.1943-5533.0001940.

[26] Y. Zhu *et al.*, "Effect of decarbonization of high carbon fly ash on workability, mechanical properties and durability of concrete," *Materials and Structures*, vol. 56, no. 9, p. 171, Nov. 2023, doi: 10.1617/s11527-023-02258-x.

[27] P. A. Hartley, G. D. Parfitt, and L. B. Pollack, "The role of the van der Waals force in the agglomeration of powders containing submicron particles," *Powder Technology*, vol. 42, no. 1, pp. 35–46, Apr. 1985, doi: 10.1016/0032-5910(85)80036-X.

[28] R. Siddique, "Utilization of silica fume in concrete: Review of hardened properties," *Resources, Conservation and Recycling*, vol. 55, no. 11, pp. 923–932, Sep. 2011, doi: 10.1016/j.resconrec.2011.06.012.

[29] D. P. Bentz and C. F. Ferraris, "Rheology and setting of high volume fly ash mixtures," *Cement and Concrete Composites*, vol. 32, no. 4, pp. 265–270, Apr. 2010, doi: 10.1016/j.cemconcomp.2010.01.008.

[30] M. D. A. Thomas, *Optimizing the Use of Fly Ash in Concrete*. Skokie, IL: Portland Cement Association, 2007, vol. 5420.

[31] J. M. Khatib, "Performance of self-compacting concrete containing fly ash," *Construction and Building Materials*, vol. 22, no. 9, pp. 1963–1971, Sep. 2008, doi: 10.1016/j.conbuildmat.2007.07.011.

[32] V. V. Potapov and D. S. Gorev, "The results of tests of the compositions of fine-grained concrete with addition of nanosilica fume and microsilica," *Modern High Technologies*, vol. 2, no. №3 2019, pp. 232–238, 2019, doi: 10.17513/snt.37471

[33] A. Hamza, S. Derogar, and C. Ince, "The effects of silica fume and hydrated lime on the strength development and durability characteristics of concrete under hot water curing condition," *MATEC Web of Conferences*, vol. 120, p. 02004, Aug. 2017, doi: 10.1051/matecconf/201712002004.

[34] G. L. Golewski, "The Role of Pozzolanic Activity of Siliceous Fly Ash in the Formation of the Structure of Sustainable Cementitious Composites," *Sustainable Chemistry*, vol. 3, no. 4, pp. 520–534, Dec. 2022, doi: 10.3390/suschem3040032.

[35] Solovyov L.P., Pronin V.A. "Increase of ecological safety of thermal power stations by recycling of the cindery waste," Modern high technologies, no 3. pp. 40-42, 2011. https://top-technologies.ru/ru/article/view?id=26834.

**Information about authors:**

*Erzhan Kuldeyev* – Candidate of Technical Sciences, Vice-Rector for Corporate Development, Satbayev University, Almaty, Kazakhstan, e.kuldeyev@satbayev.university

*Zhanar Zhumadilova* – PhD, Associate Professor, Deputy Director, Institute of Architecture and Civil Engineering named after T. Bassenov, Satbayev University, Almaty, Kazakhstan, z.zhumadilova@satbayev.university

*Adlet Zhagifarov* – MSc, PhD Student, Institute of Architecture and Civil Engineering named after T. Bassenov, Satbayev University, Almaty, Kazakhstan, a.zhagifarov@satbayev.university

*Aigerim Tolegenova* – MSc, PhD Student, Institute of Architecture and Civil Engineering named after T. Bassenov, Satbayev University, Almaty, Kazakhstan, a.tolegenova@satbayev.university

*Mussa Kuttybay* – MSc, Postdoctoral Student, Auezov University, Department of Construction and Building Materials, Shymkent, Kazakhstan, m.kuttibay@mail.ru

*Abzal Alikhan* – MSc, Junior Researcher, Institute of Architecture and Civil Engineering named after T. Bassenov, Satbayev University, Almaty, Kazakhstan, Abzal.shagirov@mail.ru

**Author Contributions:**

*Erzhan Kuldeyev* – resources, funding acquisition.
*Zhanar Zhumadilova* – analysis, editing, interpretation.
*Adlet Zhagifarov* – concept, visualization.
*Aigerim Tolegenova* – analysis, methodology, drafting.
*Mussa Kuttybai* – testing, data collection.
*Abzal Alikhan* – testing, data collection.

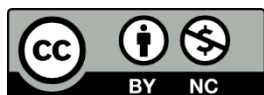**Conflict of Interest:** The authors declare no conflict of interest.

**Use of Artificial Intelligence (AI):** The authors declare that AI was not used.